THE AEROMAGNETIC FIELD AND HYDROTHERMAL CIRCULATION IN THE TROODOS OPHIOLITE, CYPRUS

by

Charles C. Walls

Submitted in partial fulfullment of the requirements
for the degree of Master of Science

at

Dalhousie University
Halifax, Nova Scotia
August, 1996

DALHOUSIE UNIVERSITY

DEPARTMENT OF EARTH SCIENCES

The undersigned hereby certify that they have read and recommend to the Faculty of Graduate Studies for acceptance a thesis entitled "The Aeromagnetic Field and Hydrothermal Circulation in the Troodos Ophiolite, Cyprus" by Charles C. Walls, in partial fulfillment of the requirements for the degree of Master of Science.

Dated: August 2, 1986

Examining Comm

(External Examiner)

(Supervisory Committee)

(Departmental Reader)

(Supervisor)

(Chair)

DALHOUSIE UNIVERSITY

DATE: August 14, 1996

AUTHOR: Charles C. Walls

TITLE: The Aeromagnetic Field and Hydrothermal Circulation in the Troodos Ophiolite, Cyprus

DEPARTMENT OF SCHOOL: Earth Sciences

DEGREE: MSc CONVOCATION: Fall YEAR: 1996

Permission is herewith granted to Dalhousie University to circulate and to have copied for non-commercial purposes, at its discretion, the above title upon the request of individuals or institutions.

Signature of Author

Table of Contents

List of Figures

List of Tables

Abstract

The Troodos ophiolite in southwestern Cyprus has commonly been studied as an analogue of oceanic crust. Hydrothermal sulphide mineralization in the Troodos formed from circulating seawater and shows many similarities to that found at mid-ocean ridges. Numerous studies indicate that hydrothermal alteration, also related to the circulation of seawater, radically decreases the magnetization of ophiolitic and oceanic rocks.

This study re-analyses an aeromagnetic survey flown in the 1960's on the northern and eastern flanks of the Troodos ophiolite (Hunting Geology and Geophysics, 1969). Errors in the aeromagnetic data have been considered in detail. The aeromagnetic data has been compared to extensive geological information from a local study area. Sample measurements indicate that the magnetization of the upper Extrusives averages about ten amperes/metre and is not arranged in a regular pattern. Based upon this, the observed magnetic anomalies were modelled with a strongly magnetized layer of unaltered upper extrusives varying from approximately two hundred metres to one kilometre in thickness. This reflects variations in the depth to the top of a hydrothermally altered zone.

Massive sulphide mines in the Troodos appear to be grouped into mining districts. The locations of discrete hydrothermal mineralization (mines, mineral prospects, gossans and umbers) were analyzed to determine if they appear regularly along the direction of spreading. No such regularity was found. However, a comparison of the mineralization locations and the aeromagnetic data suggests that some mineralization in the extrusives may occur preferentially in areas of aeromagnetic lows. The correlation is probably insufficient to be used as a tool to locate mineralization, but may indicate general relationships between hydrothermal activity and a decrease in rock magnetization.

Acknowledgements

I must first and foremost thank Dr. Jim Hall for his continual faith and support throughout the process of creating this thesis. The seven years of its creation must have tried his patience more than once and it would be difficult to overstate my gratitude.

I must also thank the members of my supervisory committee, Drs. P. Ryall, J. Verhoef and P. Schenk, for their continual advice. Their critical discussions and suggestions improved it greatly. Dr. S. Dehler and Dr. M. Zentilli suggested improvements to the final version.

Thanks also to James Hall for his assistance in collecting the field data. Lata Hall contributed the paleomagnetic measurements, for which I am in her debt.

The staff of the Geological Survey Department of Cyprus, and especially the director, Dr. G. Constantinou, contributed their friendship and support during several field seasons since 1982. Their support was essential to the success of this thesis. Thanks also to our many friends in Palekhori and elsewhere in Cyprus who assisted our fieldwork in so many ways.

Finally, I would like to thank my family and friends, especially Mom, Dad and Cathy for their support and patience.

Chapter 1

Introduction

The ore bodies of the Troodos ophiolite of Cyprus have been mined for copper since the Bronze age (Bear, 1963). They are now thought to be typical manifestations of the circulation of sea water through oceanic crust (eg. Constantinou, 1980).

This hydrothermal circulation in the Troodos ophiolite can be considered in at least two scales: a regional event which caused widespread alteration of some of the country rock, and a more episodic type which caused intense alteration in upwelling zones. The upwelling zones are marked at their higher levels by the mines and smaller examples of mineralization. Both scales are associated with a decrease in the magnetization of the rocks.

This study examines the distribution of these two manifestations of hydrothermal circulation in the Troodos ophiolite. The aeromagnetic field in the vicinity of the extrusive units on the northern flank of the Troodos will be analyzed to investigate the distribution of altered and unaltered zones. A mathematical analysis of the distribution of mines and mineralization will determine if they are regularly spaced. The pattern of these manifestations of hydrothermal circulation will be used to draw conclusions as to the nature of hydrothermal circulation in the Troodos and, by extension, in the oceanic crust.

The magnetization of the oceanic crust

The oceanic crust is divided into several layers on the basis of seismic refraction data (figure 1.1) (Salisbury et al., 1989). Layer 1 is made up of unconsolidated sediments and sedimentary rocks. Layer 2 is the upper volcanic layer of extrusives and dikes overlying layer 3, composed of gabbros and pyroxenites.

Magnetic anomalies which form stripes parallel to spreading ridges (eg. Mason and Raff, 1961; Raff and Mason, 1961) were interpreted to be due to sea floor spreading and reversals in the earth's magnetic field (Vine and Matthews, 1963). Detailed magnetic data (eg. Talwani et al., 1971) suggested that these magnetic anomalies were due to a thin, strongly magnetized layer at the top of layer 2. While deeper, less strongly magnetized sources may be important and may affect the shape of anomalies (Kidd, 1977; Arkani-Hamed, 1989), later work has confirmed the importance of this upper layer (Cande and Kent, 1985).

Field reversals are not the only cause of major anomalies. Figure 1.2 shows a profile of the magnetic field along the crest of the Reykjanes Ridge south of Iceland. As this survey is parallel to the ridge crest, no significant reversals are present. The magnetic anomaly pattern is generally accounted for by the calculated magnetic field of the topography.

Other large anomalies have less obvious causes. A long interval of normal magnetic field polarity during the late Cretaceous (Helsley and Steiner, 1969)

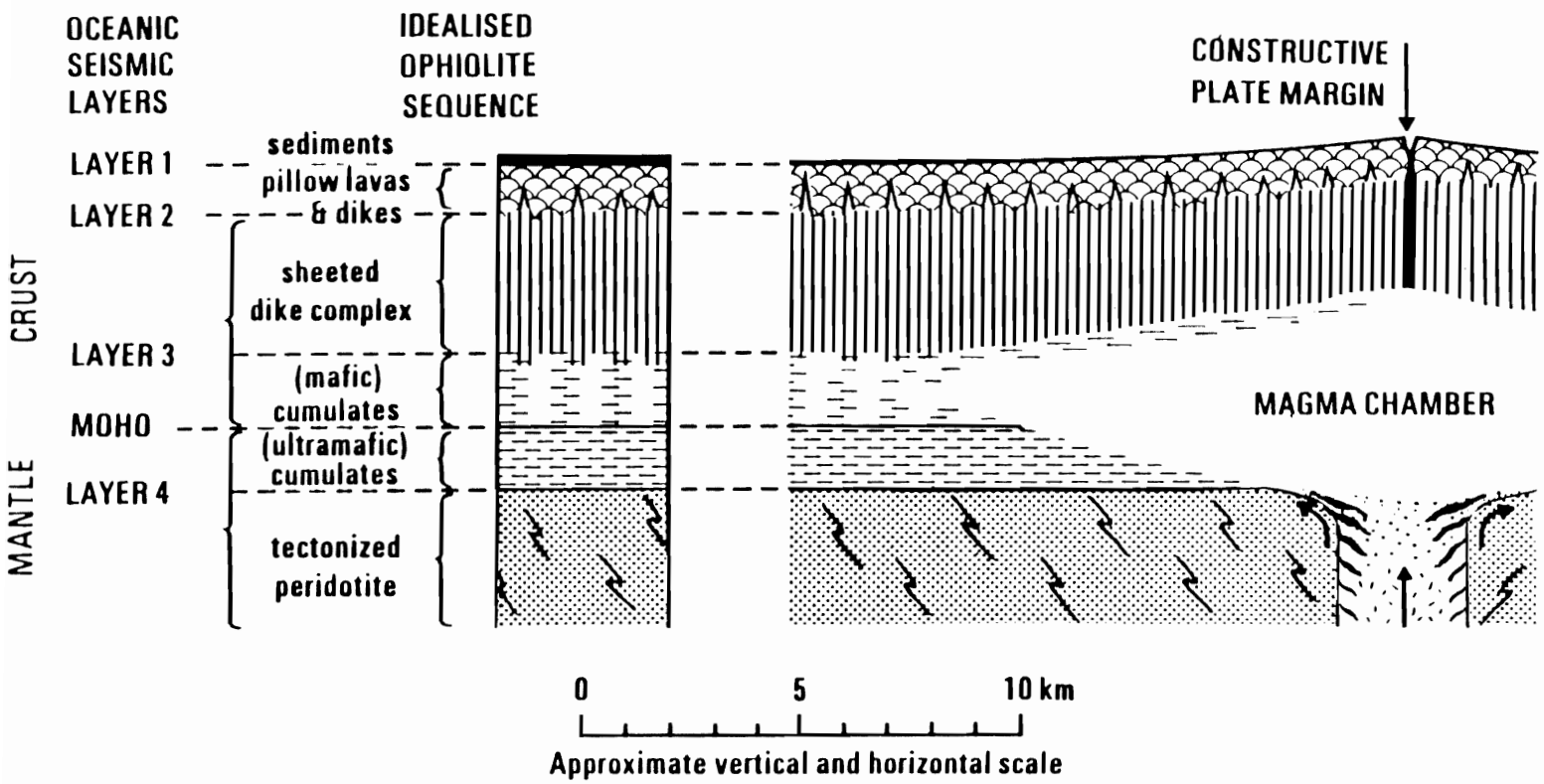

Figure 1.1. Idealized sectional view of the oceanic crust showing seismic layers (from Gass, 1980).

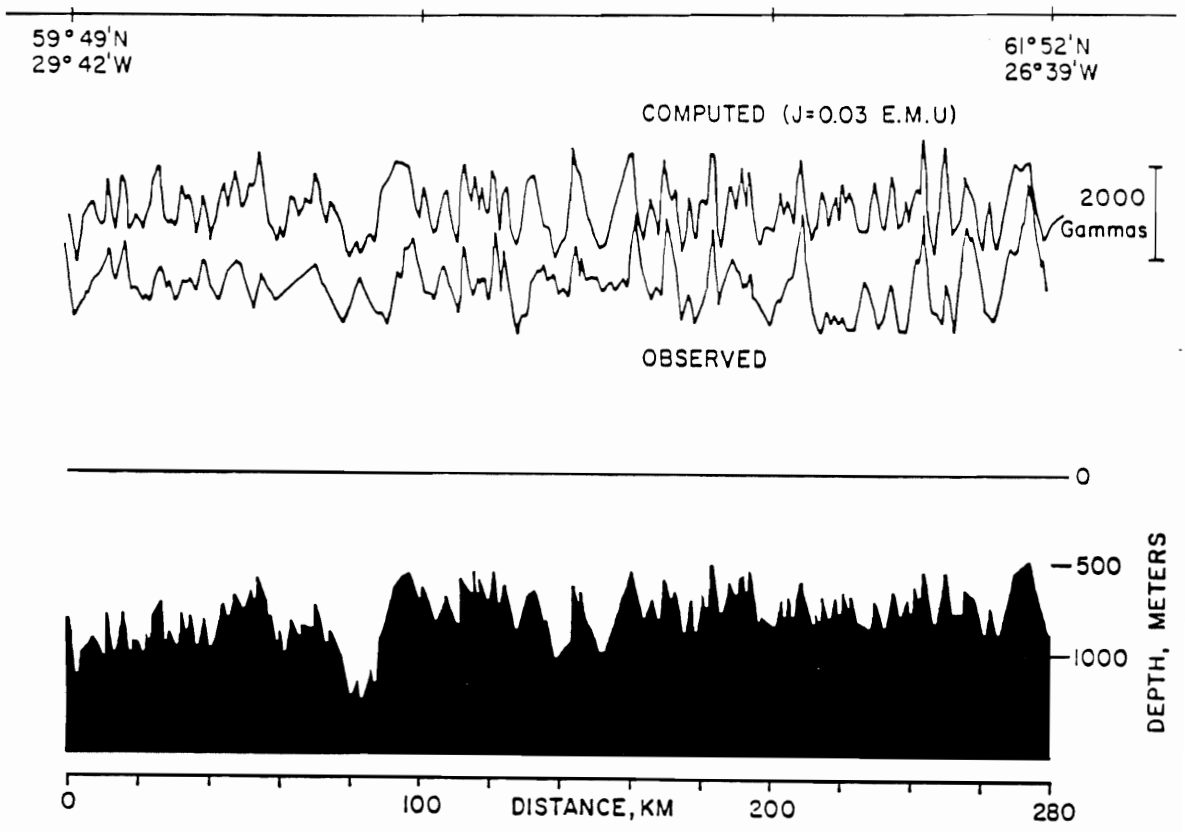

Figure 1.2. Observed and computed profiles of the magnetic field along the Reykjanes ridge crest south of Iceland. The computed profile assumes the anomaly is caused by uniformly (30 amp/m) magnetized topography, shown at the bottom. Note the close similarity (from Talwani et al., 1971).

contains numerous anomalies, only some of which can be attributed to topographic features (eg. Atwater and Severinghaus, 1989).

Early Deep Sea Drilling Project drill holes indicated that some material may have been rotated tectonically after the magnetization was established (Ade-Hall et al. 1976; Verosub and Moores, 1981). While this is important in limited areas causing local magnetic anomalies, magnetization calculated from models indicates that this cannot be a widespread effect (Cande and Kent, 1985).

The composition of oceanic basalt, which makes up the upper layer of oceanic crust, is often very uniform on a local scale (eg. Miyashiro, 1973). However, several classes of sea floor basalt have been differentiated by geochemical means (Natland, 1991). Thus, large magnetic anomalies of geochemical or petrological origin do occur, particularly where iron-rich basalts are common (Vogt, 1979). Variations in rock magnetism may be due to differences in grain size as well as differences in abundance of Fe-Ti oxides. The latter are the major carriers of magnetization (Natland, 1991).

The natural remanent magnetism of oceanic rocks shows a regular variation with increasing age (Bleil and Peterson, 1983). From a maximum at the ridge crest, the average remanent magnetization decreases rapidly to a minimum in rocks approximately 20 million years old. It then increases gradually in rocks from 20 to 120 million years of age. Low temperature oxidation of titanomagnetite is the main cause of this pattern.

Another possible origin for local magnetic anomalies is hydrothermal

activity, which generally decreases the magnetization as seen in rock samples (eg. Hall et al., 1991a). This effect would create magnetic lows that could be used to prospect for massive sulphide ore deposits on land (eg. Hunting Geology and Geophysics, 1969). Rona (1978) has suggested that magnetic lows could assist in discovering massive sulphide deposits on mid-ocean ridges. Studies since that time have confirmed a strong relationship between hydrothermal circulation and the destruction of magnetic minerals in the upper oceanic crust (Wooldridge et al., 1990). This information has been used to investigate magnetic anomalies in the vicinity of hydrothermal massive sulphide deposits at oceanic ridges and to propose possible configurations for the crust in these areas (Wooldridge et al, 1992).

Hydrothermal circulation in the oceanic crust

Hydrothermal circulation in the oceanic crust is the movement of sea water from the rock/water interface downward into the crust and back to the surface in a circulation cell (figure 1.3). The process is driven by a heat source at depth such as a magma chamber. The circulating sea water removes heat from the crust, causes widespread alteration in the recharge limb and creates intense alteration in the discharge limb. Vents, which occur at the top of the discharge limb, can be marked by massive sulphide deposits.

Active vents have been discovered on all major spreading ridges (figure

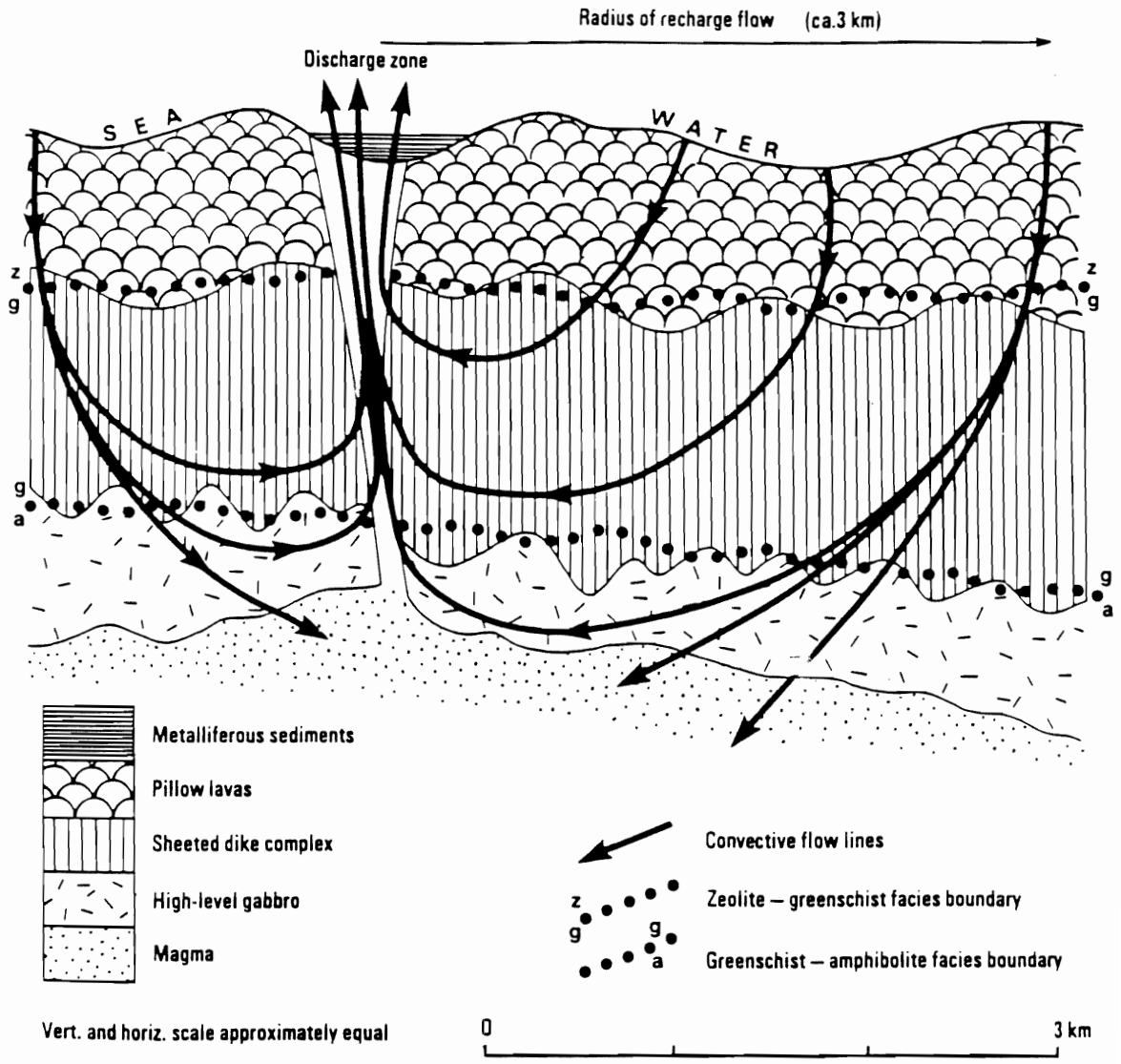

Figure 1.3. Idealized model of hydrothermal circulation in the oceanic crust (from Gass, 1980.).

1.4). Given that less than ten per cent of the world's system of spreading ridges has been investigated in sufficient detail to detect hydrothermal venting (Rona and Scott, 1993), it may be assumed that this activity is commonly associated with the formation of new crust at or near the axes of oceanic ridges.

Modelling studies of modern vents suggest that the fluid interacted with the magma chamber which provided the heat energy to drive the circulation. This interaction took place deep in the circulation cell across a high permeability boundary layer which may have been quite complicated geologically (Lowell et al., 1995). The layer may have remained thin to provide the constant heat output observed at some modern vents (Lowell and Germanovich, 1994). Two stage circulation may have been important in some cases, where circulation in a deeper layer transferred heat to convection cells in an upper circulation layer (Bischoff and Rosenbauer, 1989). These upper cells circulated sea water from the surface and emitted it at vents or vent fields.

The discharge arm of hydrothermal circulation cells are known to occur along more restricted pathways. These were probably determined by existing faults, fissures and zones of higher porosity in the section. Ascending fluids were focussed into narrow pathways with high rates of flow to emerge at vents on the sea floor. Consequently, the discharge arm controlled the rate of circulation (Lowell et al., 1995).

Venting at the sea floor may be either localized or diffuse. Localized vents, as found at some localities on the East Pacific Rise, form chimneys emitting

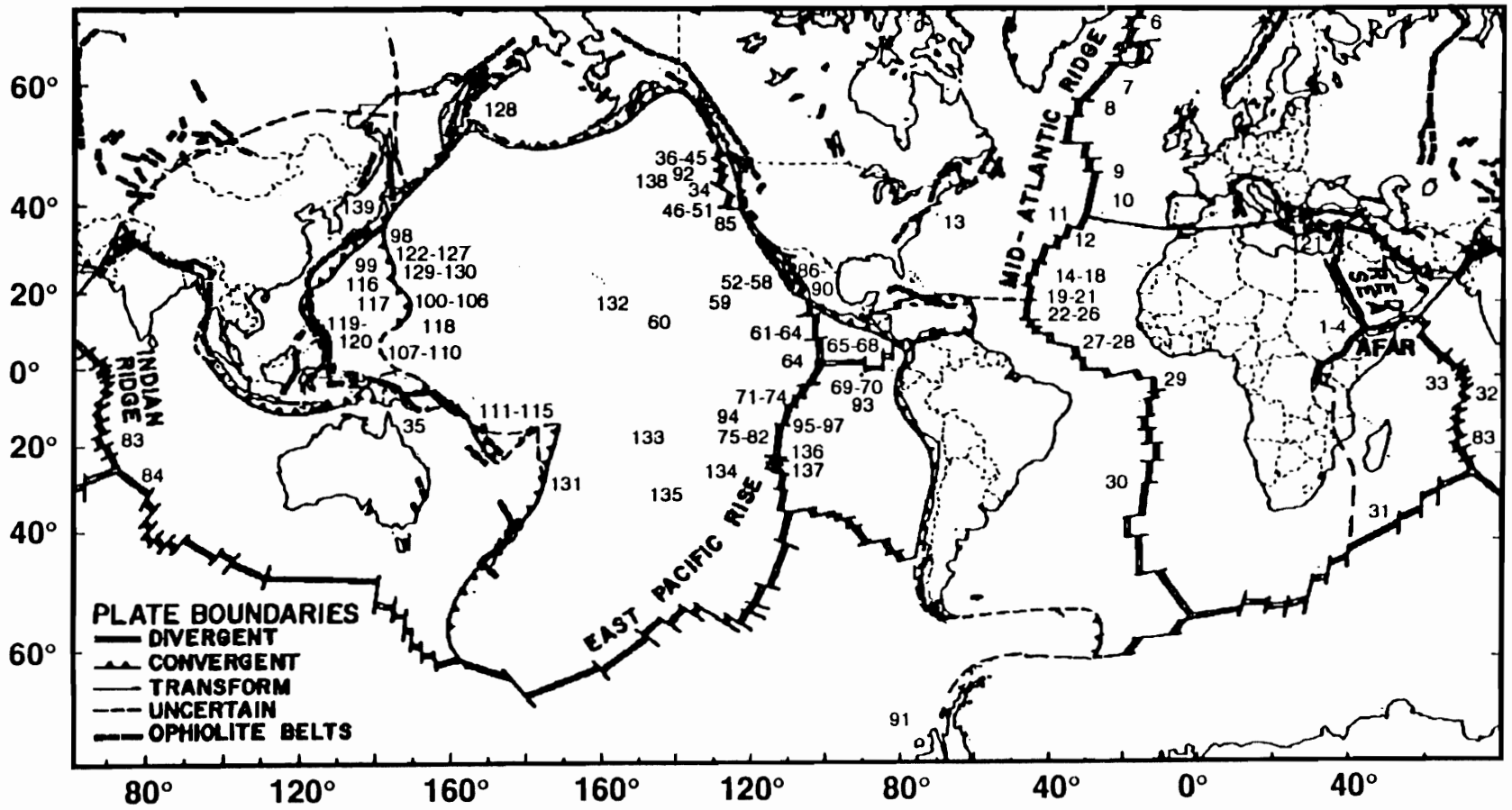

Figure 1.4. The locations of 139 known hydrothermal circulation sites in the world's oceans (from Rona and Scott, 1993).

hydrothermal fluids at up to four hundred degrees Celsius. More diffuse venting, as seen at the Galapagos Spreading Centre for example, is usually associated with lower temperatures (Lowell et al., 1995), possibly due to subsurface mixing with cold seawater (Corliss et al., 1979).

Chimneys typically have an outer shell of anhydrite grading inward to an inner shell of euhedral sulphide crystals. On the cessation of flow from the vent, the outer shell of anhydrite usually dissolves, and the sulphide remnant collapses to the sea floor forming a rubble mound. Some variability is typically seen in the sulphide mineralogy of these deposits. Pyrite is ubiquitously present. Copper dominated deposits contain chalcopyrite, bornite, chalcocite and covellite. Zinc dominated deposits are richer in sphalerite (Lydon, 1988). Pyrrhotite may or may not be present (Wooldridge et al., 1990).

Why have so few hydrothermal circulation systems been investigated in detail, given their importance and attractiveness? The answer undoubtedly lies in their inaccessibility. Conducted at the bottom of deep oceans, this research is difficult, expensive and produces limited results. Even the most intense and expensive efforts to date have produced little direct sub-surface data.

Ophiolites are pieces of seafloor that have been raised above sea level. They provide an opportunity to study some types of oceanic crust in detail with little difficulty and cost. This study will use the Troodos ophiolite of southwestern Cyprus to provide information about hydrothermal systems in oceanic-type crust. Specifically, it will look at the distribution of alteration and mineralization and the

associated magnetic field anomalies in the extrusive units of the ophiolite. These features will be compared to other geological data collected from the area.

Cyprus and the Troodos Ophiolite

The island of Cyprus is located in the eastern Mediterranean approximately 70 kilometres south of Turkey and 120 kilometres west of Lebanon. Rocks from the Troodos ophiolite in southern Cyprus are late Cretaceous in age (eg. Mukasa and Ludden, 1987).

It is assumed that the Troodos was part of a small microplate which, based on paleomagnetic measurements, has rotated ninety degrees counterclockwise since its formation (Clube et al., 1985). Geochemical studies on the volcanic rocks suggest that the ophiolite was formed in an island arc or back-arc basin environment during the closing of Tethys (Miyashiro, 1973; Muenow et al., 1990). The well developed sheeted dike complex indicates that it formed at least in part in a spreading ridge environment (Thy and Moores, 1988).

The Troodos was formed during the long Cretaceous normal magnetic polarity epoch (Staudigel et al., 1986). No significant reversals of the magnetic field are preserved. Thus, the magnetic anomalies present over the volcanics cannot be due to polarity reversals.

Two small mountain ranges dominate the island (figure 1.5). The Kyrenia range extends the length of the northern coast. The Troodos range, containing

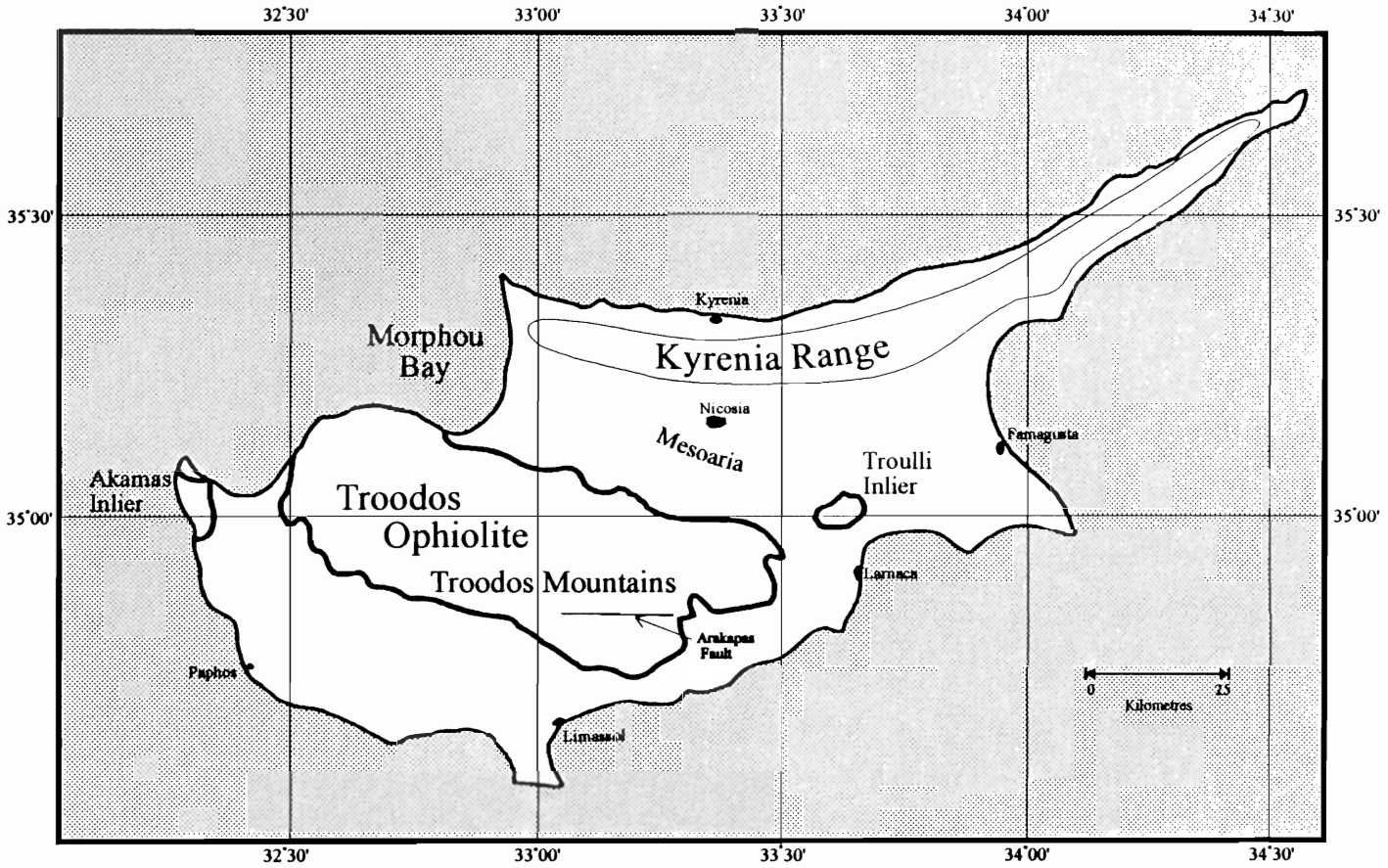

Figure 1.5. Map of Cyprus

the ophiolite, is centred in the southwestern third of the island. Its peak, Mt. Olympus, stands 1952 metres above sea level. The Troodos forms an elongated ridge trending approximately twenty degrees south of east.

Between the two ranges lies a large plain, the Mesoaria, extending from Morphou Bay in the northwest to Larnaca and Famagusta in the east. A smaller plain forms the western edge of the island. The Troulli inlier, assumed to be a continuation of the Troodos ophiolite, lies just north of Larnaca. Another inlier, the Akamas, makes up the western tip of the island.

The Troodos ophiolite was uplifted and formed into an anticlinal emplacement structure during the Pleistocene epoch (Grand et al, 1993). Erosion has since exposed a near continuous section through a type of oceanic crust.

Figure 1.6 shows the geology of the ophiolite. Upper mantle units are exposed near the topographic summit. Surrounding these are crustal ultramafics and gabbros, which are in turn surrounded and overlain by sheeted dikes. These grade upward stratigraphically into mixed pillow lavas and sheet flows. The transition zone between sheeted dikes and extrusives is termed the Basal Group. It consists of dikes with screens of extrusive material. The extrusives are in turn overlain by chalks and other marine sediments.

The southeastern section of the ophiolite is cut by a large east-west fault, the Arakapas fault, which is interpreted to be a fossil transform fault. A similar geological sequence, from ultramafics to pillow lavas occurs south of this fault.

The Troodos is one of the most complete and least deformed ophiolites

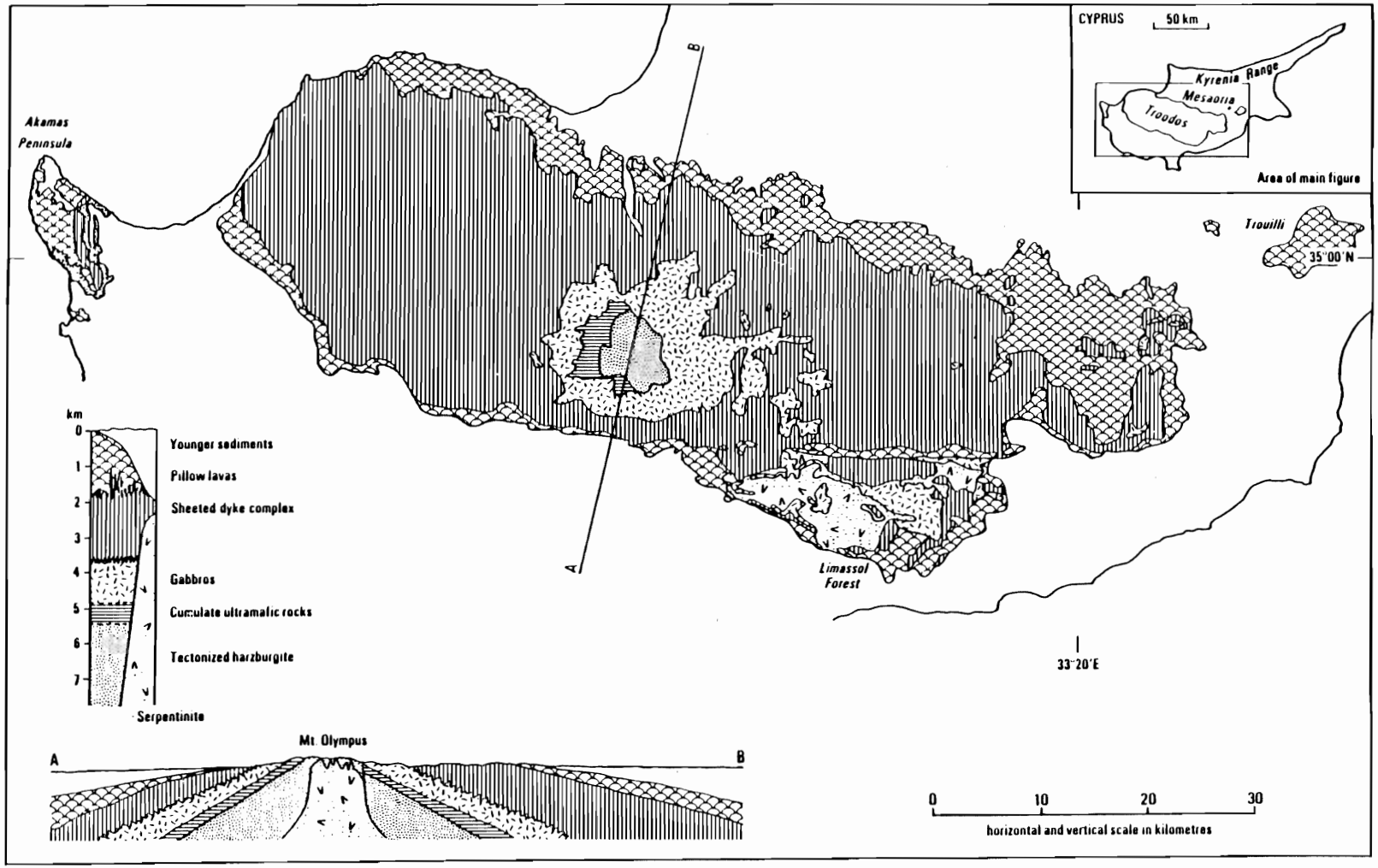

Figure 1.6. The geology of the Troodos ophiolite (from Gass, 1980).

and has been studied extensively. It retains a complete oceanic crustal sequence from the Layer 1 sediments to the Moho and down into upper mantle rocks. While it has been uplifted and eroded to expose a cross-section, the original sea floor/crustal constructional relationships between the layers of the ophiolite have been preserved.

Numerous studies of alteration have been conducted on the Troodos rocks (eg. Gillis and Robinson, 1985) which compare closely with oceanic crust in this regard (Gillis and Robinson, 1988). Yang (1991) conducted a regional study of the alteration based on samples collected along seven profiles on the north flank of the ophiolite. He divided the upper part of the ophiolite into three zones based on secondary mineralogy. These zones are observable in the field due to changes in colour and macroscopic alteration features.

The highest zone (brownstone) endured alteration at temperatures less than 200 degrees Celsius. The lowest zone (greenstone) recorded alteration at temperatures from 200 to 450 degrees Celsius. An intervening transition zone experienced temperatures of 200 to 300 degrees Celsius. This transition zone corresponds very closely to the interval where dikes make up between 25 and 50 percent of the outcrop.

The coarse magnetic structure of the Troodos follows the pattern of the exposed geology. An aeromagnetic survey flown at 2600 metres altitude found higher magnetic field values over the extrusives on the northern flank of the ophiolite (Vine et al., 1973) (figure 1.7). A negative anomaly corresponds to the

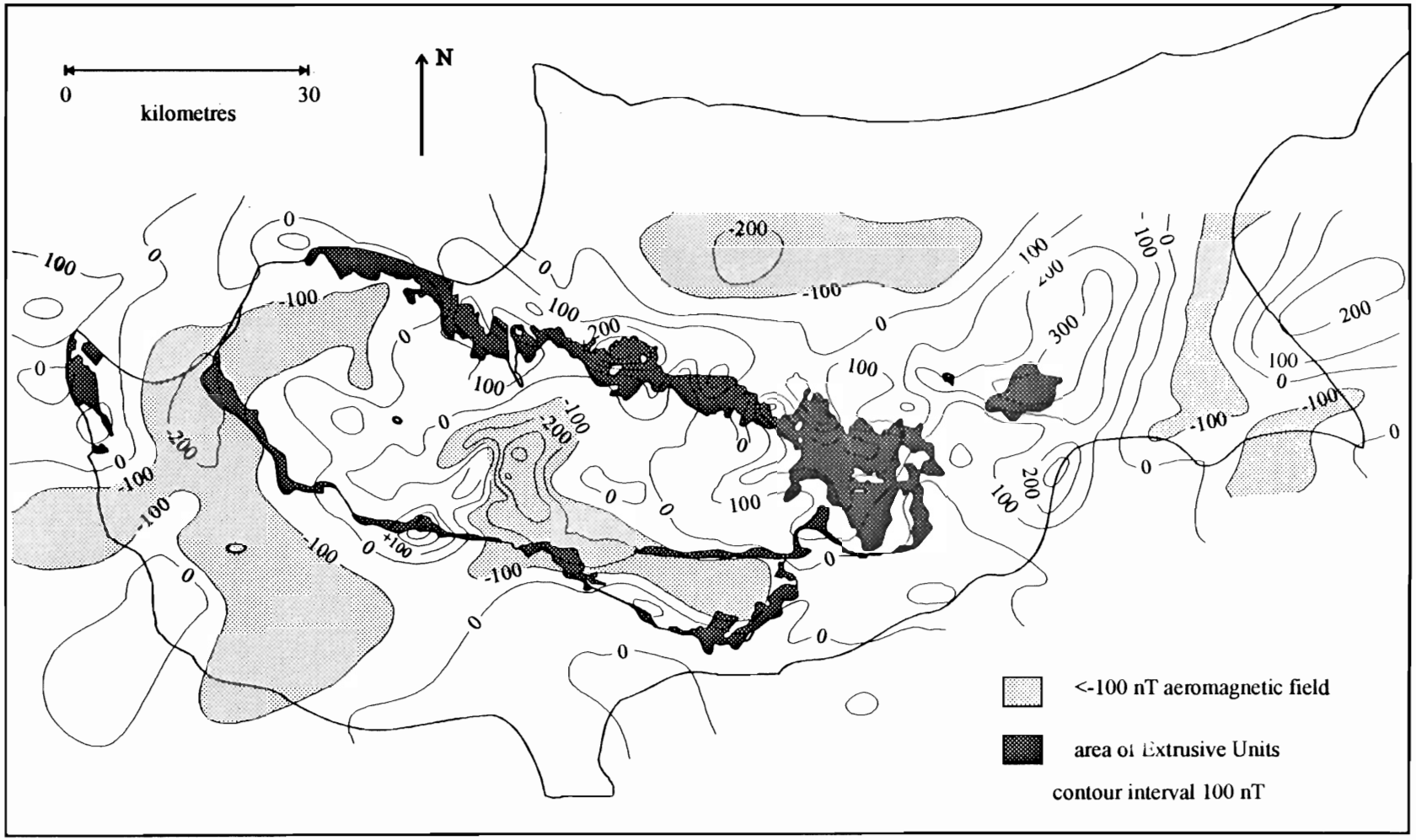

Figure 1.7. High level aeromagnetic survey of Cyprus (redrawn from Vine et al. 1973).

topographic summit where the deepest upper mantle units are exposed. The intervening sheeted dikes and upper gabbros correspond to intermediate magnetic field values.

Profiles of rock magnetization are generally consistent with this pattern (figure 1.8). Samples with the strongest remanent magnetization are found in the unaltered upper crustal extrusives. Remanence decreases sharply near the base of the extrusives. Serpentinized samples deeper in the section show strong remanent magnetization locally. The smaller volumes of stronger magnetization represented by these units limit their effect. Induced magnetization has a peak equal to about one quarter of peak remanent magnetization at the base of the extrusives and the top of the sheeted dikes due to the formation of secondary magnetite (Hall et al., 1991a).

The combined effect of both remanent and induced magnetization in the Troodos profiles shows that by far the strongest magnetization is in the extrusives. This profile, and another from the Kambia area of the ophiolite, compare well so far as information is available to a Deep Sea Drilling Project profile through the oceanic crust (figure 1.9) (Hall et al. 1991a). All show strong magnetization in the upper volcanics, a sudden decrease and then continuously low magnetization at depth.

Sulphide mineralization, in the form of gossans, sulphide ore bodies and smaller concentrations of sulphide minerals, is contained mostly in the Extrusive section of the ophiolite. Smaller and less frequent instances of mineralization are

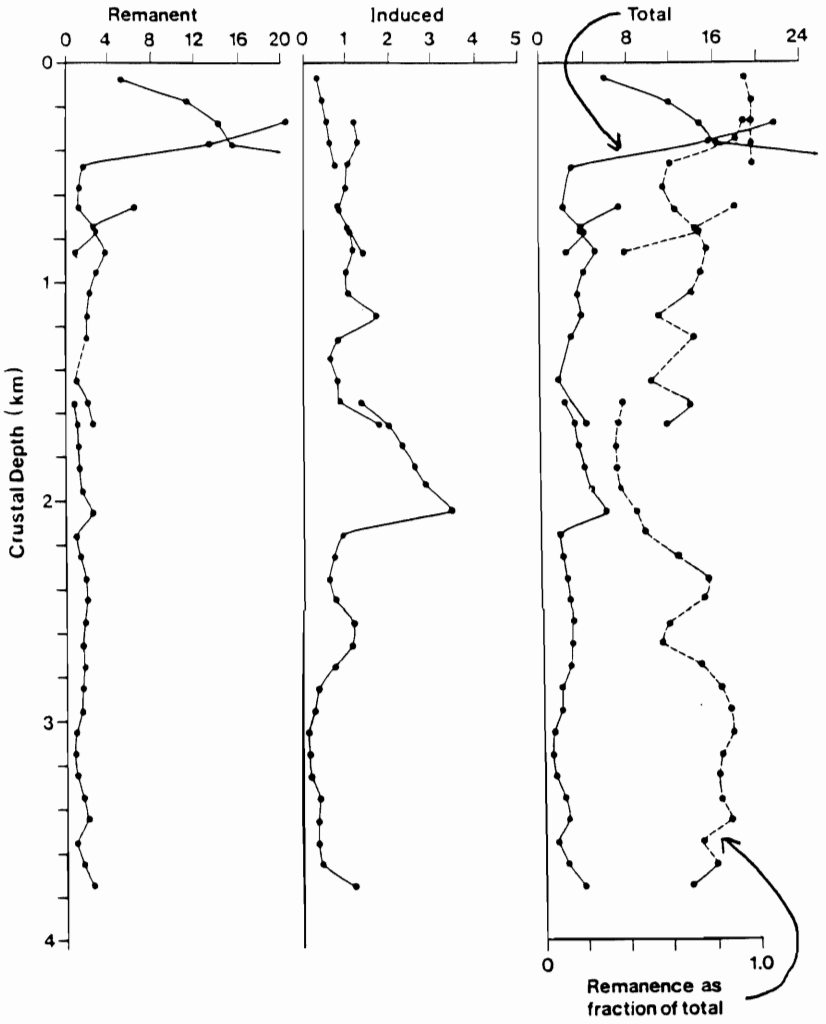

Figure 1.8. Profiles of magnetic properties with depth in a drillhole section from the northern flank of the Troodos ophiolite. The total magnetization (right column, solid line) was calculated using the formula T = J + kF where J is the remanent magnetization, k is the susceptibility and F is the earth's field for Cyprus (from Hall et al., 1991a).

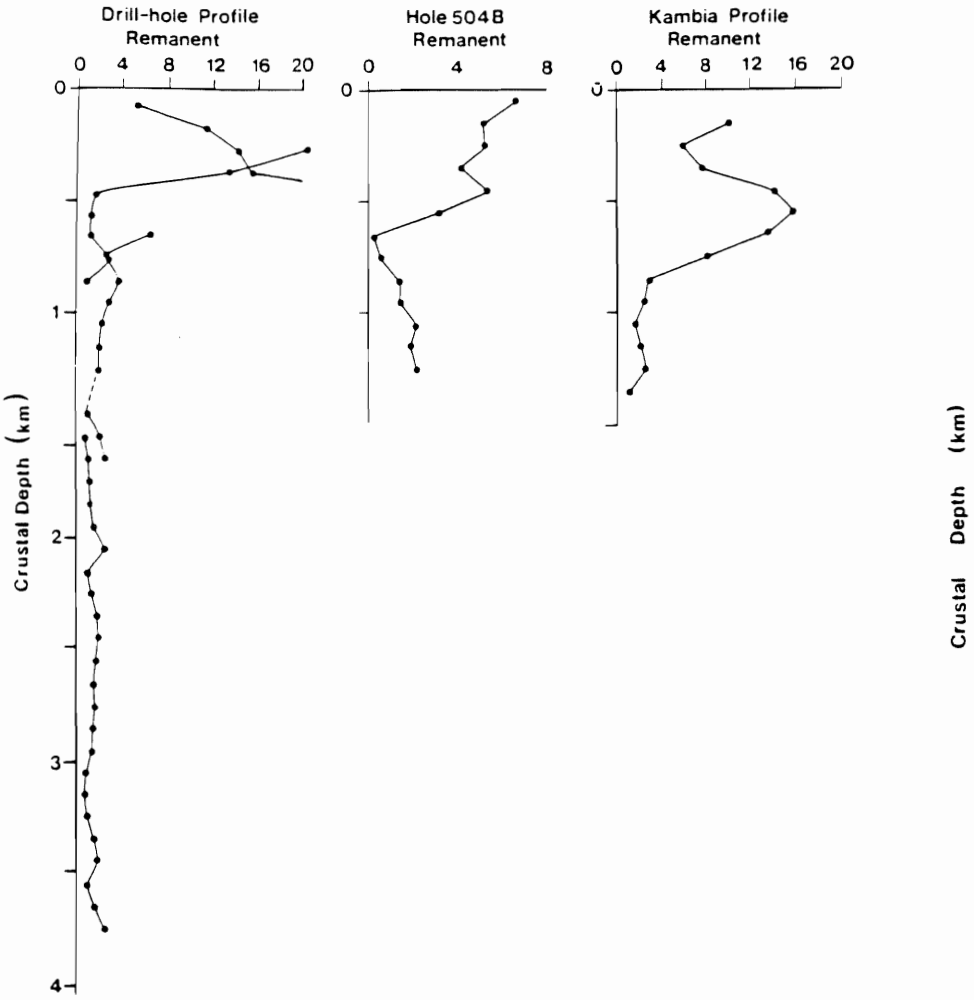

Figure 1.9. A comparison of profiles with depth of natural remanent magnetization in a drillhole section from Cyprus, the DSDP drillhole 504B and a field profile from the Kambia area of Cyprus (from Hall et al.,1991a).

found in the Basal Group, Sheeted Dikes and Gabbros. The ore bodies occur preferentially just above the level in the extrusives where dikes form approximately 25 per cent of the volume of the outcrop (Hall and Yang, 1994). This may be due to preferential preservation, whereby deeper bodies are destroyed by the intrusive activity and shallower bodies are redissolved by circulating sea water.

Sulphide mineral deposits that have been exploited commercially range in size up to twenty million tons. The most common minerals are pyrite and marcasite, with smaller amounts of chalcopyrite and sphalerite. The richest deposits contained up to 4.5 per cent copper (Bear, 1963; Geological Survey Department of Cyprus, 1982).

Gossans are the weathered tops of zones originally rich in sulphides. They are marked in the field by bright red and yellow deposits of limonite (Bear, 1963). In this study, the term gossan refers to zones of intense hydrothermal alteration which represent the former pathways of ascending hydrothermal fluids. At depth, the fluid pathways consist of sulphide-rich, highly hydrothermally altered zones and are light grey to creamy white in colour. Gossans are more numerous and widespread than ore deposits. In some cases they are demonstrably related to ore deposits. In other instances they may be the roots of ore deposits subsequently removed by erosion.

Other deposits of hydrothermal origin which are prominent in the Troodos are umbers and ochres. These are sedimentary deposits and have been exploited

commercially for pigments. Umbers are rich in manganese and iron oxides from vents which precipitated locally from the water column and often settled in depressions on the sea floor. They are characteristically dark brown to yellow in colour. Ochres are typically yellow in colour due to their iron oxide content. They occur as sediments overlying sulphide ore deposits and are interpreted to be due to submarine weathering of the ore (Constantinou, 1980)

The sulphide deposits in the Troodos, and similar examples in Oman (Haymon et al., 1984; Haymon et al., 1989), are analogues of deep sea hydrothermal vent deposits. As noted above in this regard, strong similarities exist between Troodos and oceanic type crust. Circulating fluids formed the Troodos deposits (Bear, 1963) and had, in some cases, a salinity very close to that of sea water (Spooner and Bray, 1977). Since the discovery of active vents on the sea floor, a comparison of the texture and mineralogy of East Pacific Rise and Troodos deposits shows strong similarities (Oudin et al., 1981). Indeed, fragments of vent chimneys have been found in Troodos deposits (Oudin and Constantinou, 1984).

Summary

The effect of hydrothermal circulation in the Troodos ophiolite and the oceanic crust is similar on both local and regional scales. Locally, Cyprus massive sulphide deposits have structures and minerals very similar to vent deposits.

Regionally, both the Troodos and the oceanic crust have a strongly magnetic layer at the top of layer 2. The magnetization in rocks directly below this layer in the Troodos has been decreased by hydrothermal alteration. There is some evidence that this may be the case in the oceanic crust as well.

This study will use aeromagnetic data and computer modelling to investigate the magnetic structure of the stratigraphically higher extrusive part of the Troodos ophiolite. Detailed geological data from smaller sections of the ophiolite will be combined with the magnetic results to estimate hydrothermal alteration patterns.

An analysis of the distribution of ore bodies and mineralization will determine if a regular spacing exists for these discrete, extreme manifestations of hydrothermal circulation. A comparison between the aeromagnetic data and the mineralization locations will seek relationships between the two. The findings of these studies will be extended to the oceanic crust to predict patterns that might be observed there.

Chapter 2

Aeromagnetic Data

Data Specifications

The data for this analysis were taken from an aeromagnetic survey conducted for the United Nations in the mid 1960's (Hunting Geology and Geophysics Ltd., 1969). All specifications for the data are taken from this report. The survey covers the northern and western flanks of the Troodos ophiolite (figure 2.1). Its purpose was to aid in the development of the local mineral industry. All commercial sulphide mineral deposits occur in the Extrusives. The survey straddles these units, extends into the Sediments to the north and east and into the Sheeted Dikes to the south and west.

The survey was conducted from 28 October to 11 November 1965 by the Hunting Geology and Geophysics Company of the U.K. Two aircraft were used to measure magnetics and electromagnetics. Magnetic measurements were made using a single axis fluxgate sensor mounted in the aircraft tail stinger. The sensor was maintained parallel to the earth's field by two secondary fluxgate sensors and a gimbal mechanism. The measured total field was recorded in gammas (or nanotesla (nT)) on a chart recorder. The aircraft flew at a nominal height of four hundred feet (122 metres) and an average speed of 120 to 130 knots. Lines were nominally one quarter mile (400 metre) apart and oriented north north east. A series of air photos recorded the aircraft position at regular intervals. Elevations

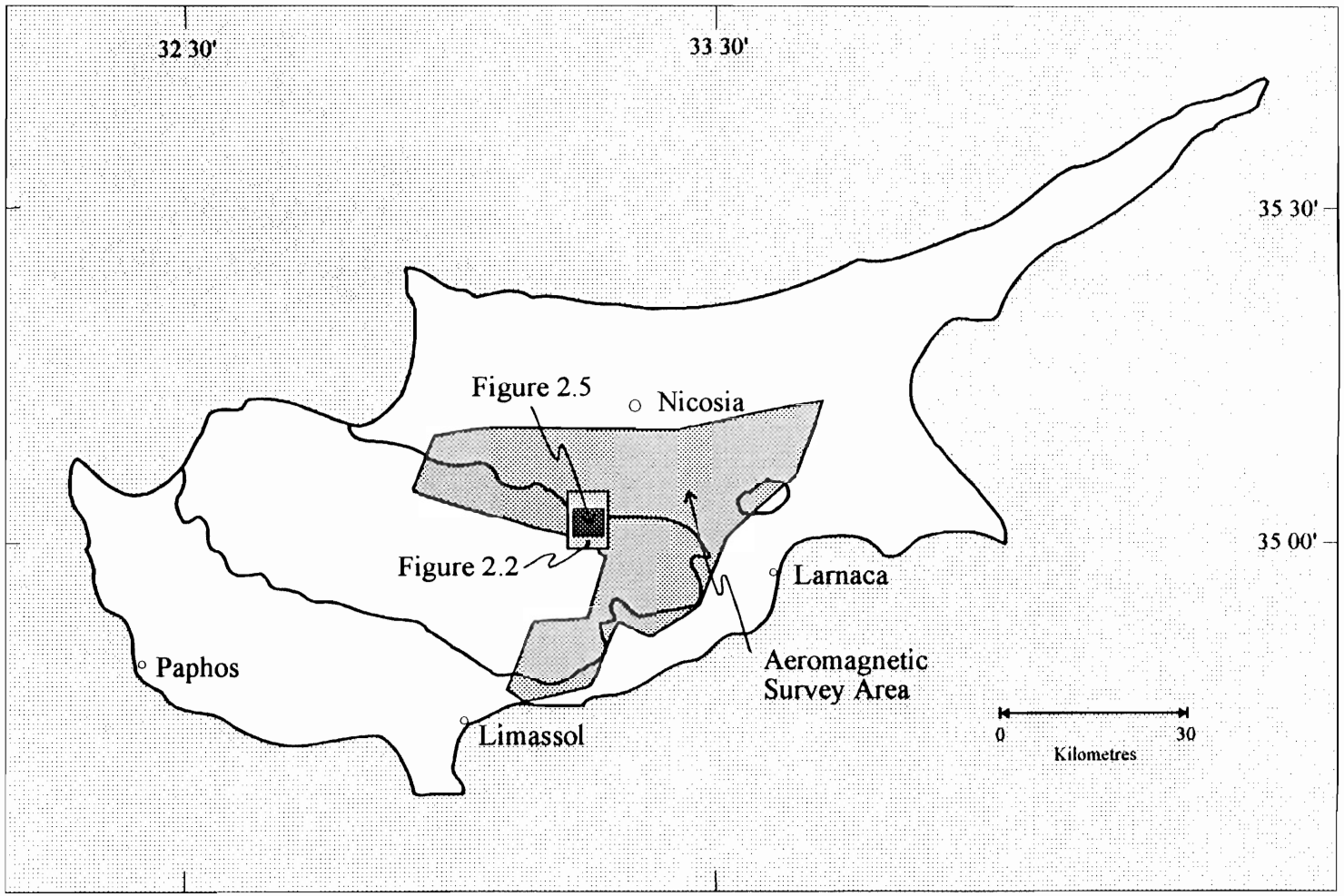

Figure 2.1. Location map showing the location of the aeromagnetic survey (modified from Hunting Geology and Geophysics, 1969). The locations of the areas shown in figures 2.2 and 2.5 are also indicated.

were measured continuously with a radio altimeter and were recorded on a chart recorder.

The data were originally plotted and contoured on 1:31680 work sheets derived from the topographic maps of the area. These used a local grid, the Cassini projection and the Clark 1866 spheroid. This system is one of the simpler methods of map depiction and was used by the British Ordnance Survey during the 19th and early 20th century. Minimal distortions appear in both area and distance when limited areas such as Cyprus are mapped. At some later time the results were apparently re-scaled to 1:50000, but this was not described in the report. A small section of one of the published 1:50000 maps is shown in figure 2.2.

The average level of the data in the aeromagnetic survey is not known to be related to any other survey or system and thus has no meaning outside this survey. Values in the original data are all positive and range from approximately 2000 to 9100 nT.

Data Quality

Data quality in the original survey may be best discussed in terms of the accuracy of the magnetic measurements and accuracy of the plotting of locations.

The survey was flown by a fixed wing aircraft in the "drape flying" mode, where the plane attempts to follows the contours of the ground at a fixed

Figure 2.2. Example section the published aeromagnetic map (after Hunting Geology and Geophysics Ltd., 1969). The scale is 1:50,000 and north is up.

elevation clearance. Obviously, errors in maintaining this elevation will have a corresponding effect on the results. Unfortunately, the detailed radio altimeter measurements are not included in the report and therefore could not be considered quantitatively.

The shape of magnetic anomalies is determined by three factors: variations in the geology and mineralogy in the area, the presence of magnetized topography, and the method of measurement (ie. drape or level flying). The latter two factors are not of geological interest and must be removed or allowed for in the interpretation.

In this case, drape flying imposes its own pattern of anomalies on aeromagnetic data (Grauch and Campbell, 1984). Even with perfect elevation control, the changing geometry creates anomalies as the aircraft approaches, climbs, descends and departs hills. The effect of topography, drape flying and possible variations in flight clearance elevation will be considered in detail later in this chapter.

Position errors have also been considered in some detail. Errors of up to one kilometre are apparent in comparing the physical features plotted on these aeromagnetic maps with the most recent 1:50000 Universal Transverse Mercator (UTM) sheets (Fairey Surveys Ltd., 1973a, b, c and d). The aeromagnetic maps are plotted using the Cassini projection and Clark 1866 spheroid. The UTM maps use the UTM projection and the International spheroid. Changes in the projection and spheroid have been eliminated as the source of error.

The physical features plotted on the aeromagnetic maps match exactly with those on a series of 1:50000 UTM maps published in the 1940's (Army Map Service, 1942a and b). Thus, errors must be due to inaccuracies in the compilation of these earlier maps. These errors were corrected in the more recent UTM sheets of the 1973 series.

Digitizing

The survey was originally part of a larger survey of groundwater and mineral resources in the area conducted jointly by the Government of Cyprus and the United Nations Special Fund (United Nations Development Project, 1970). The geophysical report and the larger survey report both contain interpretations and recommendations about the geology, structure, mineralization and geophysics of the area.

Although copies of some of the original worksheets were available, they were not reliably legible. Therefore all data were taken from the 1:50000 aeromagnetic maps which accompany the report. Locations were digitized along flight lines at every point where the flight line crossed a magnetic contour line. Magnetic values were entered by hand at the time the points were digitized.

For each digitizing session, a grid of known latitude and longitude points was also digitized. From these, conversion factors were calculated to convert digitizer coordinates to latitudes and longitudes. The numerous digitizer sessions

were combined to give a single map which was then converted to UTM coordinates.

For smaller areas where there was an obvious location error, the data from the aeromagnetic maps were shifted to match recognizable physical features with their locations from the 1973 UTM maps. Larger areas were corrected in a similar manner using average offsets of latitude/longitude points.

The data were interpolated onto an orthogonal grid to facilitate further processing. The chosen grid was 750 by 576 units in size with a one hundred metre spacing unit and was approximately centred on the spatial extent of the data. The spacing was chosen empirically to represent the data without creating artifacts while also keeping the computer file size manageably small. The dimensions were chosen to be compatible with a fast Fourier transform algorithm used in later processing.

Several interpolating algorithms were tried and the minimum curvature spline method was used for the final grid. While there is no mathematical relationship between the minimum curvature algorithm and the magnetic field, they are similar in smoothness and in having continuous second derivatives (Smith and Wessel, 1990, Briggs, 1974). The interpolation is performed by minimizing the sum of the second horizontal derivatives of the magnetic data (Watson, 1992, Webring, 1991). The gridded aeromagnetic data is shown in figure 2.3. The average level in this figure has no independent meaning and does not compare to other surveys or figures. The scale was chosen to have the same range as later

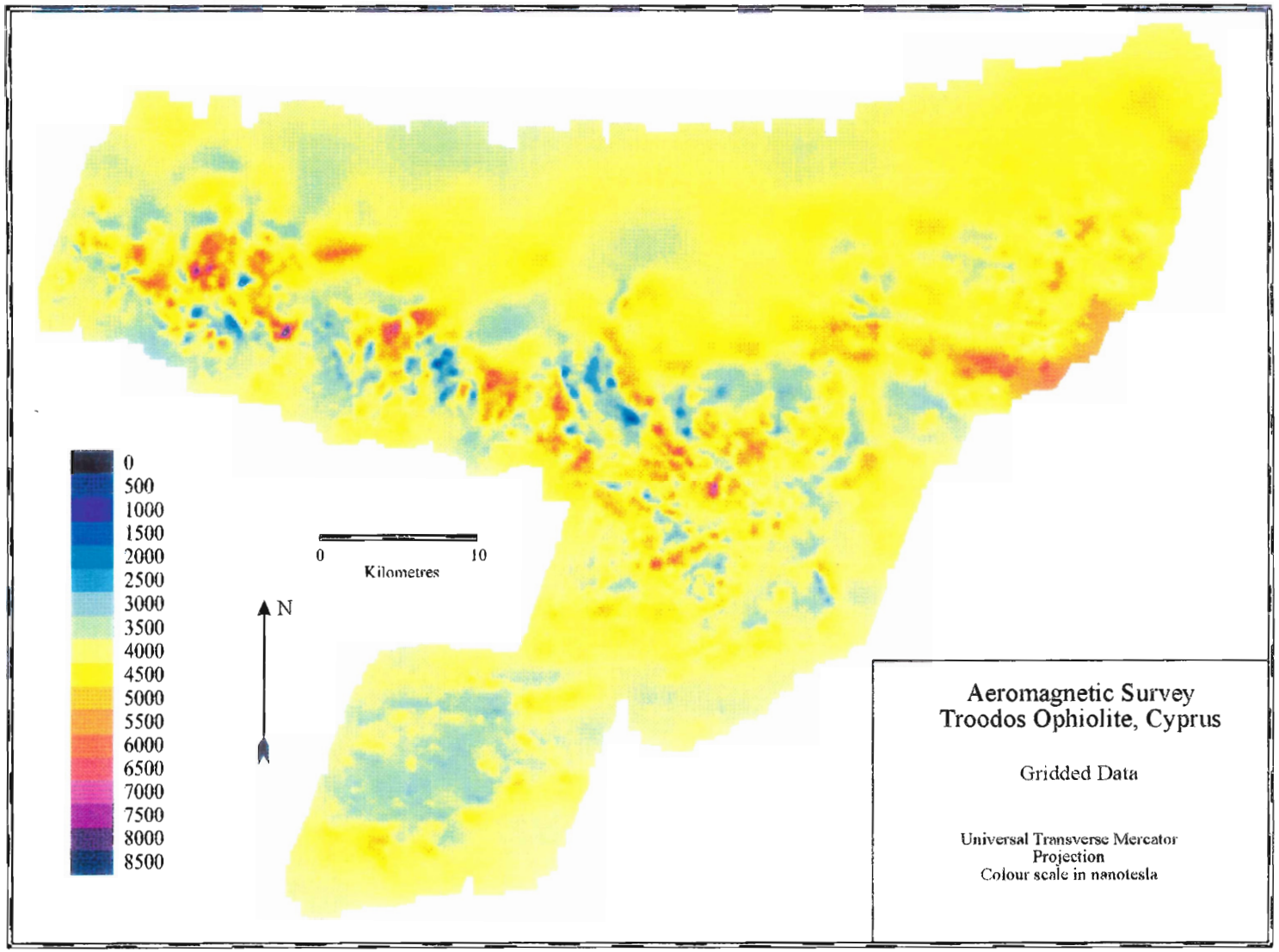

Figure 2.3 Gridded aeromagnetic survey of part of the Troodos ophiolite, Cyprus. The location is shown in figure 2.1.

figures.

Reduction to the Pole

Magnetic anomalies, in contrast to gravity anomalies, are usually asymmetric and offset from their source due to the generally substantial inclination from the vertical of the magnetic field. To simplify the interpretation of the data, they can be transformed to a situation where the magnetic vector is vertical, as it is at the magnetic poles. This process is called reduction to the pole (RTP).

The magnetic field can be defined by the fundamental relationship:

$$T = \frac{\partial V}{\partial \Gamma} \qquad (2.1)$$

where T is the magnetic field anomaly

V is the magnetic potential

Γ is the direction of the earth's field

The magnetic potential can be expanded (Baranov, 1957):

$$V = \frac{\partial U}{\partial s} \qquad (2.2)$$

where U is the gravimetric equivalent or "reduced to the pole" potential and s is the magnetization. Thus

$$T = \frac{\partial^2 U}{\partial s \, \partial \Gamma} \qquad (2.3)$$

The inverse of equation 3 can be used to determine the RTP potential from the observed anomaly. The RTP field can then be calculated by differentiating the potential. These equations can been solved analytically and numerically given suitable approximations (Baranov, 1957, Baranov and Naudy, 1964). The process is awkward with real data and can be inaccurate at low magnetic latitudes. In addition, these methods are awkward when specifying a direction of rock magnetization different from that of the earth's field.

The reduction to the pole method is more easily applied by converting data to the frequency domain using a Fourier transform. The equation for this operation is

$$F(u,v) = \int_{-\infty}^{\infty}\int_{-\infty}^{\infty} f(x,y)\, e^{i(ux+vy)}dxdy \qquad (2.4)$$

and the inverse

$$f(x,y) = \frac{1}{4\pi^2}\int_{-\infty}^{\infty}\int_{-\infty}^{\infty} F(u,v)\, e^{-i(ux+vy)}dudv \qquad (2.5)$$

where f(x,y) is a function defined in two dimensions, usually east (x) and north (y) and F(u,v) is the same function expressed in the (u,v) wavenumber domain.

These may be applied to regularly sampled data using the discrete Fourier transform

$$F(u,v) \equiv \sum_{y=0}^{N-1} \sum_{x=0}^{M-1} e^{2\pi iyv/N} e^{2\pi ixu/M} f(x,y) \qquad (2.6)$$

and the inverse

$$f(x,y) \equiv \frac{1}{NM} \sum_{y=0}^{N-1} \sum_{x=0}^{M-1} e^{-2\pi iyv/N} e^{-2\pi ixu/M} F(u,v) \qquad (2.7)$$

where N and M are the dimensions of the data set.

Once the measured magnetic field has been transformed to the frequency domain, it may be reduced to the pole by a simple geometric factor (Cordell et al., 1992; Arkani-Hamed, 1988, based on a derivation in Bhattacharyya, 1965)

$$F\{T_p\} = F\{T\} K^2 / (\mathbf{B}\cdot\mathbf{G})(\mathbf{M}\cdot\mathbf{G}) \qquad (2.8)$$

where **B** and **M** are the unit vectors along the earth's field and the direction of magnetization respectively,

G is a vector (iu,iv,K),

$K = (u^2+v^2)^{1/2}$, and

u and v are the wavenumbers in the east (x) and north (y) directions.

The geometric factor may be rewritten as (Verhoef, 1986)

$$K^2/(\mathbf{B}\cdot\mathbf{G})(\mathbf{M}\cdot\mathbf{G}) = 1/[(\sin(I_p)+i\cos(I_p)\sin(\theta+D_p))(\sin(I_r)+i\cos(I_r)\sin(\theta+D_r))] \quad (2.9)$$

where I_p and I_r are the inclinations of the earth's field and remanence, respectively,

D_p and D_r are the declinations of the earth's field and remanence, respectively, and

θ = arctan (v/u)

These formulae assume that the direction of both the earth's field and remanence remain constant over the area.

The actual process for reducing to the pole involves padding the data set with zeros and tapering, then converting to the frequency domain using a fast Fourier transform. The data is then multiplied by the geometric factor and transformed back to the spatial domain. The method is readily performed by a computer on a gridded data set and suffers no inaccuracy at low magnetic latitudes.

Figure 2.4 shows the reduced to the pole data. A declination of 2.4 degrees and an inclination of 50.6 degrees was assumed for the earth's field based on values for the International Geomagnetic Reference Field (Cordell et al., 1992). The remanent magnetization was assigned a declination of 280 degrees and an inclination of 40 degrees based approximately on average values for the ophiolite (Clube et al., 1985).

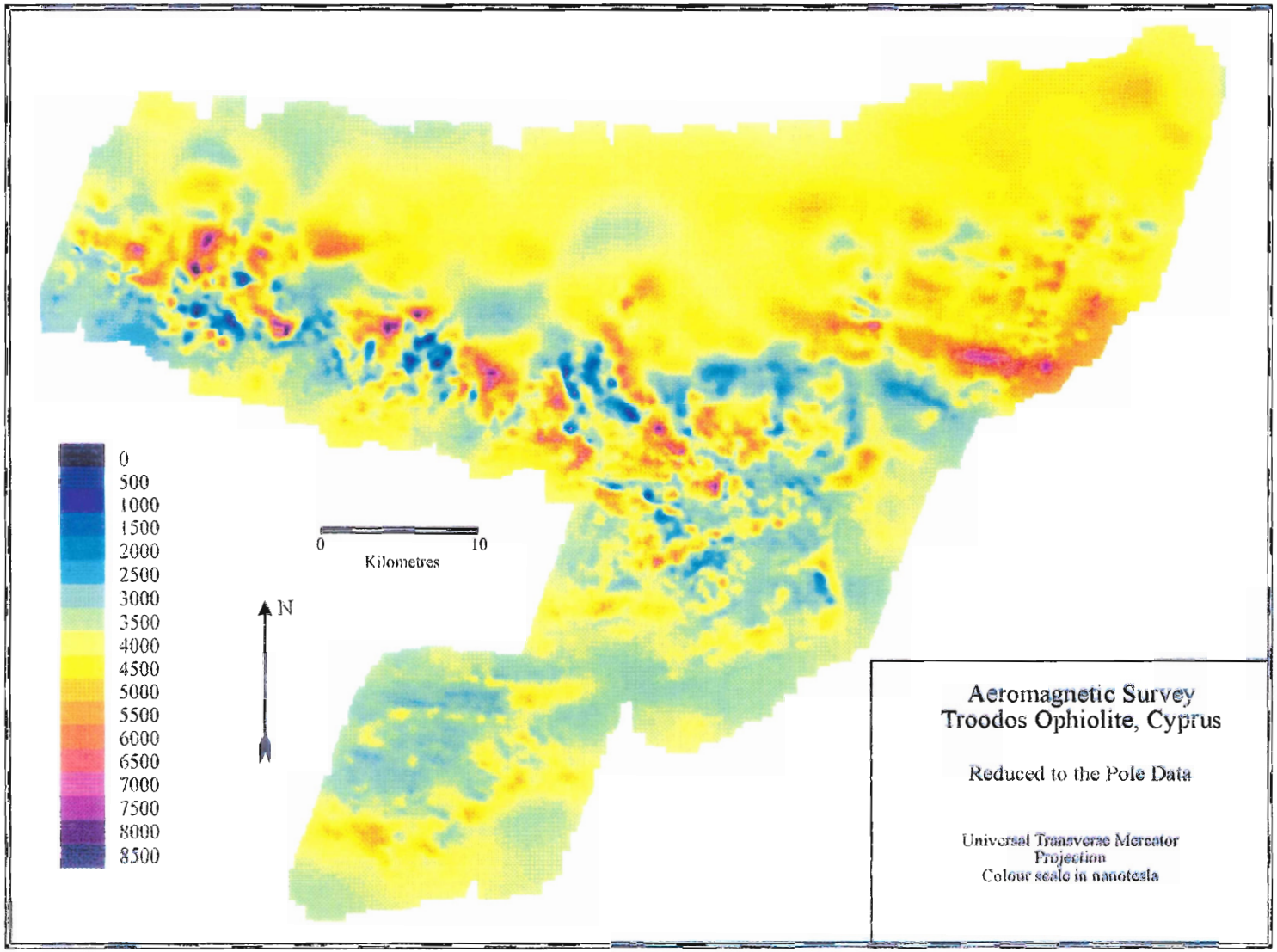

Figure 2.4 Reduced to the pole aeromagnetic survey of part of the Troodos ophiolite, Cyprus. The location is shown in figure 2.1.

The distribution of anomalies on the scale of the whole survey is only slightly changed by the RTP operation. The location of magnetic peaks and troughs are shifted slightly to the north. The shapes of the anomalies changes slightly but the RTP anomalies can be clearly related to the original aeromagnetic anomalies. Note that the scales in figures 2.3 and 2.4 are the same but they do not have the same average level.

The Effect of Topography on the Aeromagnetic Data

As noted previously, the original aeromagnetic survey was flown in the draped mode, in which a fixed wing aircraft attempts to maintain a constant clearance above the surface of the ground while collecting the data. Inevitable variations in this elevation will be reflected in the data. The problems that must be addressed are twofold: how large are the errors caused by variations in elevation, and what is the effect of drape flying on the data?

Errors in the data due to elevation inaccuracies

This problem may be considered in two parts: how large were the errors in flight elevation and how large are the magnetic anomalies caused by these errors? Part of this discussion will include consideration of the relative sizes of true anomalies as opposed to elevation-induced errors. What maximum size of elevation-induced error is significant? What effect does a typical elevation-

induced error have on the data?

Anomalies in the aeromagnetic survey range up to 7000 nanotesla (nT) in amplitude from a peak value to an adjoining trough. Typical major anomalies are from one to six kilometres long.

In order to look at details of individual anomalies, a smaller area was selected for detailed study. The area is approximately fifty square kilometres in area, centred on the village of Kambia (figure 2.1). This area was chosen because of the availability of detailed geological data which will be described and used later in the study. The aeromagnetic anomalies are shown in figure 2.5.

In the Kambia detailed study area an aeromagnetic low separates two highs. The highs are three and six kilometres long from north to south with maximum values of 5700 and 5750 nT. The low is approximately five kilometres in north-south extent and reaches a low of 2600 nT. The range of values in this limited area is approximately 3000 nT.

Thus, arbitrarily, errors of one thousand nT or more will cause major distortions in the data. Errors of one hundred to one thousand nT will affect the details of the survey but not the major patterns of the anomalies. Errors of less than one hundred nT will be insignificant.

Elevation was measured during the initial survey with a radio altimeter. The elevations were recorded on a chart recorder and were eventually compiled into a map. Unfortunately, this map is not included in the published report. The report does however, include one example of an elevation profile (figure 2.6). A

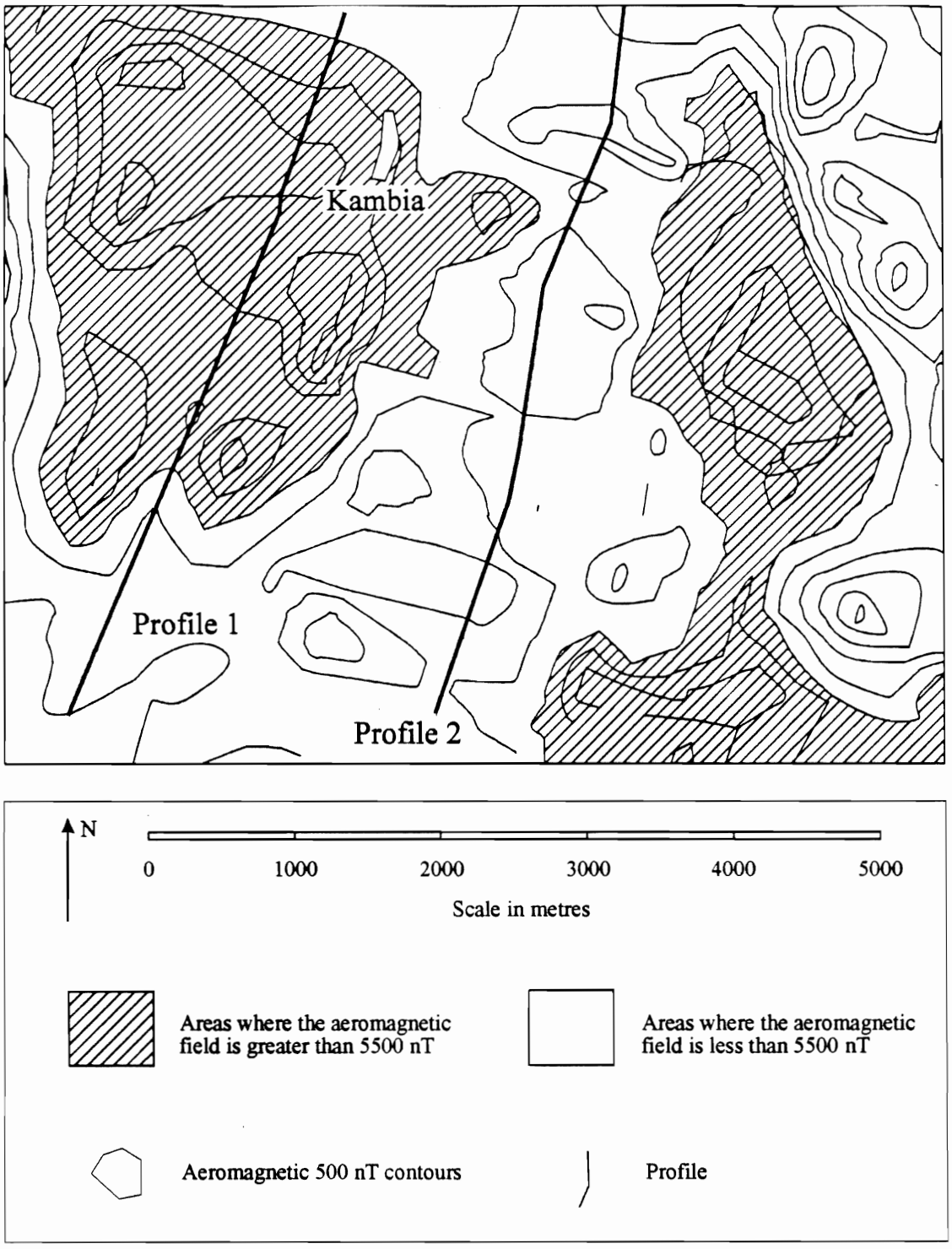

Figure 2.5. The Kambia profile area with locations of profiles and rough aeromagnetic contours. The location is shown in figure 2.1.

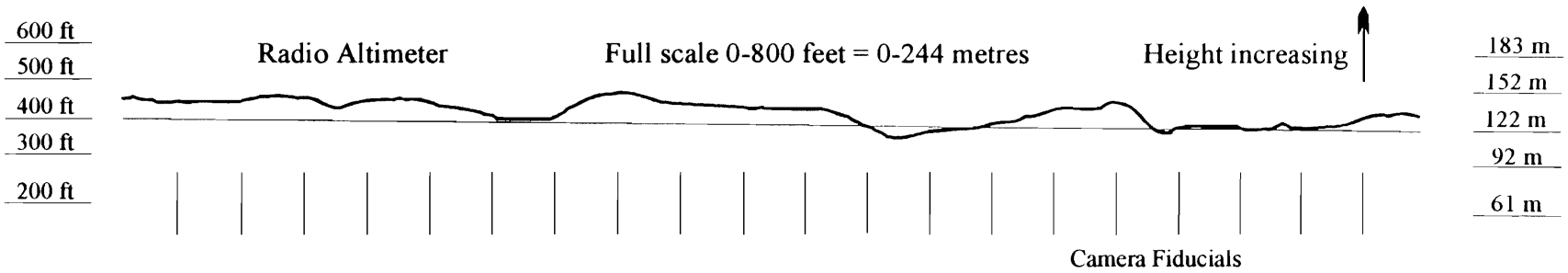

Figure 2.6. The example flight elevation profile. Redrawn from Hunting Geology and Geophysics, 1969.

table is also included listing the elevation of measurements at the peaks of larger electromagnetic anomalies and the direction (ie north or south) that each flight line was flown. In the absence of detailed information, the elevation variation can only be estimated from a likely flight profile. The effect of the variation in elevation on the magnetic field can be inferred by comparison of the aeromagnetic anomalies and the topography.

Figure 2.6, the example elevation profile, shows that the elevation varies from the nominal four hundred feet (122 metres) by up to approximately sixty feet (eighteen metres). Most of the error in this profile is in the sense of increasing elevation. It is not known if this is typical. With the low flight elevation and sometimes rough topography, the pilot probably flew high for safety. On the other hand, a list of elevations at larger electromagnetic anomalies averages less than the nominal four hundred feet (340 +/- 55 feet, 104 +/- 17 metres) with a minimum of 180 feet (55 metres) and a maximum of 520 feet (159 metres).

With this rather approximate estimate of the range of variation of elevations, calculation can give an estimate of the range in resultant magnetic anomalies. We will consider three simplified situations where flight elevations above flat level ground are varied and the effect on magnetic anomalies examined.

Let us assume the magnetic source is a point pole. This situation cannot strictly occur in natural conditions, but is an acceptable approximation when half of the dipole is at sufficient depth that it does not contribute significantly to the anomaly. This would correspond geologically to a narrow cylindrical body of

considerable vertical extent from the surface downwards. If the body outcrops at the surface then the distance from the source monopole to the measurement is the flight elevation.

The magnetic anomaly amplitude will then vary in inverse proportion to the square of the elevation.

$$\text{ie. } M \propto 1/h^2 \qquad (2.10)$$

If 122 metres is taken as the nominal flight elevation, the magnitude of the anomaly will increase by approximately nineteen per cent if the elevation decreases to 112 metres. Should the elevation increase to 132 metres, the anomaly amplitude will decrease by approximately fifteen per cent.

As an opposite extreme we can consider the case where the earth is uniformly magnetized for a great distance in all directions. In this case there is no change in the source-measurement geometry for small changes in elevation and there is no change in magnitude of the magnetic field due to errors in elevation.

The actual situation in Cyprus would probably vary between these two extremes. For a more complete description of the effect of variations in measurement elevation, the situation can be examined in the wavenumber domain.

Figure 2.7 shows a series of plots of the change in anomaly magnitude as a function of wavelength for elevation differences of -20 to +20 metres. These

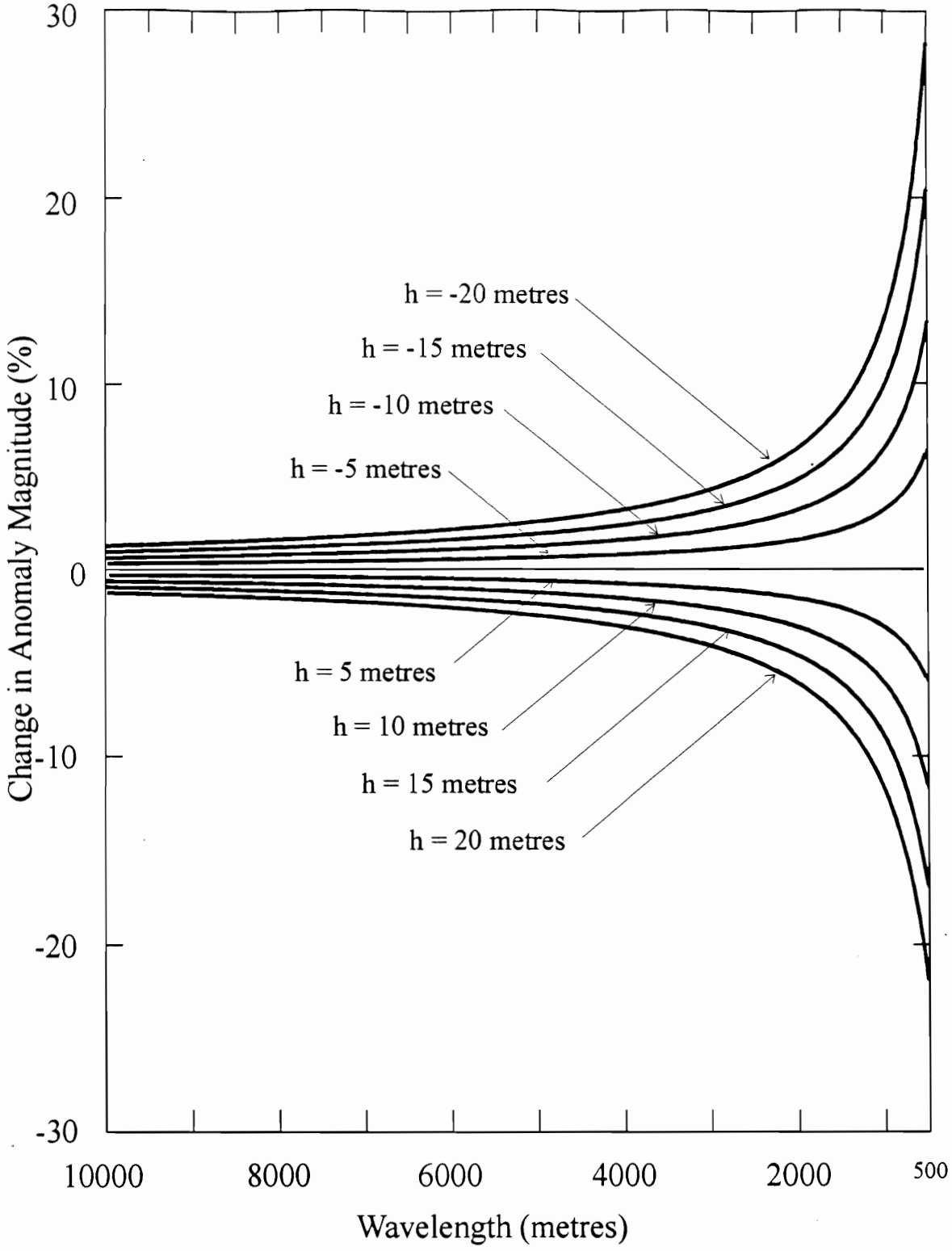

Figure 2.7. The variation in magnetic field strength with elevation in the wavenumber domain. Elevation changes (h) are positive with increasing altitude.

curves are plots of the upward continuation factor in the wave number domain (Caress and Parker, 1989)

$$f = e^{-kh} \qquad (2.11)$$

where $k = 2\pi/l$ is the wavenumber

h is the elevation change.

The nominal flight line spacing is four hundred metres which gives a minimum unbiased wavelength of approximately eight hundred metres. The longest wavelength shown on the plot is 10000 metres. At this and longer wavelengths, elevation differences have little effect on the anomaly magnitude.

From figure 2.7, elevation variations only affect the shortest wavelength anomalies, and only at significant elevation variations. Changes greater than 10 per cent only occur at elevation variations of greater than ten metres and then only for anomalies with wavelengths less than 1500 metres. At eight hundred metres wavelength, an increase in elevation of twenty metres will decrease the size of the anomaly by approximately 15 percent. A decrease in elevation of twenty metres will increase the anomaly by eighteen percent.

Modelling can be used to estimate the size and character of expected anomalies. In this case models will simulate cases where drape flown measurements are collected over a topographic step fifty metres high.

Figure 2.8 gives some indication of the anomalies which may be encountered in this situation. The model dimensions are as shown in the

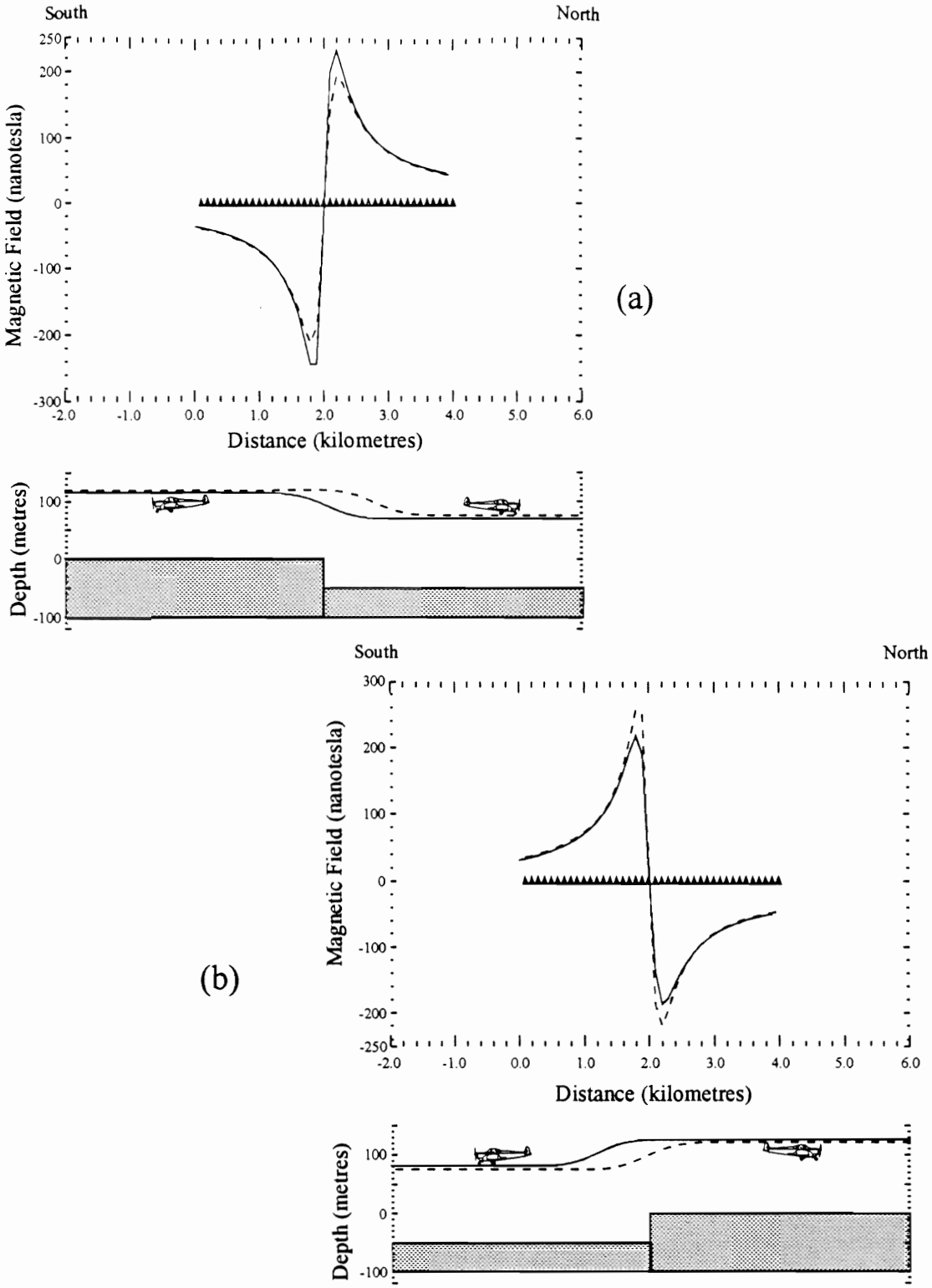

Figure 2.8. The calculated aeromagnetic field of a topographic step feature (a) increasing in elevation southward and (b) increasing in elevation northward. Model dimensions, flight profiles and flight directions are as shown in the bottom of each diagram. Magnetization is as for Cyprus and is described in the text.

diagram. The measurement altitude was a nominal 122 metres but the plane was assumed to not rise quickly enough when approaching a hill and to not drop quickly enough when leaving a hill. The assumed profiles are show at the top of the cross section part of the diagram. The dashed line is a profile from south to north; the solid line is the same profile from north to south. Magnetic intensities and directions were as for Cyprus.

Leaving a topographic step to the south, a negative anomaly is encountered followed by a positive. Approaching the same feature from the north, a small positive anomaly is followed by a steep negative at the boundary.

Of critical interest is the minimal difference between the north directed and south directed profiles over the same topographic step. The total magnitude of the anomaly due to the topographic feature is approximately five hundred nanotesla. The difference in anomaly magnitude due to the change in direction of the flight path is about one hundred nanotesla.

For a more empirical investigation of the effect of topography on this aeromagnetic data, two profiles across the Kambia area were examined. Profile one crosses the left aeromagnetic high and profile two the central magnetic low. The locations of the profiles are shown in figure 2.5.

Profiles one and two were constructed directly along flight lines where direct comparisons between the aeromagnetic data and topography were possible. The profiles were constructed by drawing a line between points taken from the intersection of the flight line and the aeromagnetic or topographic contours. The

difference in the level of the raw aeromagnetic data and the RTP aeromagnetic data is not real and they have been plotted separately for clarity. The estimated flight path is smoothed from the topographic profile. The aeromagnetic and topographic data, with flight directions, are shown in figures 2.9 and 2.10. As can be seen, a small topographic effect is present in the data. The aircraft must have been unable to follow small variations in elevation. Further, elevation accuracy was questionable as the plane approached, cleared and departed from large hills and valleys. Example locations are shown in shaded areas on the diagrams.

The topographic effect in the data is minor in amplitude compared to the amplitudes of the larger anomalies. Where such an effect appears to be clearly defined, it would seem to be a few hundred nanotesla in magnitude compared to the thousands of nanotesla of variation in the major anomalies of the dataset. Topographic effects are not seen in adjacent lines or away from the flight lines in the gridded dataset.

The effect of drape flying on the data

Drape flying is used to reduce the effect of the magnetized topography in a magnetic profile or a map and to allow more direct interpretation of variations in remanent magnetization or susceptibility. However, this approach can also impose its own systematic patterns in the data, as anomalies will occur due to the changing geometry of the earth and the flight path. Thus, drape flying does not produce the same results as constant elevation surveying over level ground

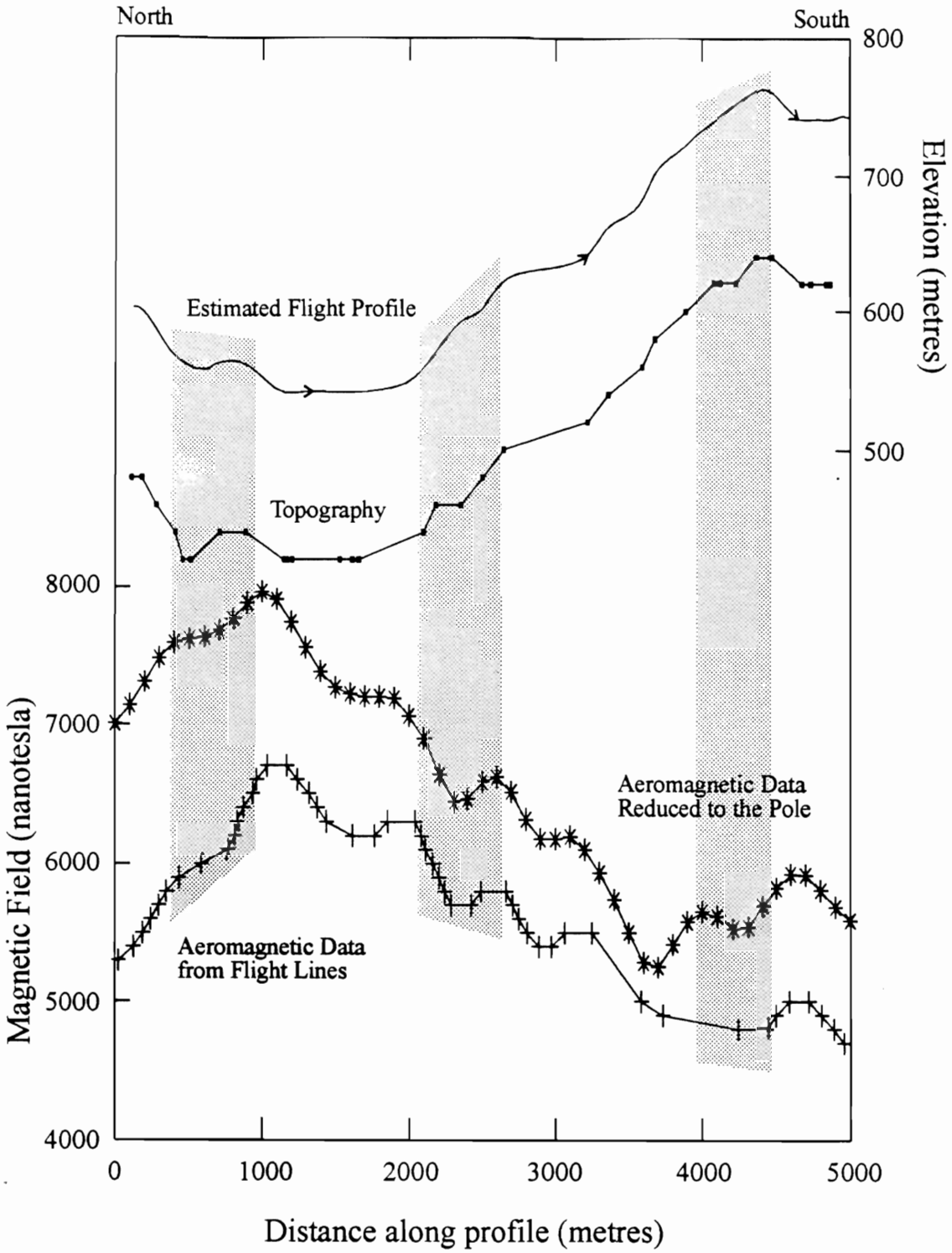

Figure 2.9. Example profile 1. Location is shown in figure 2.5.

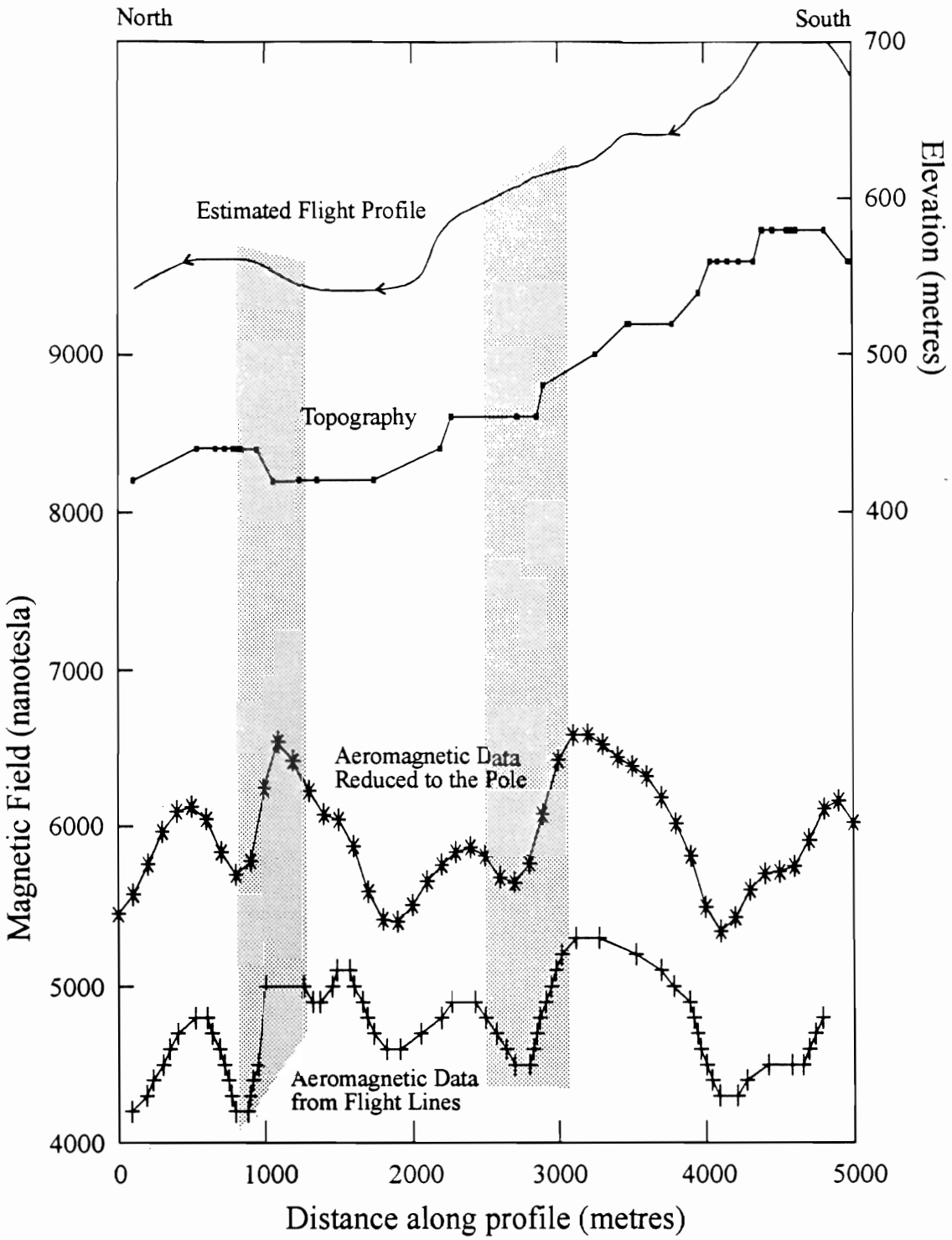

Figure 2.10. Example profile 2. Location is shown in figure 2.5.

(Grauch and Campbell, 1984)(figure 2.11). In this special case, drape flying over magnetized topography increases the amplitude of the anomaly when compared with level flight.

Level flown data can be converted to drape flown by computational methods but there is a danger in making the data more complicated and more difficult to interpret. In addition, when interpreting drape flown data some anomalies may result from or be exaggerated by the topography.

Summary

Topographic effects in the data have been investigated using theoretical calculations, models and profiles of observed magnetic and topographic data. The theoretical calculations suggest that the errors should be less than 20 per cent of the total anomaly and may be much less. The models and profiles indicate that the errors will be not more than a few hundred nanotesla (nT) in magnitude.

Thus, widespread minor topographic effects are likely in the data but will be small compared to the larger anomalies of the dataset. This will have an effect on the detail of the dataset. In addition, the detail may be affected by the drape flying method but, again, the expected effects are relatively minor when compared to the magnitudes of the major anomalies. The major effects of the topography can be compensated for by using forward modelling in the interpretation process.

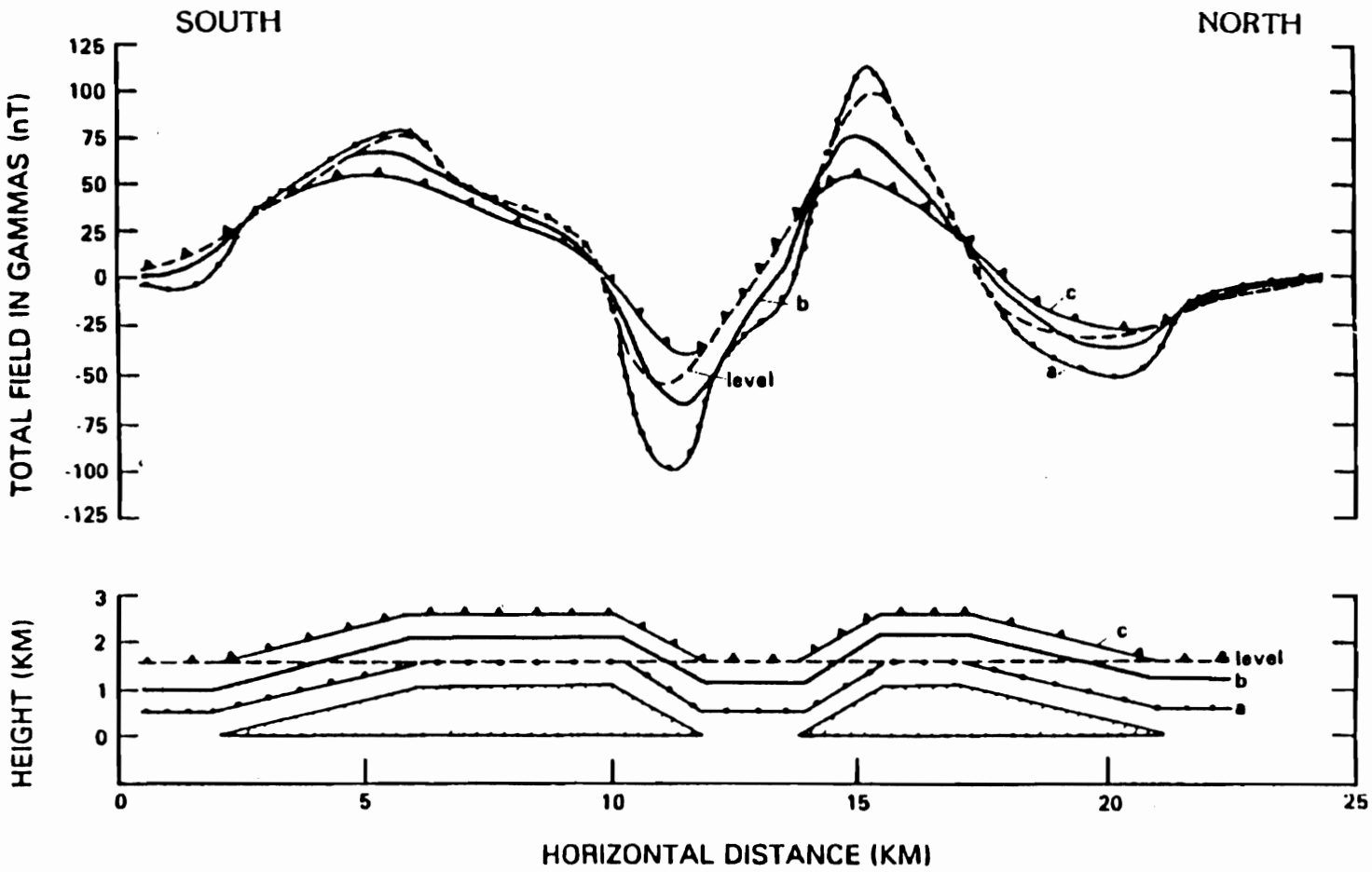

Figure 2.11. The calculated magnetic field of a model simulating magnetized mountainous terrain. The four profiles are level flight with an elevation of 1.5 km, (a) draped flight with a maximum height of 1.5 km, (b) draped flight with an average elevation of 1.5 km and (c) draped flight with a minimum elevation of 1.5 km. The model prisms are 1 km high and extend 10 km east-west. The magnetic field was 50,000 nT, the remanence was 0 and the susceptibility was 5x10-4 cgs units. From Grauch and Campbell, 1984.

Modelling

Having prepared the data, forward modelling was used to test possible configurations for the distribution of magnetization. While modelling cannot identify a unique configuration, it may be used to limit the possible configurations.

Magnetic models can be calculated in two dimensions (a profile across an infinitely long body), two and one half dimensions (a profile across a body with limited strike extent) or three dimensions. As variation along strike was significant and important, three dimensional models were used exclusively in this study. Two dimensional models could also have been used to quickly develop and refine more detailed models for limited areas along profiles. This was felt to be of less value due to the possible weakness in detail of the data discussed earlier.

In selecting the modelling program, the manner of specifying the input parameters was considered. In addition to being able to vary the distribution of magnetization for the model over the study area, it was also necessary to vary the elevation of the top surface to account for the relief. This is particularly important in areas where strongly magnetized material is found at the surface. The depths of the bases of the magnetic bodies also needed to vary over the study area. Since the survey was flown in draped mode the elevation at which the magnetic field was calculated was also required to vary over the area of the survey.

The magnetic anomaly, B, calculated at any point at a radial distance r

from a body of unspecified shape is given by (Sharma, 1986):

$$B = \frac{\mu_0}{4\pi} \text{grad}^2 \iiint_v J/r \, dv \qquad (2.11)$$

where J is the magnetization, r is the distance from the measurement point to the volume element dv and v is the volume of the body.

A number of tabular or prismatic bodies are often combined to create an approximation of a source volume of irregular shape (Talwani, 1965). This simplifies the evaluation of the integral, and allows an easy method of describing the bodies. The volume integral may also be converted to a surface integral using Green's theorem and the calculation then carried out over the surface of the body. In either case the integral may be calculated analytically, numerically, or by a combination of both. The analytic calculation removes the need for approximations inherent in the numeric calculation.

The calculations were performed using a slightly modified version of MAGPOLY developed at the USGS and made available as part of the PF version 2.11 software package (Cordell et al., 1992). This program uses the Talwani method and evaluates the integral exactly. The modifications increased the array size to allow for more measurement points and bodies.

The input to the program consisted of three files: a body description file, a data file and a measurement elevation file. The body description file contained parameters for the earth's magnetic field in the area and a description of

individual vertical prisms. The earth's field was assigned a declination of 2.4 degrees, an inclination of 50.6 degrees and a magnitude of 43,500 nT. These values were taken from the aeromagnetic survey memoir (Hunting Geology and Geophysics Ltd., 1969) and the International Geomagnetic Reference Field for 1965 (Cordell et al., 1992).

Each prism was described by the position of its four vertical edges and by the elevation of its upper and lower surfaces. In addition, each prism was assigned a value of magnetization, susceptibility, magnetic inclination and magnetic declination.

The body description file was created by a small utility program. The top elevation of the prism was determined from a gridded value of the topographic surface. These were interpolated from detailed contours digitized from 1:50000 topographic maps. The bottom surface of the prism was either set to a uniform distance from the top surface or to a constant value.

The magnetization of each prism, the topography, and variations in the top and bottom prism depths were determined and/or displayed using the IDRISI geographic information system. They were then stored as text files and were combined using the small utility program into the body description file.

The Kambia data file, containing a grid of aeromagnetic data, is a subset of the larger aeromagnetic survey described earlier. The gridded data, as opposed to the reduced-to-the-pole (RTP) data was used because the modelling program calculated anomaly values using the declination and inclination of the earth's and

remanent fields for the area. The measurement elevations were taken as being 122 metres above the topographic elevation.

The modelling program created three files. The first listed all of the input parameters and data which were checked to ensure that they were read correctly. The second contained a grid of calculated magnetic anomaly values for the model. The third contained a grid of the difference, or residuals, between the observed and calculated values.

The calculated and residual grids were imported into the IDRISI program to be displayed and printed. They were also compared to the original data and other information such as topography, dike percentage, contacts and faults. This and the RTP data were considered and the model was refined for a successive iteration. In this way, several series of models were constructed with different distributions of magnetization and different configurations of prisms.

Figure 2.12 shows the sequence of data processing from the collection of the data to the final diagram.

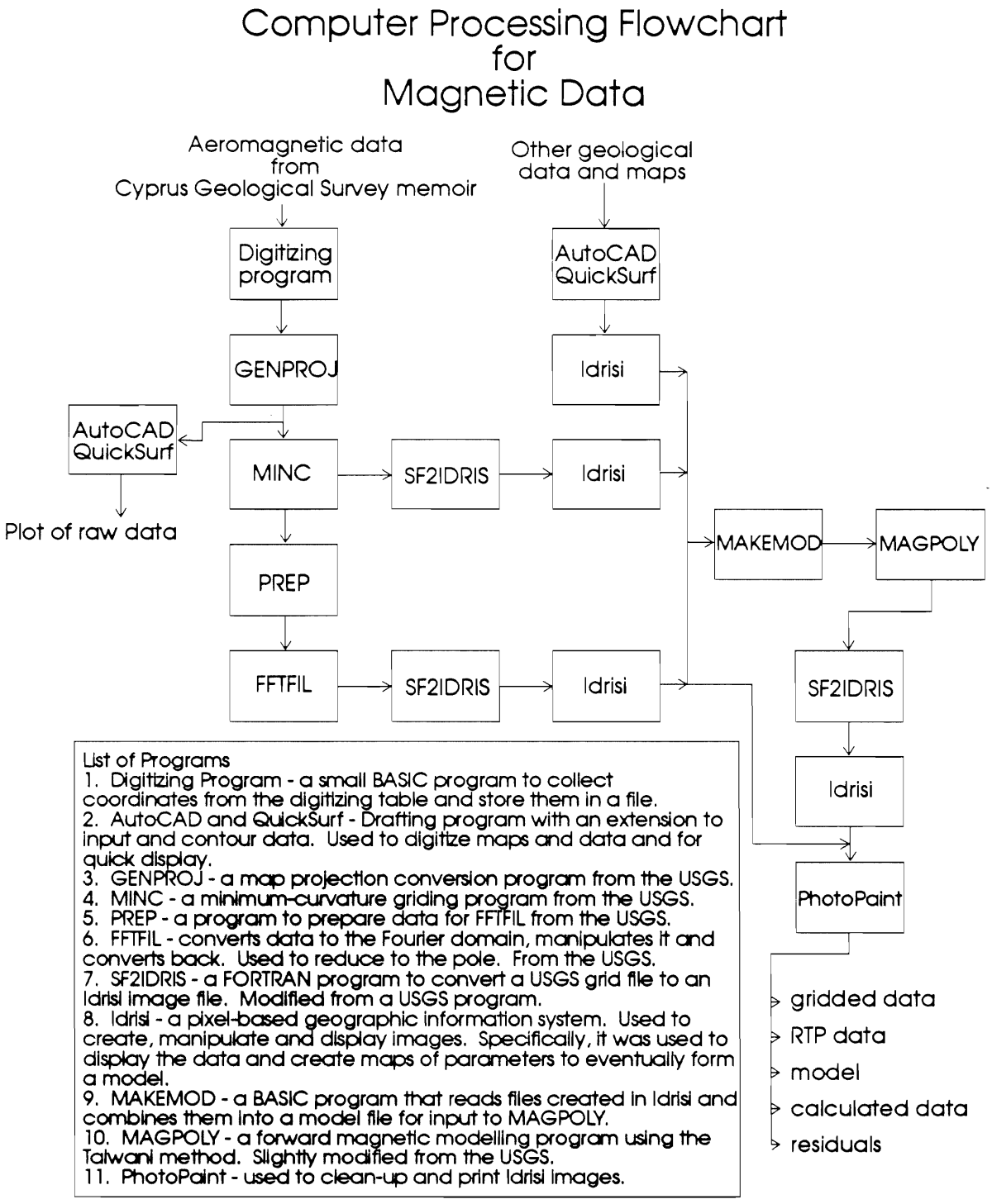

Figure 2.12. Flowchart showing the sequence of computer programs used to process the data.

Chapter 3

Relationships Between Magnetic Anomalies and Geological Features, and Magnetic Modelling

Results

The area chosen for detailed study and modelling is roughly centred on the village of Kambia on the northern flank of the ophiolite (figure 3.1). The area was selected because of the availability of detailed geological information as well as aeromagnetic coverage. The aeromagnetic data as shown in figure 3.2 is a subset of the original data discussed earlier. The grid spacing is one hundred metres by one hundred metres and the area is 8.2 kilometres in the east-west direction by 13.1 kilometres from north to south. The same data reduced to the pole is shown in figure 3.3. The RTP conversion used a magnetization direction of 300 degrees declination and 75 degrees inclination. The earth's field was as before. It may be located geographically using the roads and villages in overlay 1 which is located in the pocket in the back cover.

Aeromagnetic Data

The ophiolite in the northern part of the area lies beneath essentially non-magnetic sediment cover. This cover increases in thickness rather regularly towards the north away from the contact with the Extrusives shown in overlay 2.

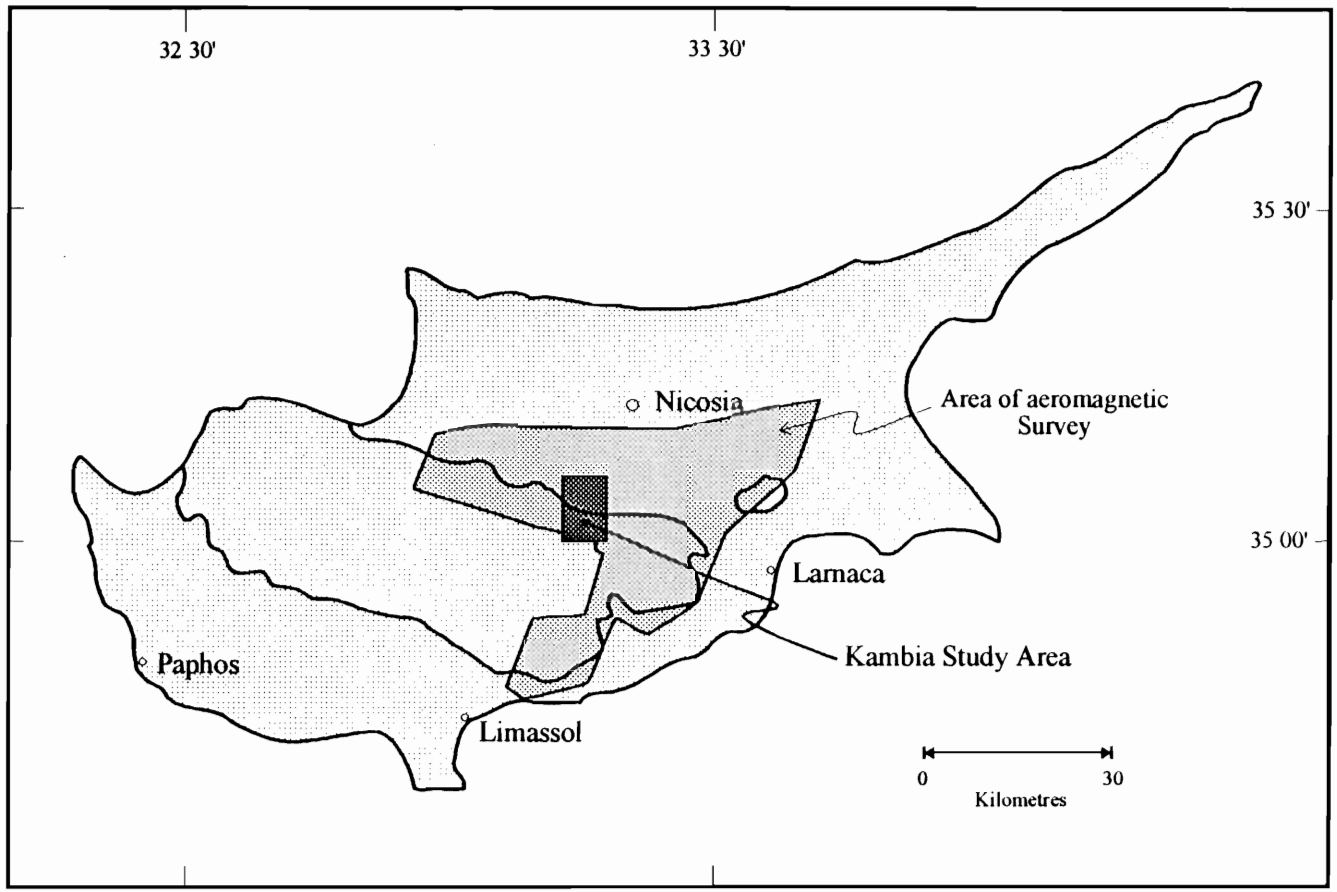

Figure 3.1 Map showing the location of the Kambia study area.

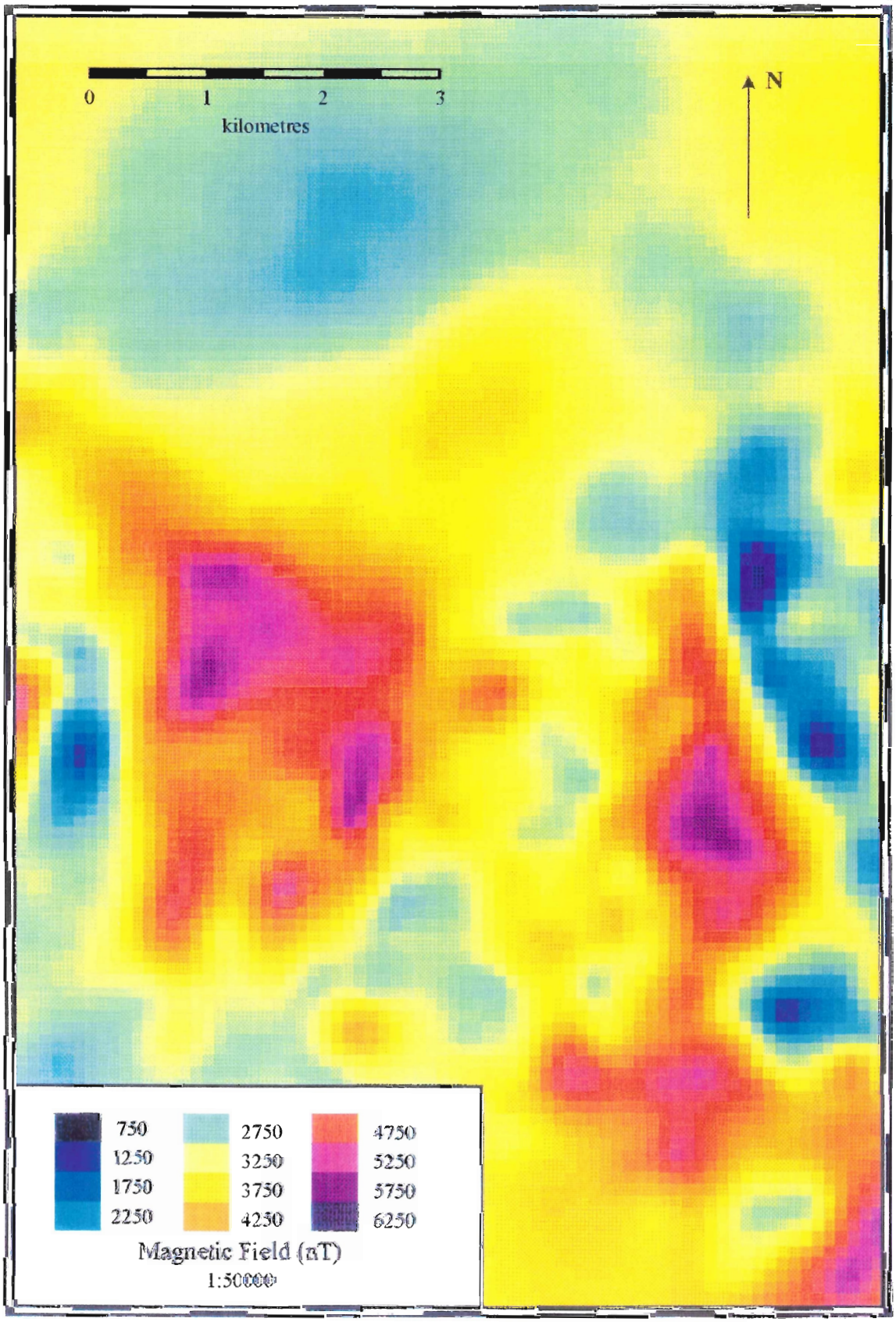

Figure 3.2. The gridded magnetic field of the Kambia study area.

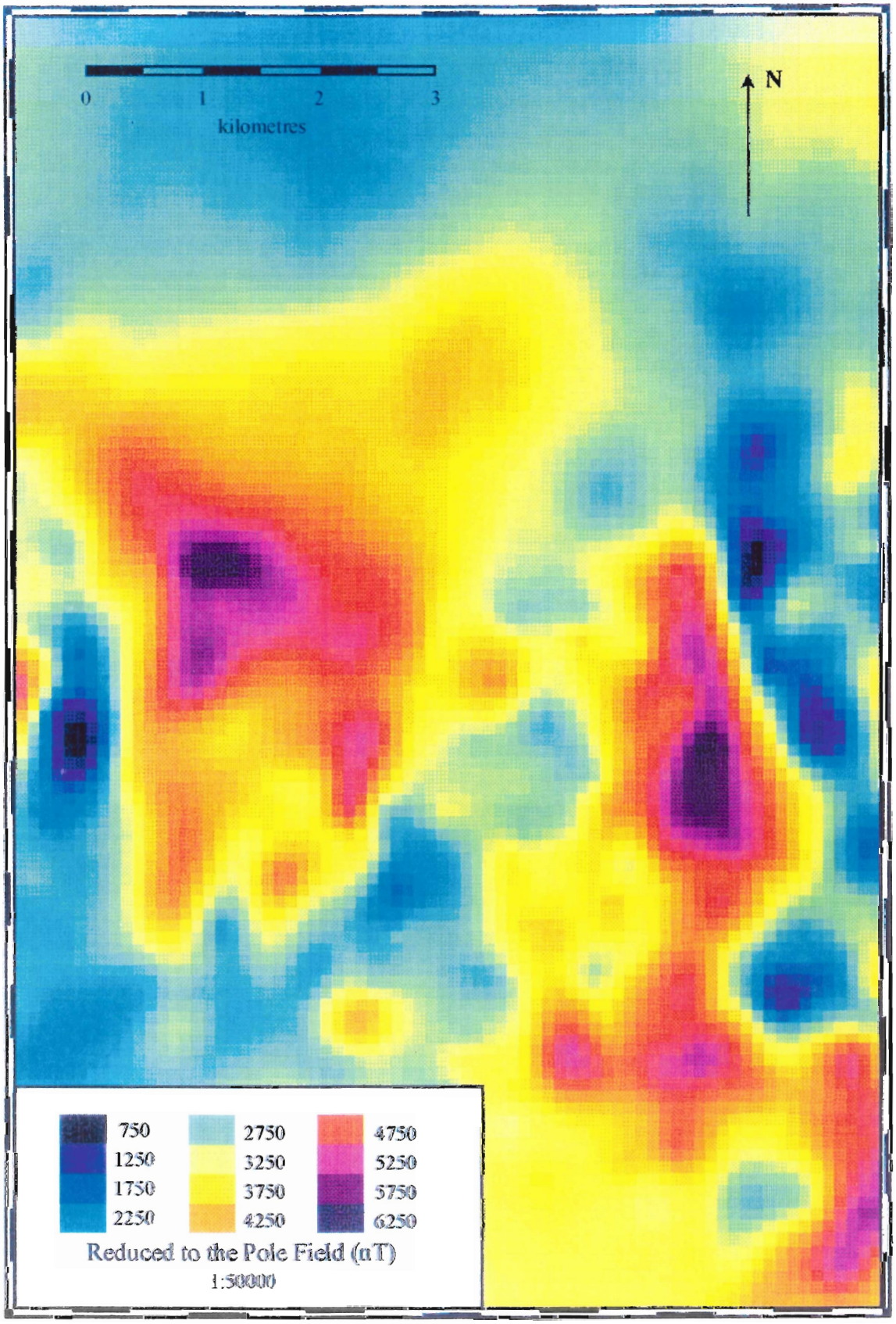

Figure 3.3. The reduced-to-the-pole field for the Kambia study area.

This area shows only the broad low amplitude anomalies expected of more deeply buried sources. The southwest corner of the area also shows relatively low magnetic relief. This is due to two causes. First, the extreme southwest corner is outside the area of the survey and has no data. Second, the remainder of the area corresponds to the outcrop of the Basal Group, which is known to be much less magnetic than the overlying Extrusives. This decrease in magnetization was introduced in chapter one with data from other studies covering different parts of the Troodos ophiolite (figures 1.8 and 1.9) and will be discussed more thoroughly later in reference to the Kambia area. The location of the approximate contact of the Basal Group with the Extrusives is also shown in overlay 2.

Between these two areas lies a band of high magnetic relief corresponding closely to the outcrop area of the Extrusives. This area is dominated by two large magnetic highs. Between them is a shallow, irregularly shaped trough oriented roughly north- south. Adjacent to the eastern edge of the survey area is a region of deeper magnetic lows which is not considered in this study.

Magnetic Samples

168 samples have been collected from the study area over the course of several field seasons and measured for their magnetic properties. Much of this has been published previously (Hall et al., 1991a). A number of new samples were collected recently to fill gaps in the earlier collections. These new samples also ensure that there are statistically significant numbers of samples from the

area of each of the two major highs and of the central low. The distribution of all samples and their natural remanent magnetism is shown in overlay 3. The magnetic properties are listed in appendices A and B and are summarized statistically in table 1 and figures 3.4 and 3.5.

Several points are obvious from overlay 3 and figure 3.4. Magnetization decreases a factor of four in going from the Extrusives to the Basal Group. The magnetization in the Extrusives, while variable, averages close to ten amperes/metre. No obvious geographical pattern of values occurs within the Extrusives. This is a significant result since a difference in values between the areas of magnetic highs and lows would suggest a simple explanation for the anomaly pattern.

The measured declinations and inclinations of the sample magnetization are remarkably consistent, with average values of 317 degrees and 67 degrees downward, respectively. This is roughly similar to the average values for the Troodos ophiolite of 274 degrees and 36 degrees (Clube et al., 1985) after correction is made for the uniform westward local tectonic dip of the Extrusive units in the study area. This averages 32 degrees in dip and 290 degrees in dip direction (Hall, in preparation).

The susceptibility generally increases with depth in the section (overlay 4) with values of 10 to 20 x 10^{-3} SI units in the Extrusives and values of 50 to 100 x 10^{-3} SI units in the Basal Group. Values for Q, the ratio of remanent to induced magnetization, are almost always greater than one, indicating the dominance of

Table 1

		n	minimum	maximum	average	std. dev.	median	skewness	kurtosis
Magnetization	Left High	15	1.22	18.30	7.27	4.49	6.63	0.77	0.49
	Right High	34	0.01	19.25	5.45	3.87	5.00	1.55	3.07
	Middle Low	52	0.90	77.50	12.82	14.26	8.85	3.06	10.42
	All Extrusives	131	0.01	77.50	8.55	10.24	5.90	4.16	22.86
	Basal Group	31	0.06	5.40	2.22	1.37	1.80	0.68	-0.33
	All Data	168	0.01	77.50	7.15	9.43	4.61	4.51	25.52
		n	minimum	maximum	average	std. dev.	median	skewness	kurtosis
Susceptibility	Left High	15	9.32	47.37	20.60	11.69	15.00	0.98	-0.15
	Right High	34	10.11	50.69	23.45	8.12	23.92	1.26	3.00
	Middle Low	52	8.53	47.37	20.25	10.31	20.05	0.95	0.25
	All Extrusives	131	1.58	88.42	25.70	16.39	22.42	1.65	2.78
	Basal Group	31	3.16	111.64	62.26	26.62	61.58	-0.14	-0.31
	All Data	168	1.58	111.63	32.92	23.32	24.40	1.30	1.10

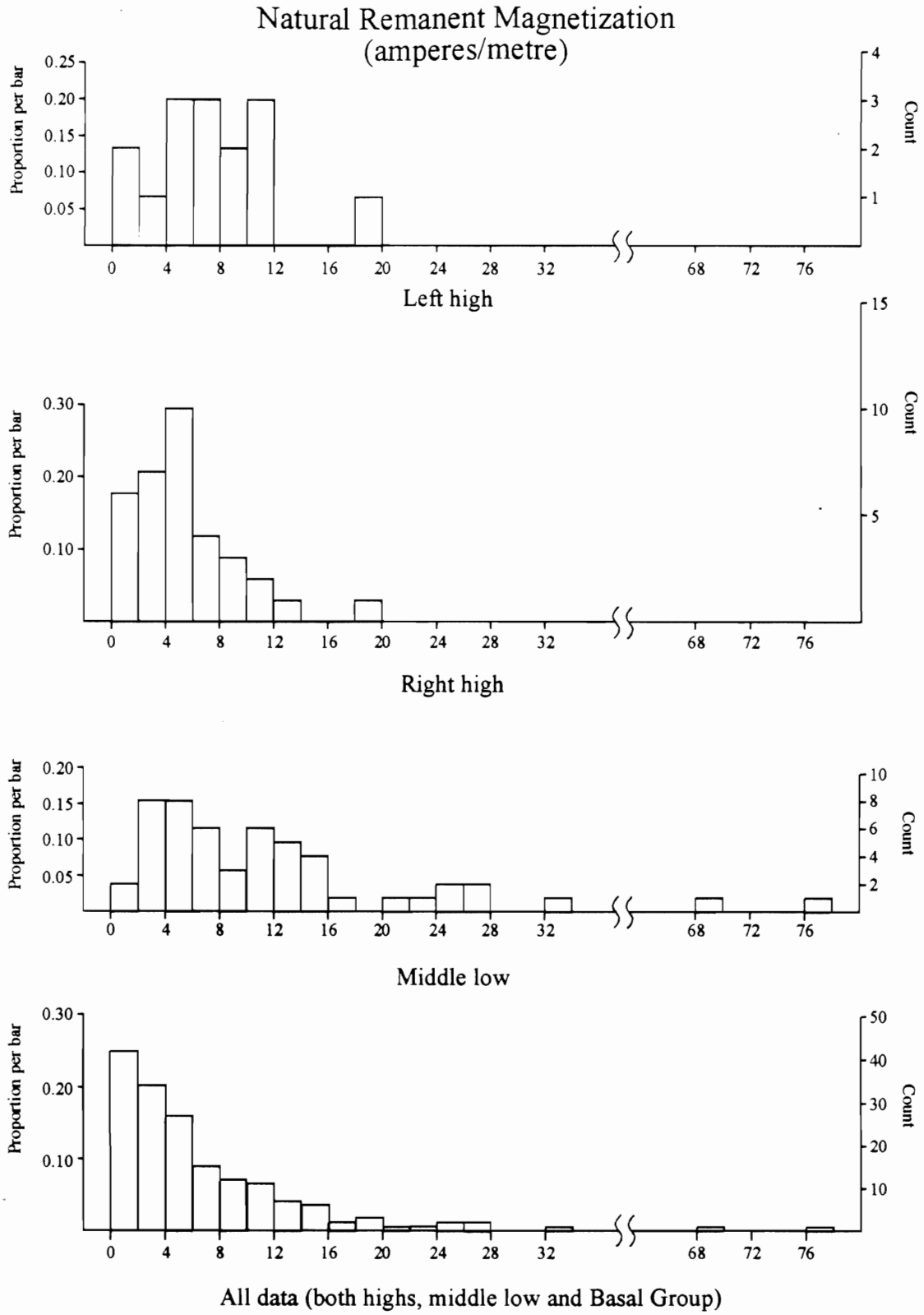

Figure 3.4 Histograms of natural remanent magnetization in samples from the Kambia study area.

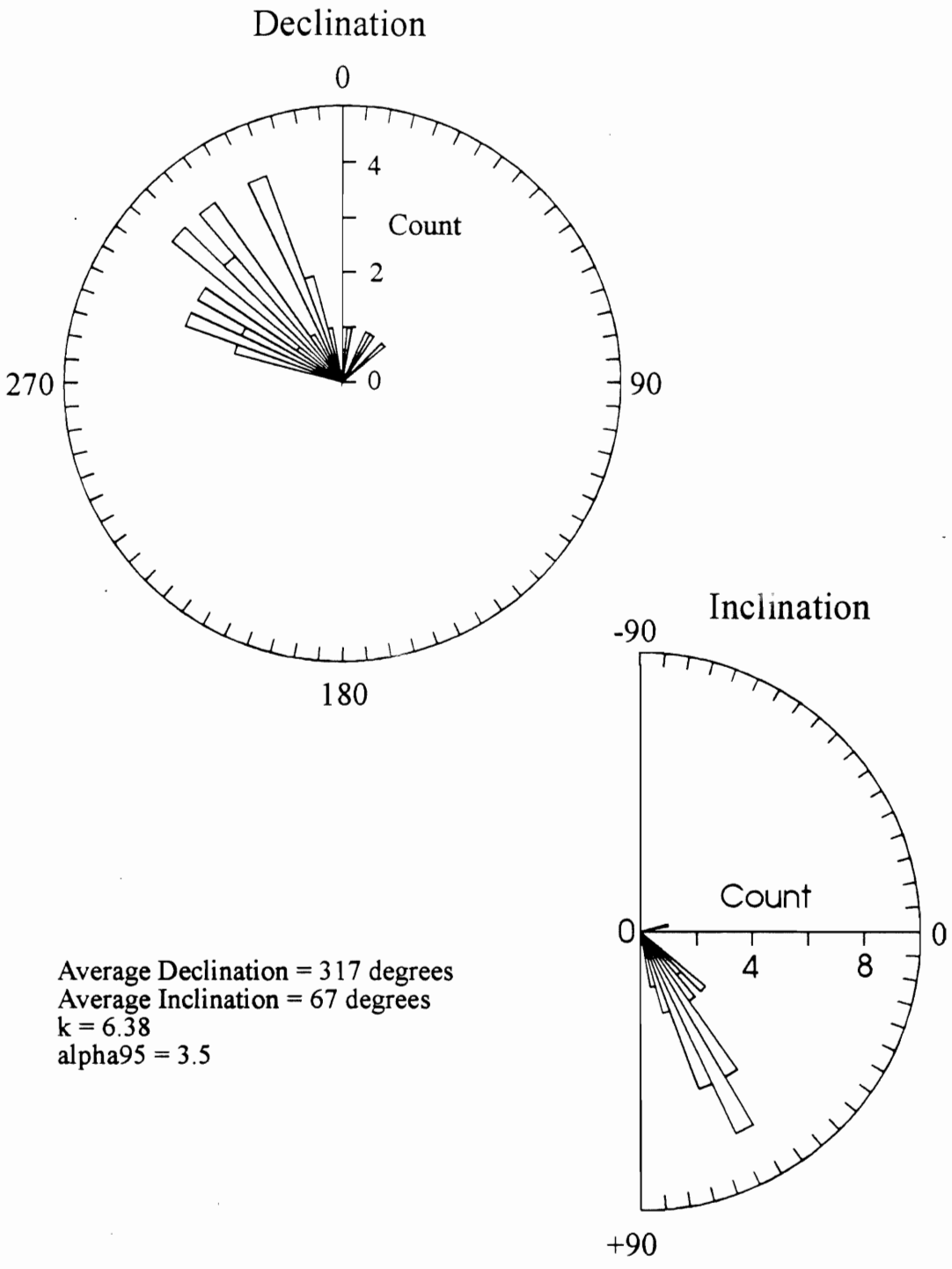

Figure 3.5. Declinations and inclinations of samples from the Kambia study area.

remanent magnetization in the area.

Correlations

Topography

Comparison of the geology (overlay 2) with the topography (figure 3.6) shows the Basal Group in the high ground to the southwest and the Sediments in the low ground to the north. This situation is generally consistent with the overall morphology of the ophiolite where the more hydrothermally altered and indurated Basal Group and Sheeted Complex, and other deeper lithologies, form the higher ground. The north and east flowing rivers and their valleys are generally not reflected in the aeromagnetic data (figure 3.2). No obvious topographic features correspond to the two highs or intervening low.

The geology of the area underlain by Extrusives

Yang (1991) measured the percentage of dikes and the ratio of pillowed to sheet flows along several profiles across the northern flank of the ophiolite. The measurement stations within the local area and the resulting contours are shown in overlays 5 and 6.

The 75 percent dike contour crosses the area in a smooth curve (overlay 5 on figure 3.3) but two projections in the 50 percent and 25 percent contours point towards the area of the Extrusives. These projections roughly correspond to the

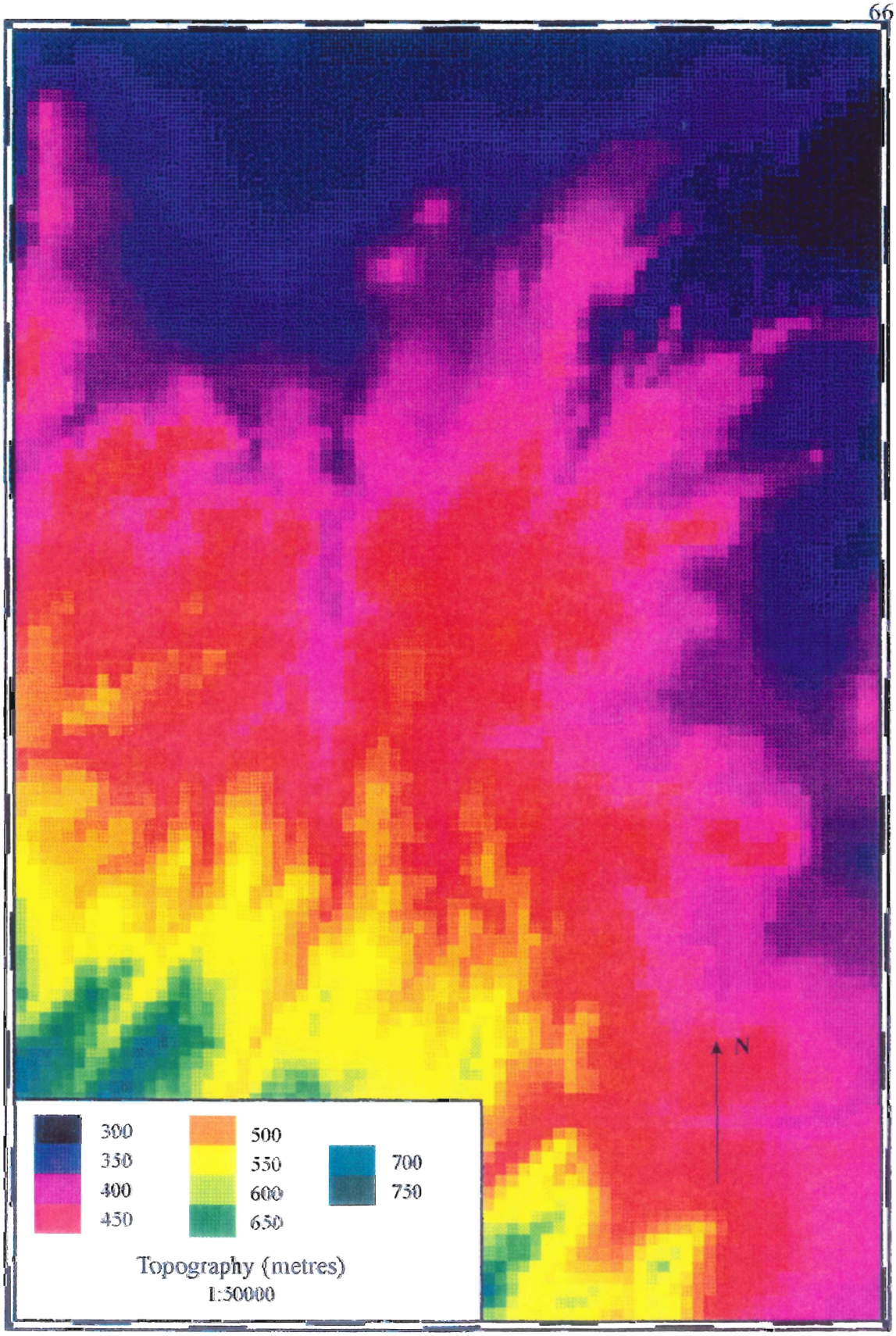

Figure 3.6. The topography of the Kambia study area.

large aeromagnetic highs. The western projection is poorly defined by the data and the contours may not represent the true shape. The measurement locations are noted on the overlay and higher dike percentages do occur in the area of the western projection. Thus, the shape of this projection is in question but there is no doubt that higher dike percentages form a ridge or outlier extending north into the Extrusives. The eastern projection is less pronounced. This may be due to its position where the strike of the contours and the Basal Group turn fairly sharply to the south. The magnetic high could represent its subsurface extension as a dike ridge in the predominantly north north east dike direction.

The central magnetic low over the Extrusives closely matches the area where sheet flows constitute 75 per cent or more of the Extrusives (overlay 6 on figure 3.3). Such areas occur at regular intervals along the northern outcrop of the Extrusives and are separated by areas where pillow lavas are more common. The eastern boundary is well defined by data collected by Yang (1991) and by more recent data (Hall, in preparation). The short western boundary that terminates at its southern end in a protrusion of the dike contours is less well defined.

Tectonics

Overlay 7 shows the faults in the area (Bear, 1960; Gass, 1960). Most faults strike north north east-south south west and the number of faults increases to the south. A smaller number of faults, which strike normal to the first set, may

be transform direction faults (Grand et al., 1993). Some faults are not well defined in the field (Bear, 1960) and Hall (in preparation) confirms the difficulty in identifying all but the most obvious.

The major fault pattern parallels or follows the boundaries of the major aeromagnetic anomalies in some but not all locations.

Grand et al. (1993) have classified the deformation of Cyprus into three phases. In order of decreasing age, they are 1) the deformation during formation of the ophiolite, 2) a post-formational compression phase and 3) a later tensional phase. The initial phase, by the orientation of dikes and the orientation and movement of faults, occurred during the formation of a north-south (present day direction) spreading ridge. Later phases often reactivated the same faults which can exhibit evidence of several successive movements. Part of the intermediate age compressional phase is represented by the Kyrenia range to the north. The latest extensional phase was interpreted to be related to the uplift of the present antiformal structure.

Small scale tectonic rotations are present in the upper section of the ophiolite (Grand et al., 1993). Many of these occurred after the initial formtion of the ophiolite and are small and insignificant on the scale of the whole ophiolite. The direction of these rotations was consistent with that noted above in the discussion of palaeomagnetic directions. Larger rotations (at least ninety degrees in some cases) may have taken place during the formation of the ophiolite as evidenced by vertical dikes cutting shallowly dipping dikes (Varga and Moores,

1985).

The number of faults seems to increase sharply south of the Extrusive-Basal Group boundary as seen in overlays 7 and 2. As noted earlier, this increase also corresponds to a magnetic boundary between the less magnetic Basal Group and the strongly magnetized Extrusives. The increase may be the result of better exposure in the Basal Group.

Alteration and Mineralization

Gossans are numerous in the area and three ore bodies have been mined. Comparing this mineralization (overlay 8) (Bear, 1960), with the faults (overlay 7) and the reduced to the pole aeromagnetic data (figure 3.3), results in two patterns becoming evident:

First, the gossans are usually associated with faults. This suggests that the faults have acted as conduits for high temperature fluid circulation. This is also consistent with the relationship between hydrothermal circulation and the pattern of magnetization. Hydrothermal circulation progressively decreases the magnetization of the rocks and is also associated with faults. The more closely spaced faults in the Basal Group may allow the hydrothermal fluid to pervasively alter the entire unit, causing its uniformly lower magnetization.

Second, the gossans are largely, but not exclusively, in the area of the central aeromagnetic low and not in the areas of the highs. Numerous smaller gossans occur in the Basal Group to the south of its boundary with the Extrusives.

They probably represent the roots of high temperature hydrothermal discharge conduits (Constantinou and Govett, 1973; Constantinou, 1980). The upper sections of these conduits and any mineralization have been removed by erosion along with the overlying Extrusives. Two of the three mined ore bodies are located within the area of the central low.

Magnetic modelling

See chapter 2 for the method. In order to apply the model appropriately to the local geological situation in the Kambia area, the following conditions were assumed. The situation is summarized in figure 3.7.

1. The soil and other unconsolidated cover on the Extrusives is thin and the strongly magnetized material is exposed at the surface.
2. The volcanics dip beneath non-magnetic sediments to the north. A non-magnetic body increasing in thickness from the Extrusive-Sediment contact northward at an angle of eight degrees downward from the topographic surface approximately represents this situation. The upper surface of the strongly magnetized bodies is at the lower surface of this wedge.

Several values of dip were tried. The eight degrees estimate was calculated from a model of anticlinal emplacement structure of the ophiolite (Hall et al, 1991a).

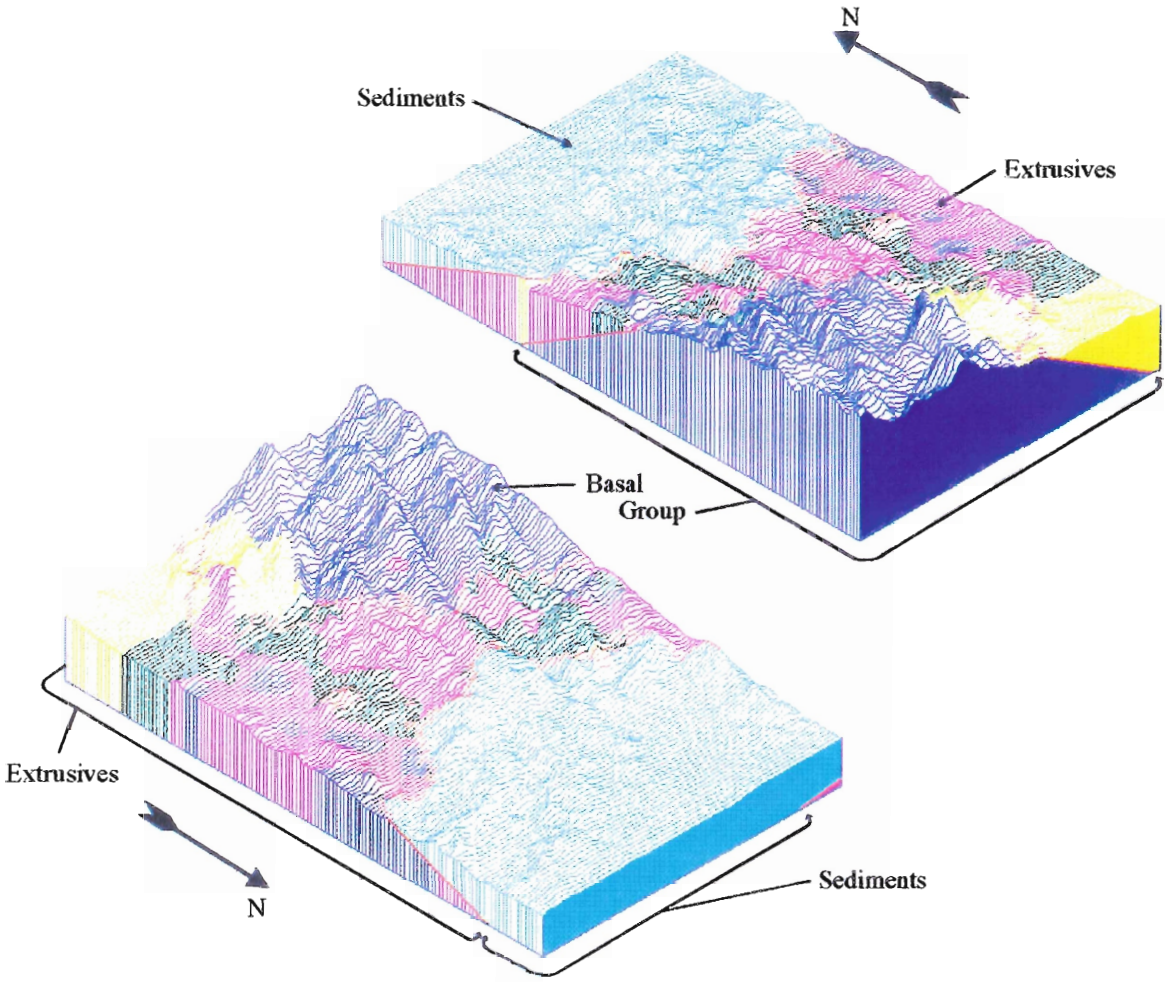

Figure 3.7. Sample model configuration showing the Basal Group dipping beneath the Extrusives which in turn dip beneath the non-magnetic sediments. The different colours within the Extrusives indicate bodies with contrasting magnetic properties which depend on the type of model.

3. The Basal Group underlies the Extrusives over the entire area. A wedge of low magnetization material (one ampere/metre) extends beneath the Extrusives to simulate this. The dip of this interface, calculated from the same model as above, was set at ten degrees, extending north from a line within the Basal Group. Several locations for this line were tried. The mapped Basal Group-Extrusives boundary (Bear, 1960) shown on overlay 2 appeared to be too far north and truncated the Extrusives near the contact to the point where they would require a very high magnetization to account for the observed anomalies. As the correspondence between the Basal Group contact and the decrease in magnetization is only approximate, the line was relocated towards the south. This allowed the highly magnetized Extrusives to have a minimum thickness of a few hundred metres in the south. The new boundary was also consistent with the southern limit of strong sample magnetization as seen in overlay 3.

4. Magnetization was set to one ampere/metre for the Basal Group bodies and zero for the northern Sediments.

The magnetizations and shapes of the bodies in the Extrusive area were then varied and the resulting anomaly calculated and compared with the observed anomalies to investigate possible origins for these anomalies. In the most general way, these may reasonably arise from one or more of several factors:

1. variations in the topography
2. errors in flight elevation
3. variable depth of burial of the Extrusives beneath non-magnetic cover other than the northern Sediments which have already been described
4. variable directions of magnetic remanence in the Extrusives
5. variations in the strength of magnetization of the Extrusives
6. variations in the thickness of the strongly magnetized Extrusives above less magnetic material below, or
7. smaller bodies of very strongly magnetized material located at depth within the strongly magnetized Extrusives.

The first two items have been discussed previously and can be rejected as explanations. A model of the topography with uniform magnetization was calculated to confirm the earlier result. As expected, the effect of the topography may be visible in the details of the data, but fails to account for the large-area anomalies. The effect of errors due to flight elevation variation is assumed to be similar or less than that due to topography.

Strong arguments also exist against the third option in which the strongly magnetized bodies are buried beneath substantial non-magnetic cover such as soil and alluvium. First, such cover is not observed in the field. The exposures are uniformly good over much of the area in natural outcrops, in bulldozed farm terraces, and in stream valleys. In no case was more than a few metres of

overburden observed. Samples collected from outcrops in the area of aeromagnetic lows do not show consistently lower magnetic intensity. This places the strongly magnetized material at or very near the surface.

Option four, where the anomalies are caused by variations in remanence direction, is also tenuous. The directions measured in samples are remarkably uniform (figure 3.5) and are consistent with the well defined Troodos direction as rotated by the uniform local tectonic tilt. This tilt extends across large parts of at least the central low and eastern high. The approximate uniformity of the tilt over the area is well controlled by field observations of the orientation of dikes and of columns in the colonnades of sheet flows.

Grand et al. (1993), as noted earlier, found there was little post-formational rotation of blocks within the ophiolite. Varga and Moores (1985) suggest that larger rotations occurred during the formation of the ophiolite, but the dips are uniform over large blocks. One small block with a large rotation was observed in the Kambia area (J.M. Hall, personal communication) and is the cause of the one reversed magnetic inclination in the sample set (figure 3.5). This block is too small to have a major effect on the interpretation, but could be responsible for a small local anomaly.

A model with variable magnetic intensity and constant direction (option five) was first constructed, calculated and refined to match the aeromagnetic data. The distribution of magnetization is shown in figure 3.8. It varies from seven to ten amperes/metre in the aeromagnetic highs to five to seven amperes/metre in

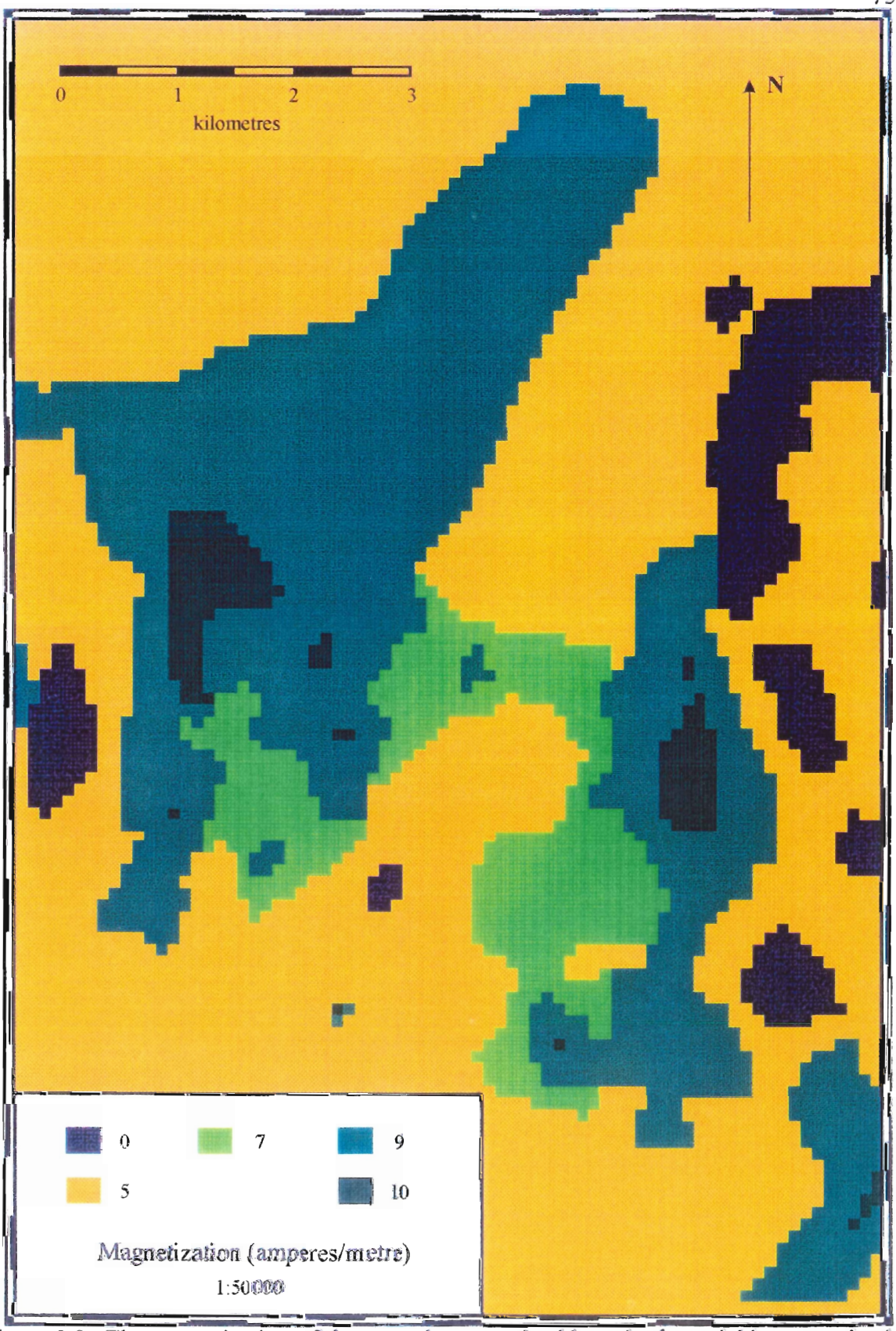

Figure 3.8. The magnetization of the strongly magnetized layer in the variable magnetization model. The basal group, which was given a one ampere/meter magnetization, is not shown.

the intervening low. This compares with the average magnetization of 8.5 amperes/metre for all samples from the Extrusives (Table 3). All bodies were constrained to be two thousand metres thick. This arbitrary thickness is greater than the maximum thickness of the extrusives. In this model the Basal Group does not extend beneath the Extrusives.

The calculated field (figure 3.9) shows the general two highs and middle low pattern of the original data (figure 3.2). The residuals (figure 3.10) do not show such a pattern, indicating that the match between the model and data is generally good. Higher values of residuals in the area of the large low to the east indicate imperfections in the model. As detailed knowledge of the geology and magnetization was not obtained for this sub-area, this was allowed to remain. Over the remainder of the study area, small variations in the residuals indicate local imperfections in the model. One standard deviation of the residual field values was 365 nT, which can be compared to that of the model calculated field (697 nT) and the original data (662 nT) to give a rough estimate of goodness of fit over the whole area.

As noted earlier, no regular distribution of magnetization is seen in the surface samples. The sample magnetizations show a higher average value in the area of the central low (12.82 amperes/metre) than in the left and right magnetic highs (7.27 and 5.45 amperes/metre respectively). In order for the variable magnetization model to be valid either the sampling must have been biased or the magnetization of the surface material in the area must have be fortuitously altered

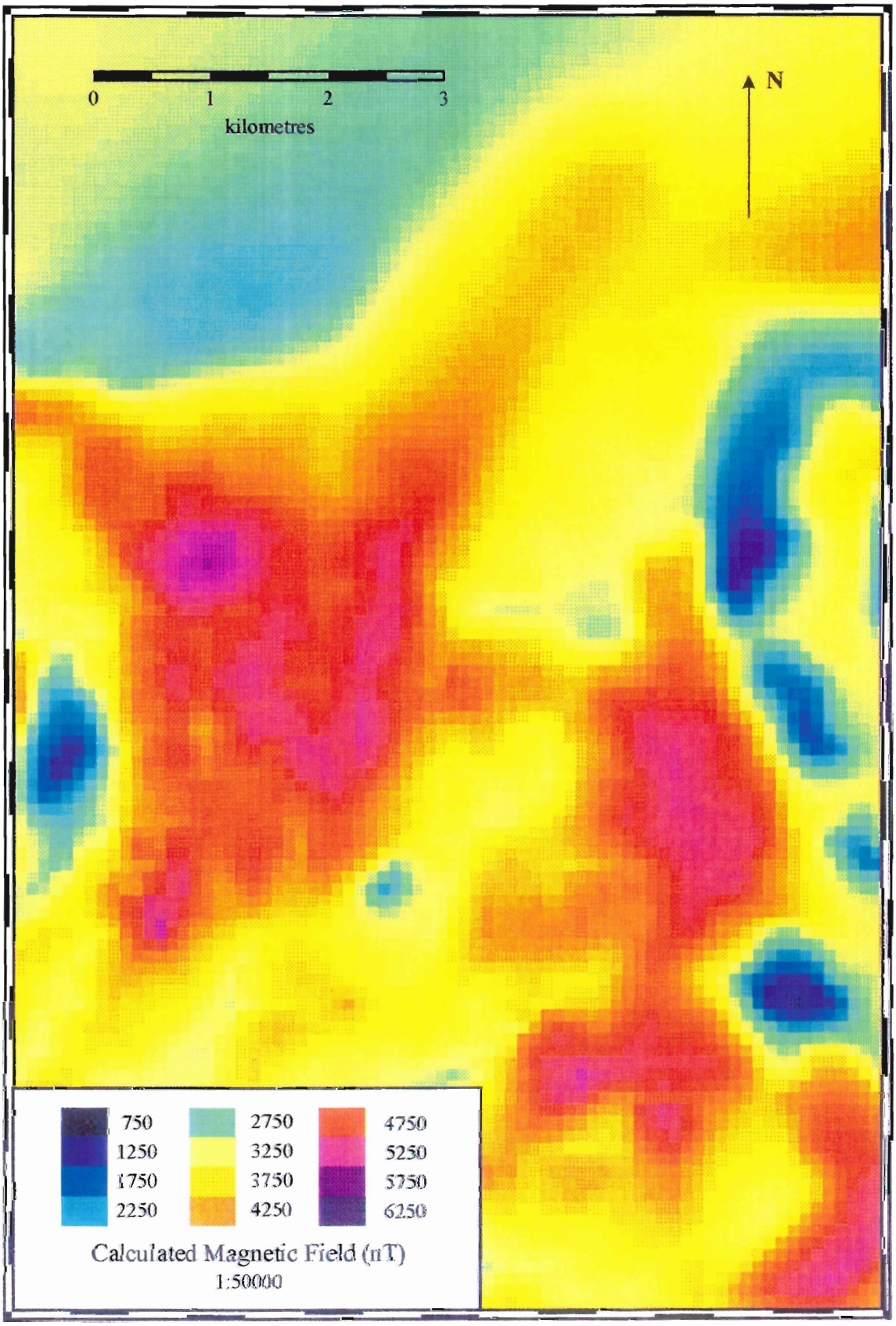

Figure 3.9. The calculated magnetic field of the variable magnetization model.

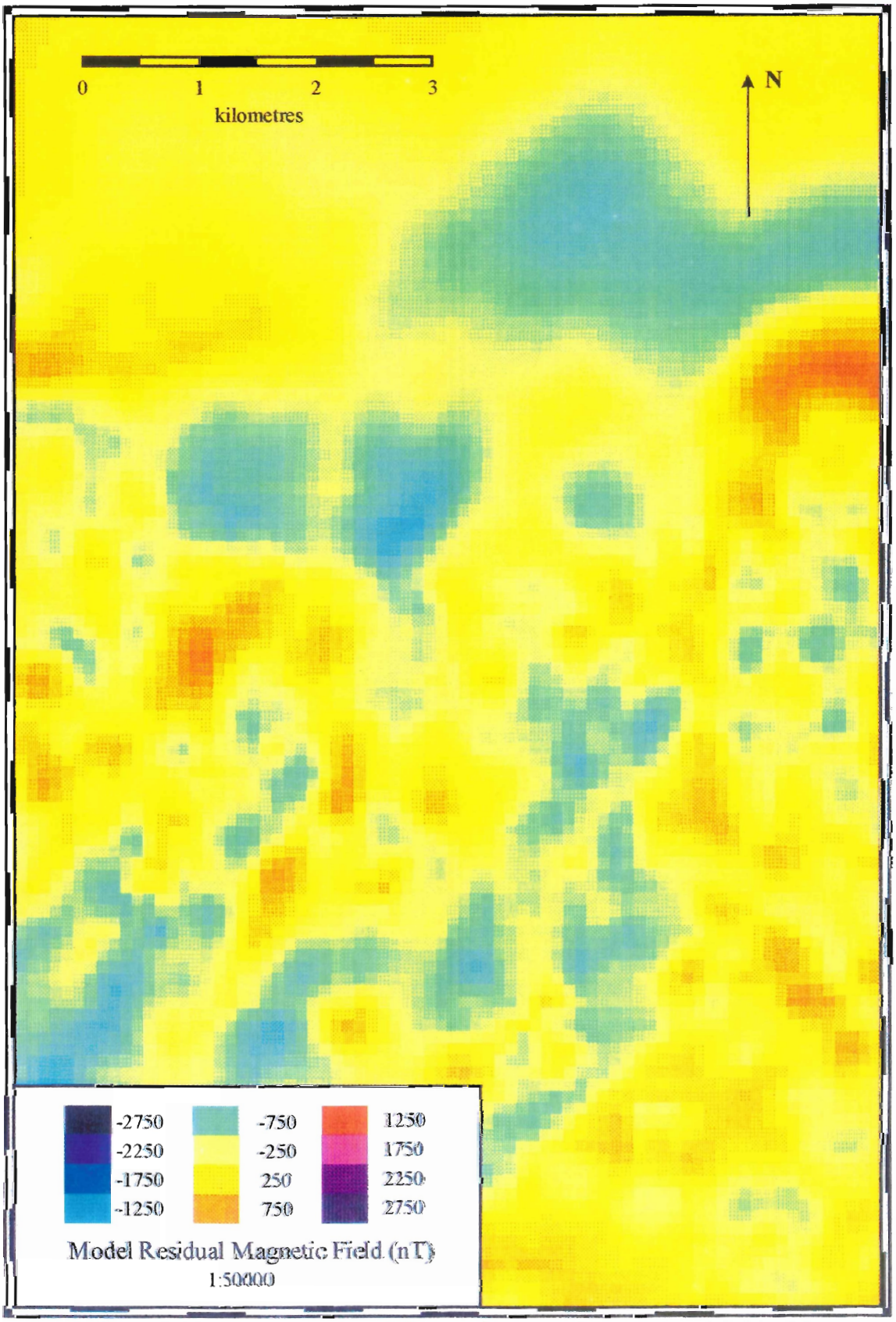

Figure 3.10. The residual or difference between the calculated field of the variable magnetization model and the gridded aeromagnetic data.

to obliterate the general magnetic pattern. This would have to have happened after the uplift and erosion of the ophiolite to occur at the present erosional surface.

Considerable effort was made to obtain fresh samples from as much of the area as possible. This effort covered several field seasons and was ultimately limited by available exposures and the need to cover a large area. The samples were collected from the areas of both of the highs and the intervening low. They represent most subdivisions of the model as shown in figure 3.8. The only consistent pattern is that of lower magnetization in the Basal Group. A sampling bias might omit weakly magnetized, less indurated units because of difficulty in recovering samples or because of a lack of exposure. However, this would be expected more in areas of pillow lavas and less in the central area of sheet flows.

Similarly, if a surface alteration event homogenized the magnetization, a lessening of this effect would be expected in the fresh exposures in the bottom of stream valleys. No evidence of this effect is seen in this study, in other surface studies or in drill core studies from elsewhere in the northern flank of the ophiolite (Hall et al., 1991b).

An alternative model which allows for uniform surface magnetization is seen in figure 3.11. Here the magnetization has been set at a uniform ten amperes/metre for the Extrusives and one ampere/metre for the Basal Group. The variable in the model is the thickness of the bodies beneath the topographic surface, except where they are truncated by the Basal Group.

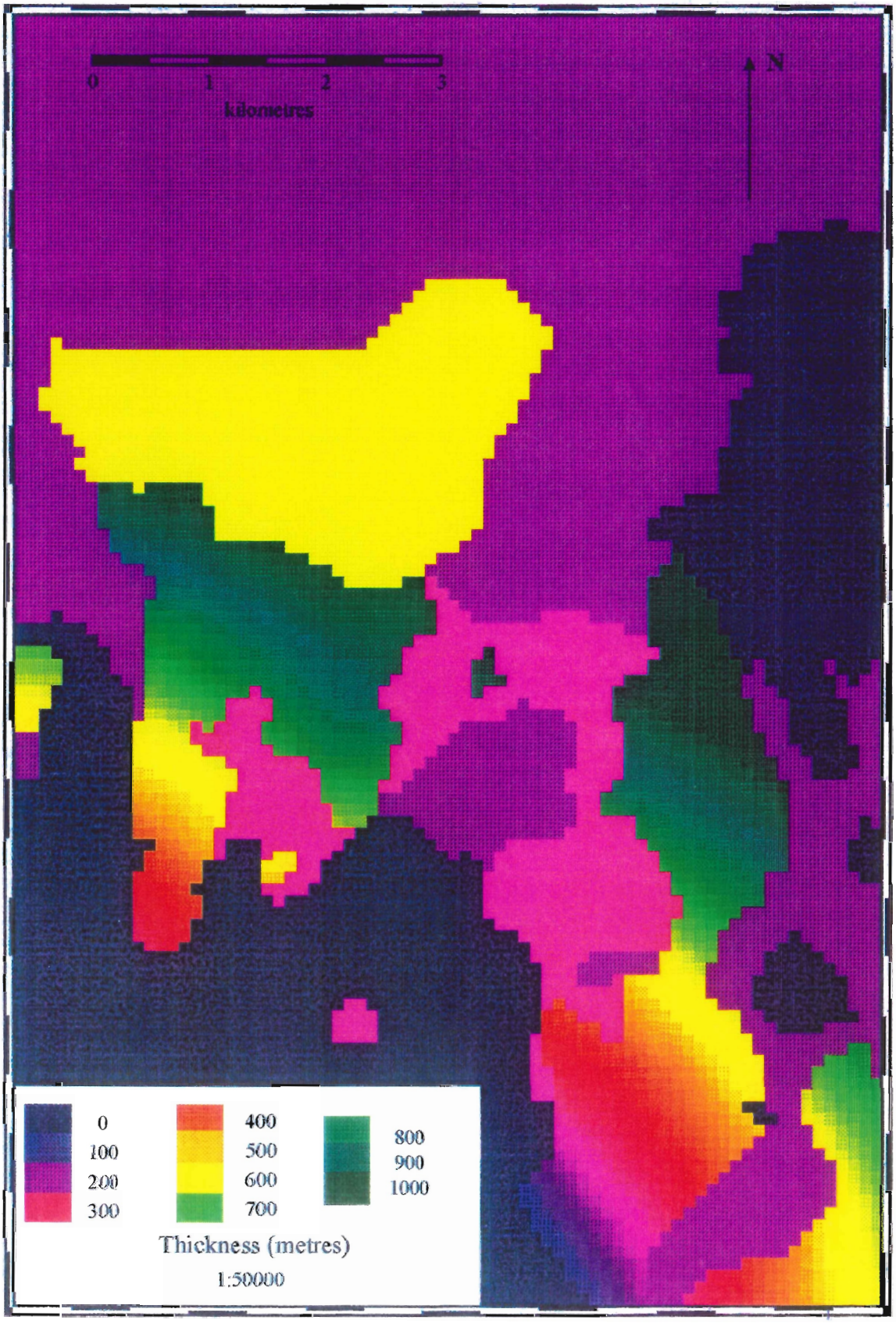

Figure 3.11. The thickness of the strongly magnetized layer in the variable depth model.

In the areas of the aeromagnetic highs, the strongly magnetized material is set to be up to 1000 metres thick, the estimated thickness of the entire Extrusive group. This drops to a thickness of 250 metres in the intervening low.

The calculated field of this model (figure 3.12) again shows a general match to the original data (figure 3.2) with two highs and a middle low. The residuals (figure 3.13) again show small variations indicating local imperfections. A large residual in the southeast corner is outside the area of detailed geological knowledge and magnetic samples. One standard deviation for the residuals in this model is 350 nT and that for the calculated field of the model was 625 nT. These are similar to the values for the previous model.

Finally, the possibility exists of very strongly magnetized material buried within the Extrusives in the vicinity of the two magnetic highs. This just might be possible, based on a few scattered very high values of sample remanence as seen in figure 3.4 and overlay 3. The two highest values of remanence are found in the Extrusives just above the Basal Group contact. This would suggest that in the unlikely event of such sources existing further down dip to the north, they are likely to be deeply buried.

A model of this situation is shown in figure 3.14. The Basal Group is given a magnetization of one ampere/metre and the area of the large low to the east is unmagnetized. The Sediment cover increases in thickness to the north and the Basal Group underlies the section as for the variable depth model. The Extrusives are given a general uniform magnetization of ten amperes/metre.

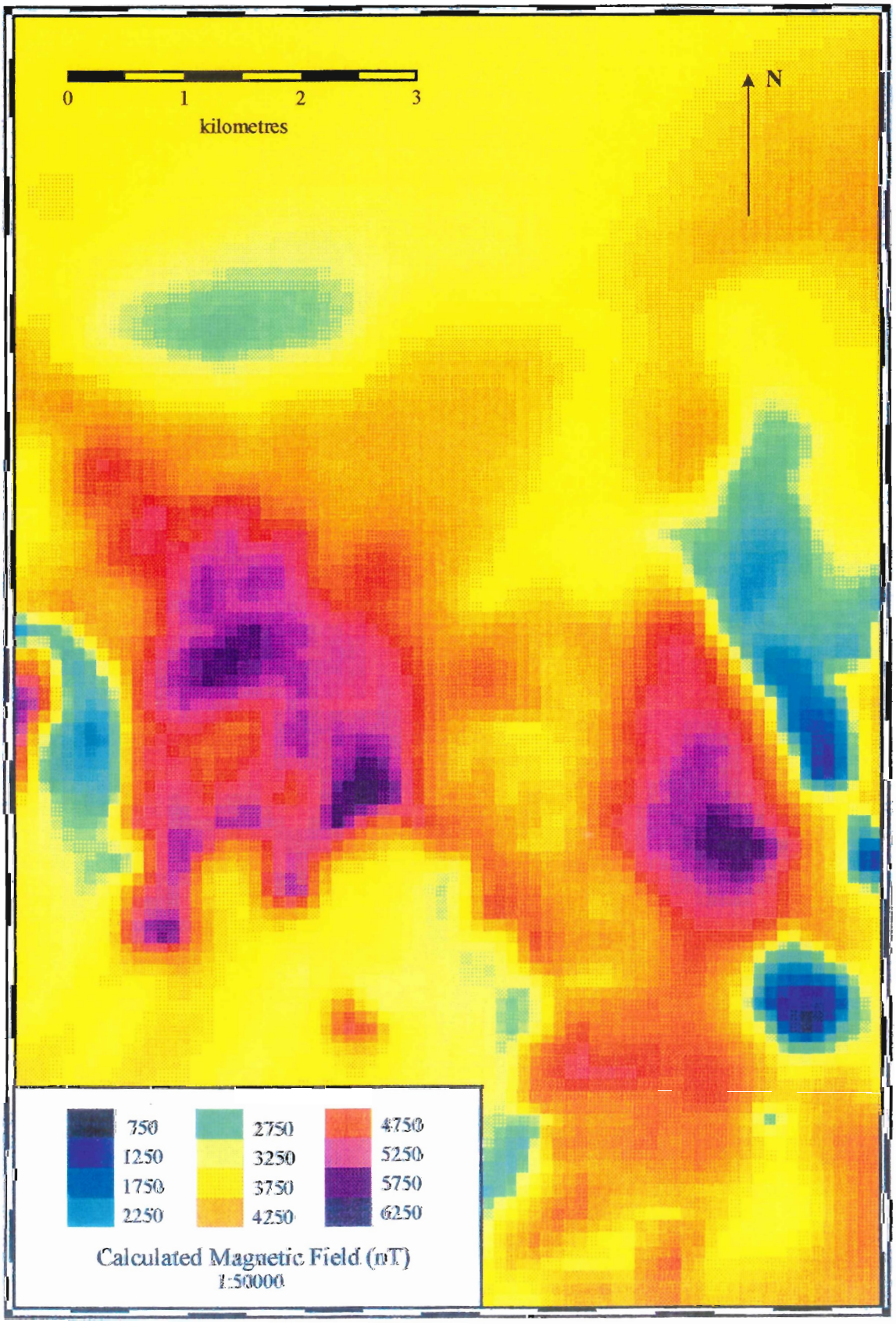

Figure 3.12. The calculated magnetic field of the variable depth model.

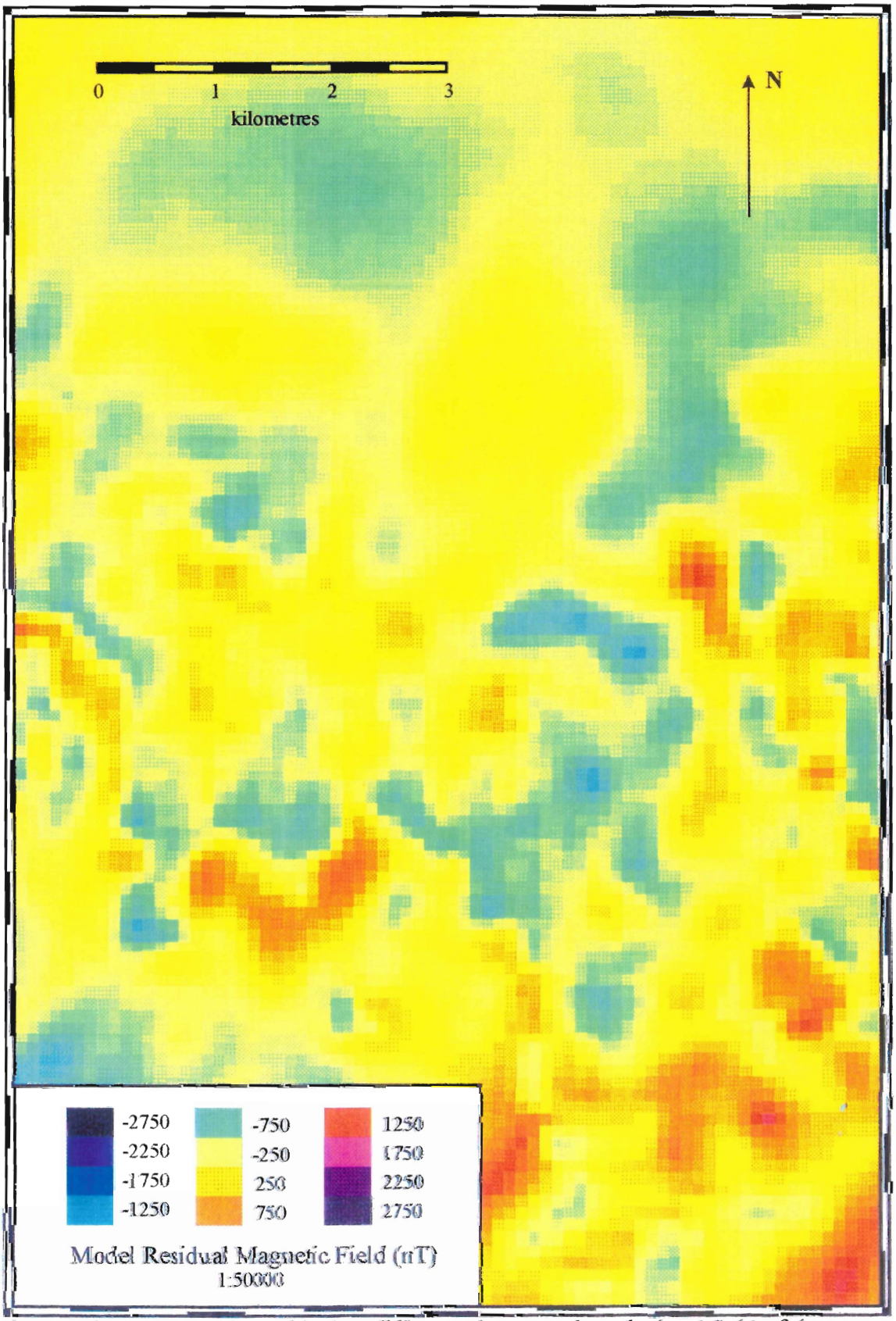

Figure 3.13. The residual or difference between the calculated field of the variable depth model and the gridded aeromagnetic data.

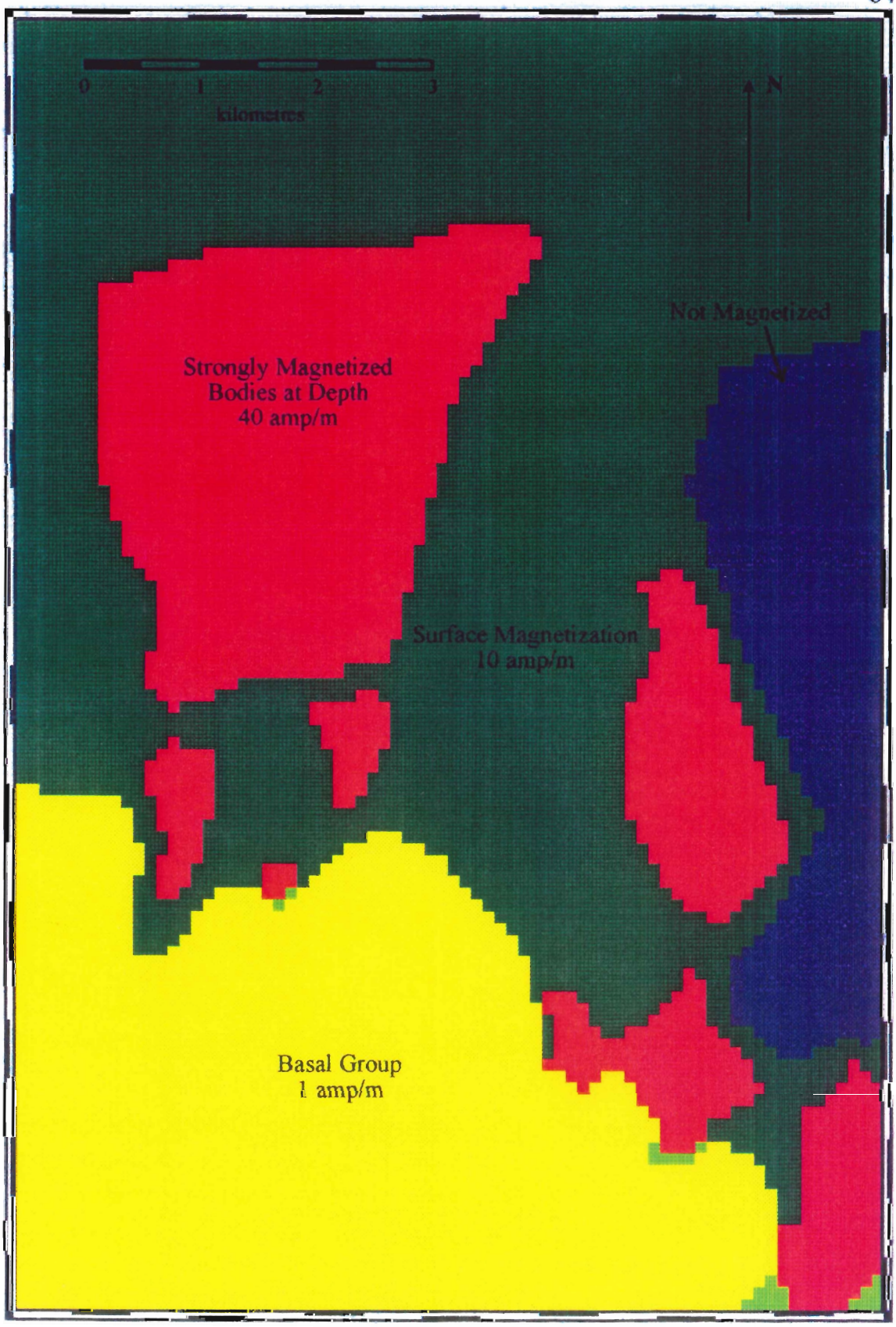

Figure 3.14. The distribution of magnetization in the deep body model.

Their thickness varies from approximately one hundred metres in some areas near the basal group contact to over one thousand metres in the north of the area. In selected areas very strongly magnetized bodies (forty amperes/metre) of two hundred metres thickness are placed at the base of the Extrusives.

The calculated magnetic anomaly is shown in figure 3.15 and the difference between the calculated and measured field is shown in figure 3.16. This model shows general but less perfect agreement with the original data (figure 3.2) when compared to the previous models. This is reflected in the residuals, which are larger in several sub-areas. One standard deviation for the residuals is 818 nT and for the model is 884 nT. Both of these are larger than those for the previous model, and the residuals are much larger. The model could be refined to reduce the residuals and improve the fit.

The quality of the magnetic modelling

The quality of the original aeromagnetic data has been discussed earlier. It was concluded that there may be small errors due to topography and survey procedures, the major anomalies are real and substantially accurate.

Each of the three models may be compared to the original data using the residuals which have already been mentioned. To provide a further comparison, a profile was constructed randomly across the two major highs and intervening low. The four curves are shown in figure 3.17.

Due to time constraints, refinement of each model was ended when the

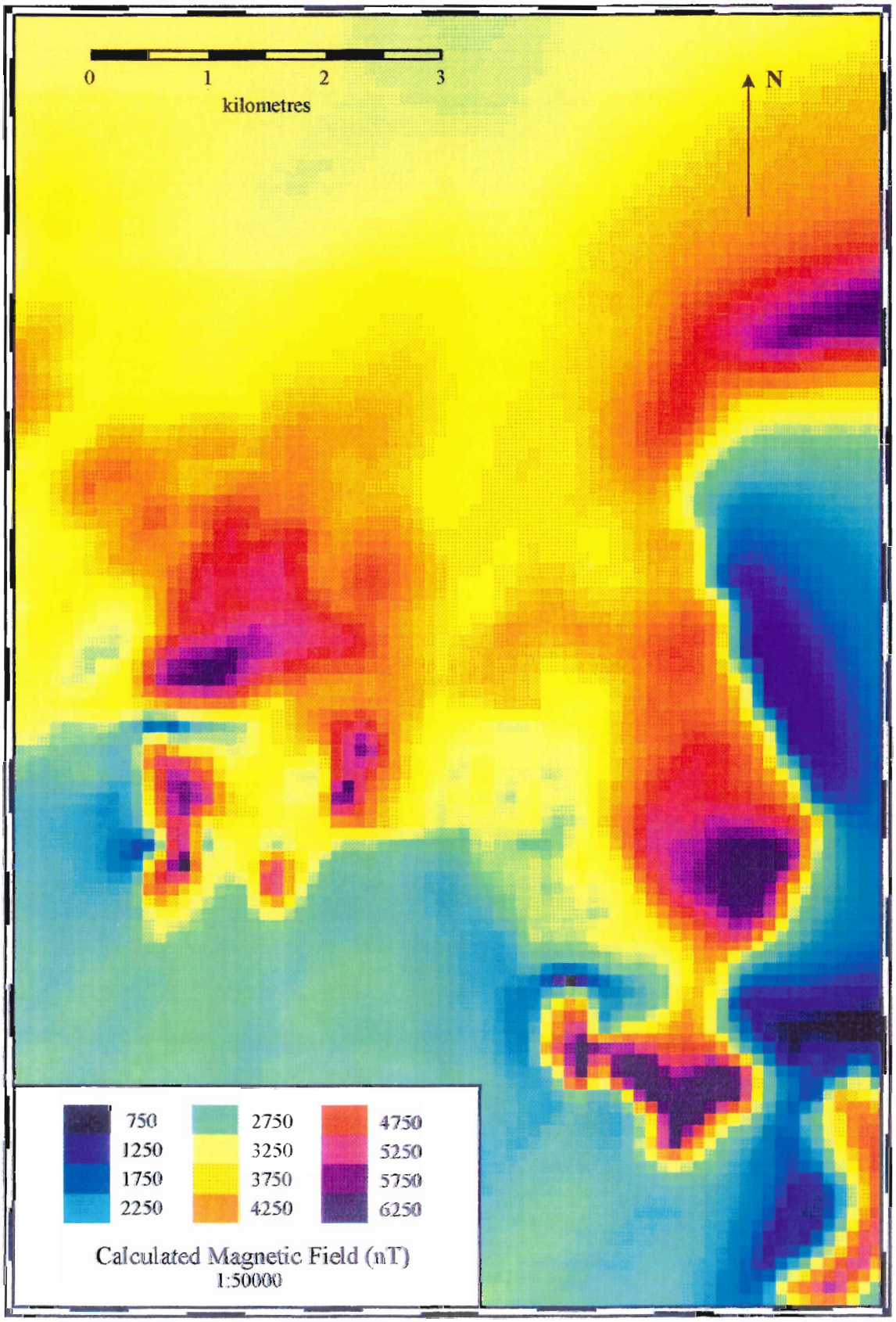

Figure 3.15. The calculated magnetic field of the deep body model.

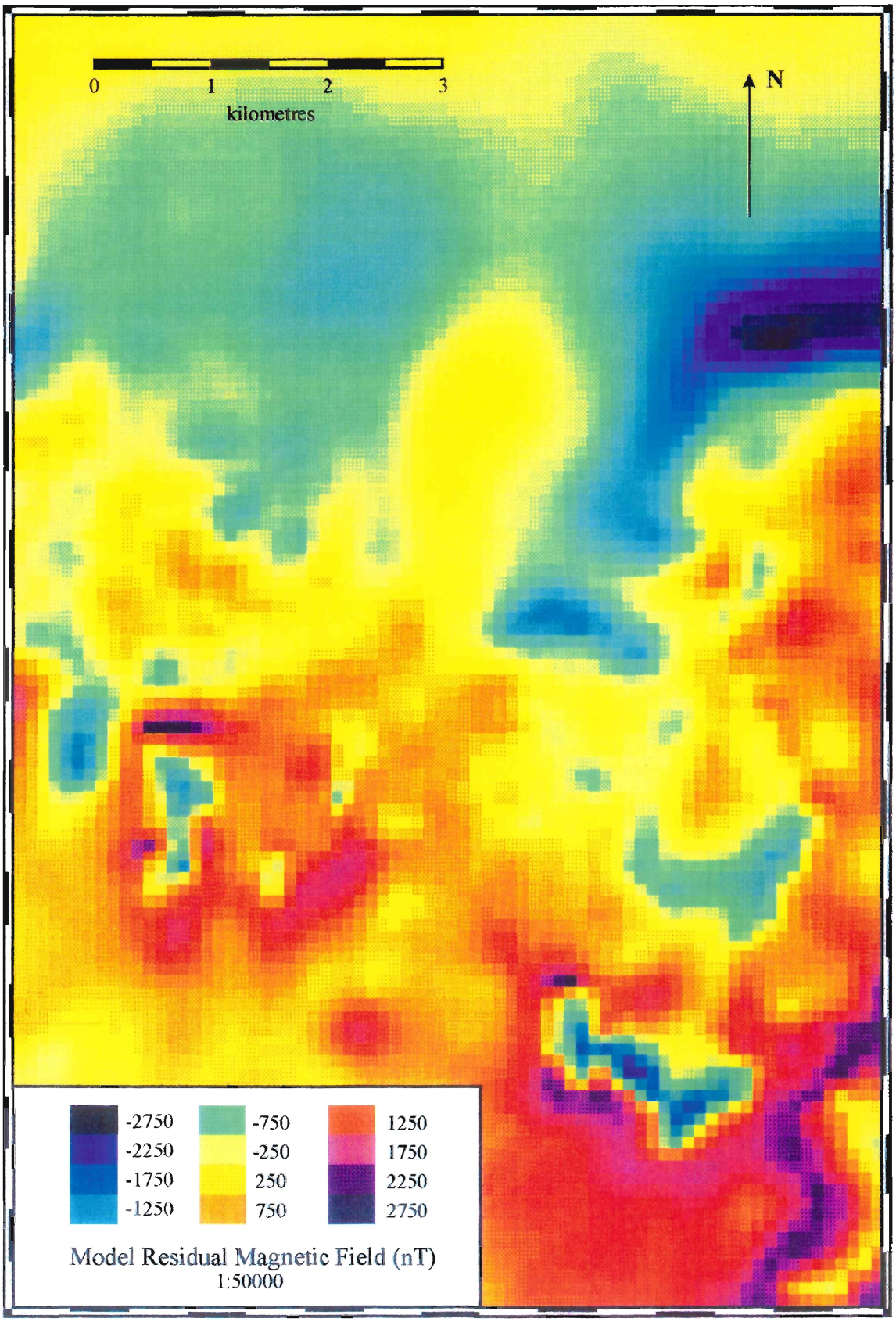

Figure 3.16. The residual or difference between the calculated field of the deep body model and the gridded aeromagentic data.

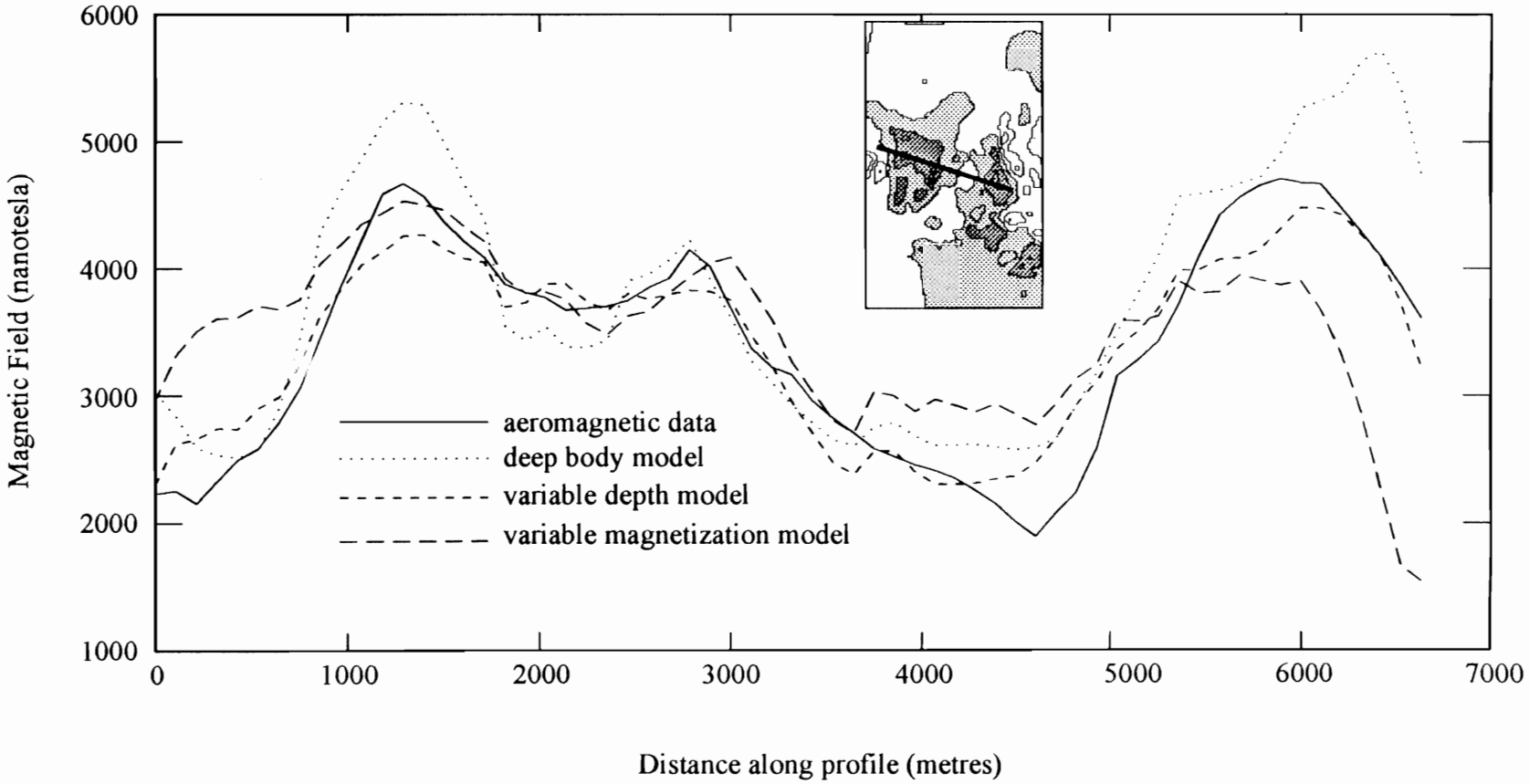

Figure 3.17. Profiles of gridded and calculated magnetic field to compare the models with the original data. The average level of each profile is arbitrary and profiles have been plotted on top of each other for comparison purposes.

calculated magnetic field roughly matched the original gridded data. This is seen in figure 3.17 in that all of the curves have the same general shape. The deep body model was not refined to the same detail as the other two. Any of the models could be further refined to reach a closer match.

Summary

The measured magnetic field in the area is dominated by two magnetic highs separated by a low. These are bounded on the south by the less magnetic Basal Group and fade under the non-magnetic Sediments to the north.

The magnetization as measured in samples shows no observable pattern aside from the lower magnetization seen in the Basal Group. Samples from the Extrusives average about ten amperes/metre whether from the vicinity of the highs or the low of the anomalies. In addition, the average declination and inclination are 317 and 67 degrees respectively for the extrusives in the area, with little variation.

A limited amount of data suggests that the two highs may occur in areas where the dikes form over 25 per cent of the Extrusives. The central low corresponds to an area where over 75 per cent of the extrusive rocks are made up of sheet flows and less than 25 per cent are pillow lavas. The mineralization and mines are generally but not exclusively concentrated in the area of the central low.

These anomalies may be attributed to three possible sources:

1. variable magnetization in the Extrusives
2. variable depth of the strongly magnetized Extrusives, or
3. bodies of very strongly magnetized material at depth in the Extrusives.

Magnetic modelling has determined that any of these options could account for the anomalies. The relative likelihood of each or all being present in the area will be discussed in the final chapter.

Chapter 4

Spectral Analysis of Mineralization Locations in the Troodos

Introduction

Anomalies in the aeromagnetic field may provide information about the distribution of regional hydrothermal alteration and, by inference, hydrothermal circulation on a similar scale. This will be discussed further in chapter five. In addition, there are much smaller discrete occurrences of intense hydrothermal mineralization in the form of mines, mineral prospects and gossans. The small magnetic signature of these occurrences will be difficult to see in the aeromagnetic survey where the flight lines are four hundred metres apart. The general nature of these deposits has been discussed in chapter one.

The ore bodies of Cyprus are grouped into mining districts (figure 4.1). These are limited in area and are separated by non-productive zones containing no mines and less mineralization than the mining districts. Presumably the zones are related to constructional features of the ophiolitic oceanic crust.

As noted previously, it is now accepted that the Cyprus sulphide deposits were formed as a result of circulating sea water and may be analogous to ocean floor deposits. The pattern of this circulation below the sea floor is still unclear (Lowell et al., 1995). It is usually assumed that the sea water is drawn down from the water/rock interface over a large diffuse recharge area. Discharge of high

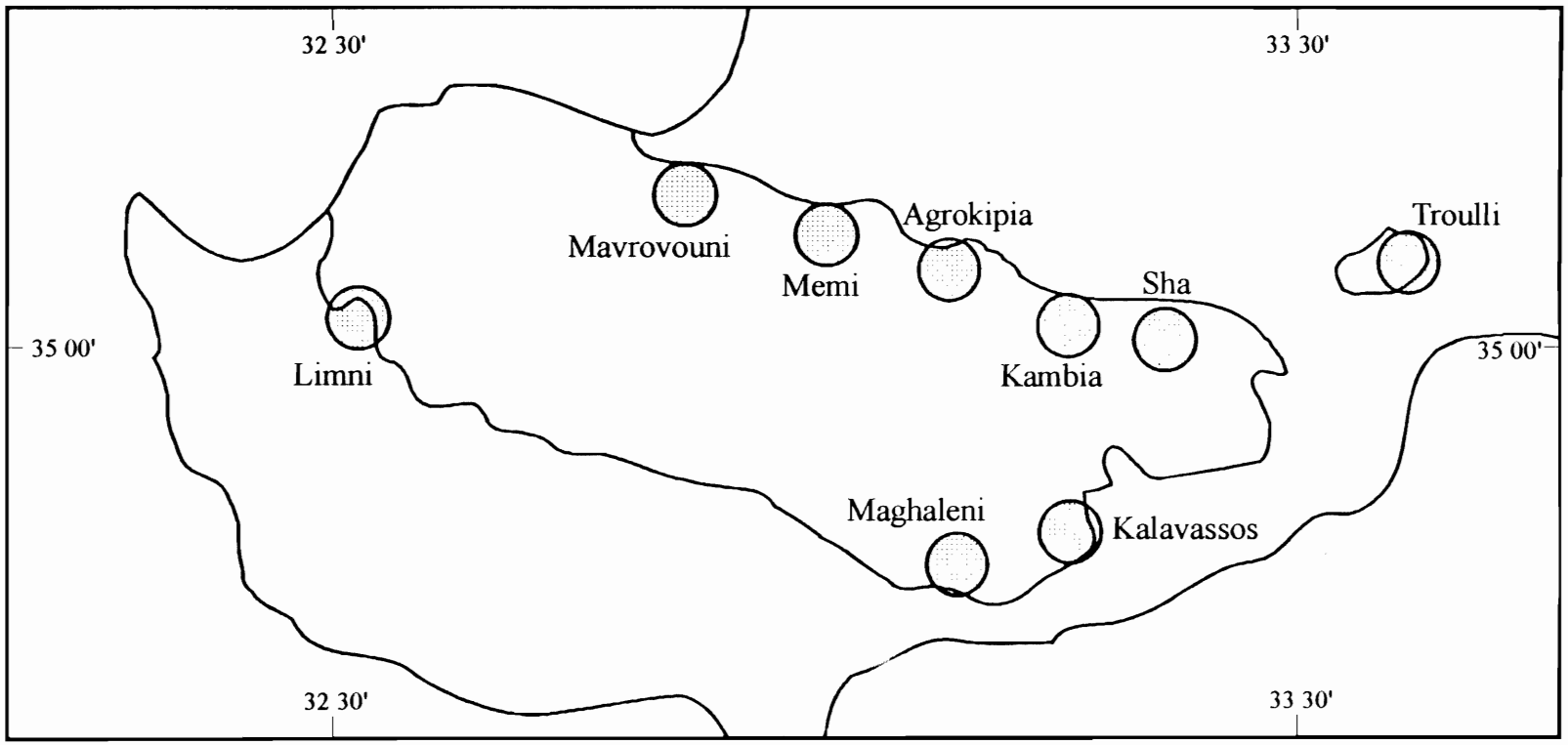

Figure 4.1. Idealized mining districts in the Troodos ophiolite. Locations were chosen from Geological Survey of Cyprus, 1982.

temperature fluid at the sea floor can be either focussed as is seen in the black smokers of the East Pacific Rise, or diffuse as is seen at the Galapagos Spreading Centre. Focussing may occur deep in the upper crust (eg. Richardson et al., 1987) or closer to the surface (Lowell, 1990).

The spatial distribution of deposits on the sea floor is poorly determined as well. The length of the system of mid-oceanic ridges and their difficulty of access combine to limit the amount of detailed knowledge of such bodies and their distribution, although this situation is changing rapidly with further exploration. Away from the ridges, volcanic and sedimentary activity have buried most deposits.

In Cyprus, sulphide bodies have been sought over several millennia for commercial reasons and many (but perhaps not all) at or near the present erosional surface are known. Spooner (1977) suggested that they have a regular spacing due to their formation as part of regularly spaced hydrothermal circulation cells. These cells must have persisted for some time to produce the larger ore deposits.

If ore deposits occur regularly, they may be related to regular variations in other features of the ophiolite. Hall et al. (1989) identified and quantified the regular variation of a number of these features on the north flank of the Troodos. The features were of two types: the thickness of the upper rock units of the ophiolite and the number and size of mineralization occurrences. The study found a strong periodic variation in the total thickness of the extrusive units

(Pillow Lavas and Basal Group). This corresponds to a regular variation in the proximity of the Sheeted Dike Complex to the surface (figure 4.2). Less regularity was found in the distribution of mineralization but there was some suggestion that it might correspond with the variation in extrusive thickness.

Hall and Yang (1994) also looked at the distribution of ore bodies in the Troodos and compared it to the percentage of dikes at different levels in the section. Their finding that ore bodies are preferentially found just above the 25 per cent dike level was postulated to be due to optimal conditions for preservation at that level (figure 4.3).

The intersection of these two conditions should constrain the location of ore bodies (figure 4.4). As these conditions seem to occur regularly, so should the mineralization.

Method

A previous study (Hall et al, 1989) had examined the regular occurrence of mineralization along much of the northern flank of the Troodos. While the results of that study were promising, they were not unequivocal. This analysis is intended to extend that study by using a large data set over a larger area.

The locations of known ore bodies, prospects, gossans, and other mineralization were digitized by hand from the geological maps published by the Geological Survey Department of Cyprus (Wilson and Ingham, 1959; Carr and

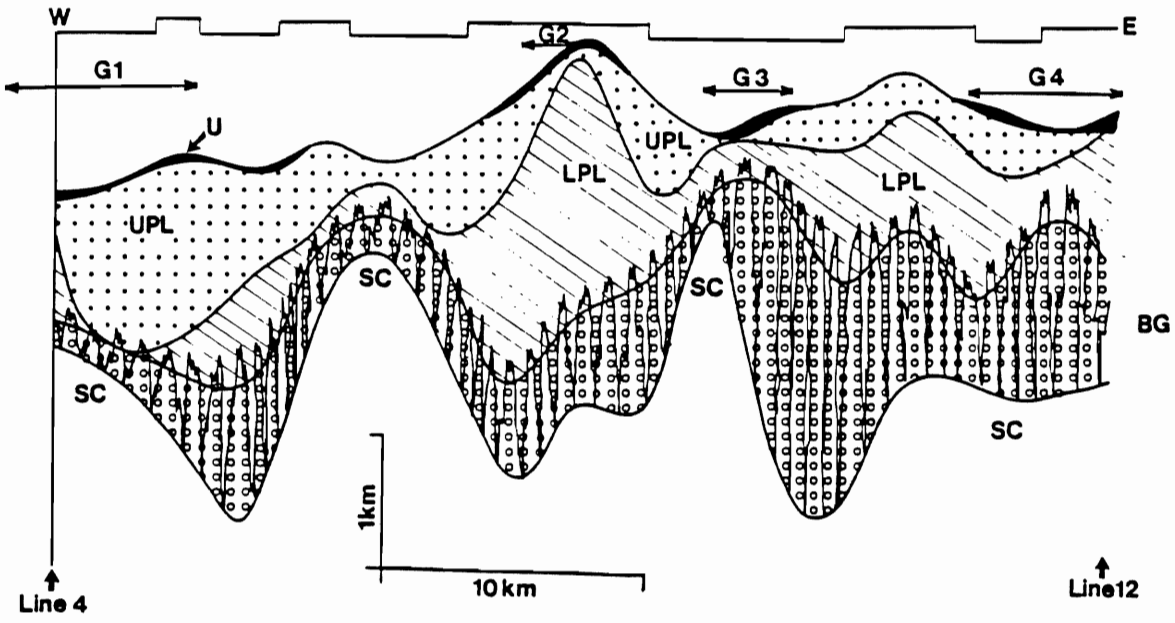

Figure 4.2. Variations in the thickness of the extrusive units on the northern flank of the Troodos ophiolite. SC - Sheeted Complex, BG - Basal Group, LPL & UPL - Pillow lava units which are subdivisions of the Extrusives, U - Umbers, G1-G4 - Mineralized zones. From Hall et al., 1989.

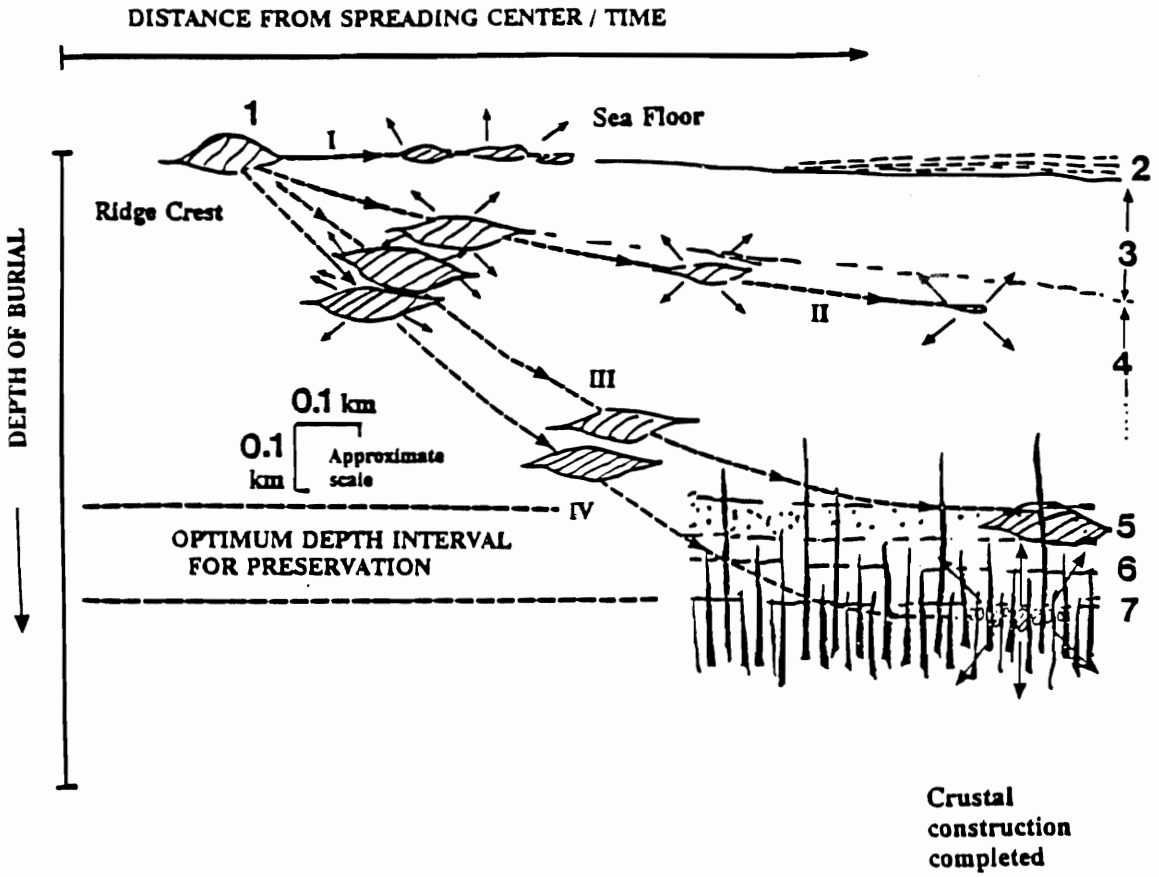

Figure 4.3. A model for preferential preservation of ore bodies in the Troodos ophiolite at about the 25 per cent dike level. Ore bodies at shallow depths are dissolved by circulating cold sea water (I & II). At deeper depths they are destroyed by hydrothermal metamorphism (IV). From Hall and Yang (1994).

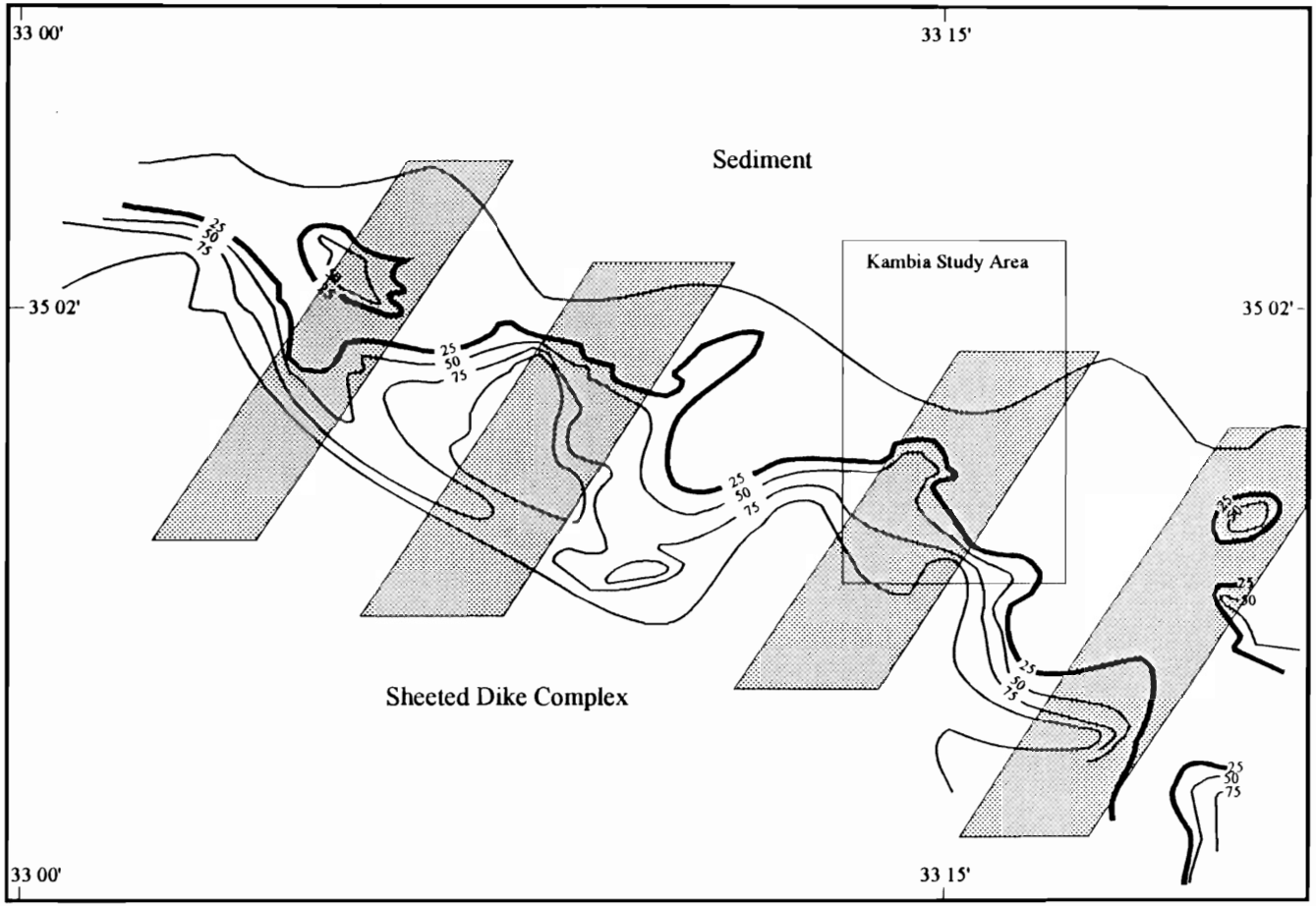

Figure 4.4. A map showing the zones of mineralization (shaded) from Hall et al. (1989) and the dike percentage from Hall and Yang (1994). The 25 per cent dike level is shown in bold.

Bear, 1960; Bear, 1960; Gass, 1960; Moore, 1960; Bear and Morel, 1960; Pantazis, 1967; Lapierre, 1971). One dimensional data series were generated from the two dimensional location data by accumulating the number of mineralization occurrences per easting kilometre. The complete data set is shown in figure 4.5a and the corresponding data series in figure 4.5b.

The one dimensional data series was of interest as it was parallel to the spreading direction. Since the data has a large north-south extent and the most periodic data series might be subparallel to the spreading direction, the data set was rotated by angles of -40 degrees through +40 degrees in increments of integer degrees. A data series was constructed and analyzed as described below for each rotation. The analysis was performed on both the complete data set of all known mineralization locations and a subset consisting of mine locations only.

To investigate regular variations, the data series were converted to the frequency domain using a Fourier Transform. A power spectrum for a range of frequencies was then calculated and displayed. Regular occurrences of mines and mineralization or variations in the quantity of such should appear as peaks in the power spectrum.

The Fourier Transform is a one dimensional case of that described earlier (equation 2.6). The expression for discrete data is:

$$F_u = \sum_{k=0}^{N-1} f_x \, e^{2\pi i k n/N} \qquad (4.1)$$

where F_u is the series in the frequency domain,

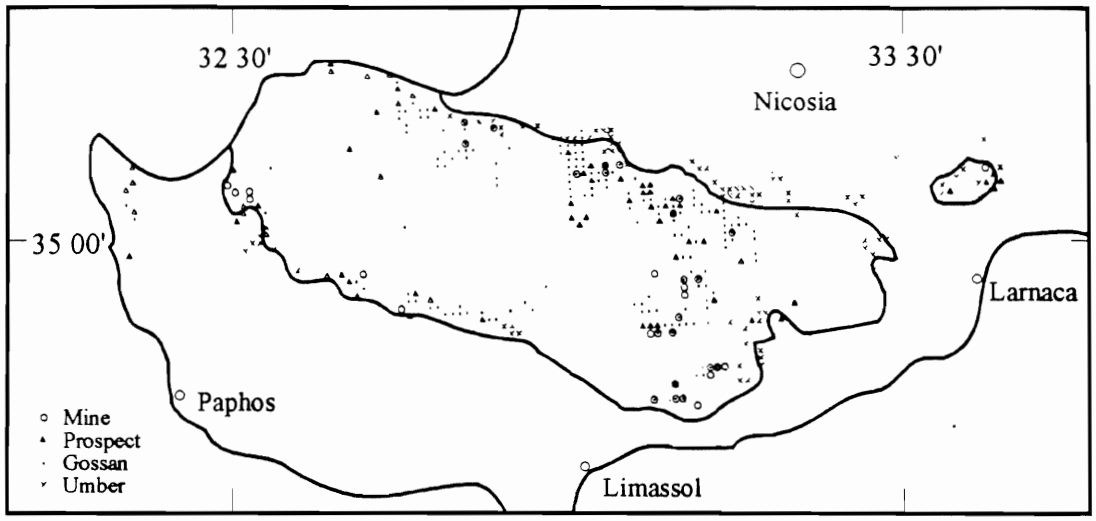

(a)

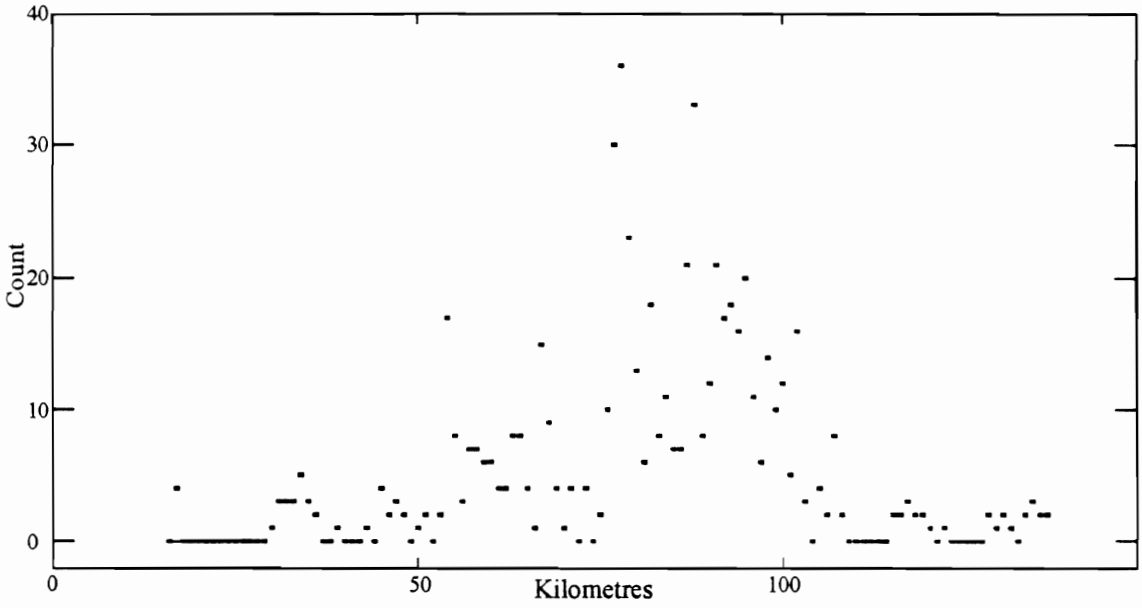

(b)

Figure 4.5. Diagram showing (a) the location of mineralization in the Troodos ophiolite and (b) a profile of this mineralization.

f_x is the series in the space domain,

n is the number of elements in the frequency data series, and

N is the number of elements in the spatial data set.

The power spectrum was calculated by the maximum entropy method using the expression (from Press et al., 1986):

$$P_f \approx \sum_{j=-M}^{M} \phi_j z^j \qquad (4.2)$$

where $z \equiv e^{2\pi i f\delta}$,

$$\phi \equiv \langle f_i f_{i+j} \rangle \qquad j = ...-3,-2,-1,0,1,2,3,...,$$

$$\approx (1/N+1-j) \sum_{i=0}^{N-j} f_i f_{i+j} \qquad j = 0,1,2,...,N,$$

$f\delta$ is the spacing of points in the frequency domain,

f_i is the data series,

N is the number of elements in the data series, and

M is the number of points to be calculated in the frequency domain.

Fourier series can only be used to approximate continuously varying data. The mineralization location data series used here are similar to continuously varying data as they are averages over each easting kilometre. Nevertheless the data is not strictly continuously varying: mineralization is either present or not. It was feared that this would cause some errors in the analysis.

Walsh functions are similar to Fourier series except that they use rectangular waveforms instead of sine and cosine waves. They are thus more appropriate in approximating episodic data such as the mines and mineralization data series. Walsh Transforms are used in a similar manner to Fourier Transforms (Beauchamp, 1975).

The analysis was repeated using an available Walsh Transform computer program (Huang, 1991). Only the complete mineralization data set was used. A data series was constructed by assuming an average width for each mineralization occurrence (100 and 300 metres were tried). The series was constructed in the east-west direction and amplitudes of +1 were assigned if mineralization was present and -1 if not. The data set was rotated by zero and twenty degrees to correct for the rotation of the ophiolite based on experience from the Fourier analysis

Results

Results were generally disappointing. Power spectra are shown in figures 4.6, 4.8, 4.9 and 4.10. These uniformly show a concentration of power in the lower frequencies representing the overall extent of the data. Little information is present in higher frequencies which would represent regularity within the data set.

The Fourier spectrum does show small peaks at wavelengths of approximately 12, 5 and 3.5 kilometres (figure 4.6). The much higher first point

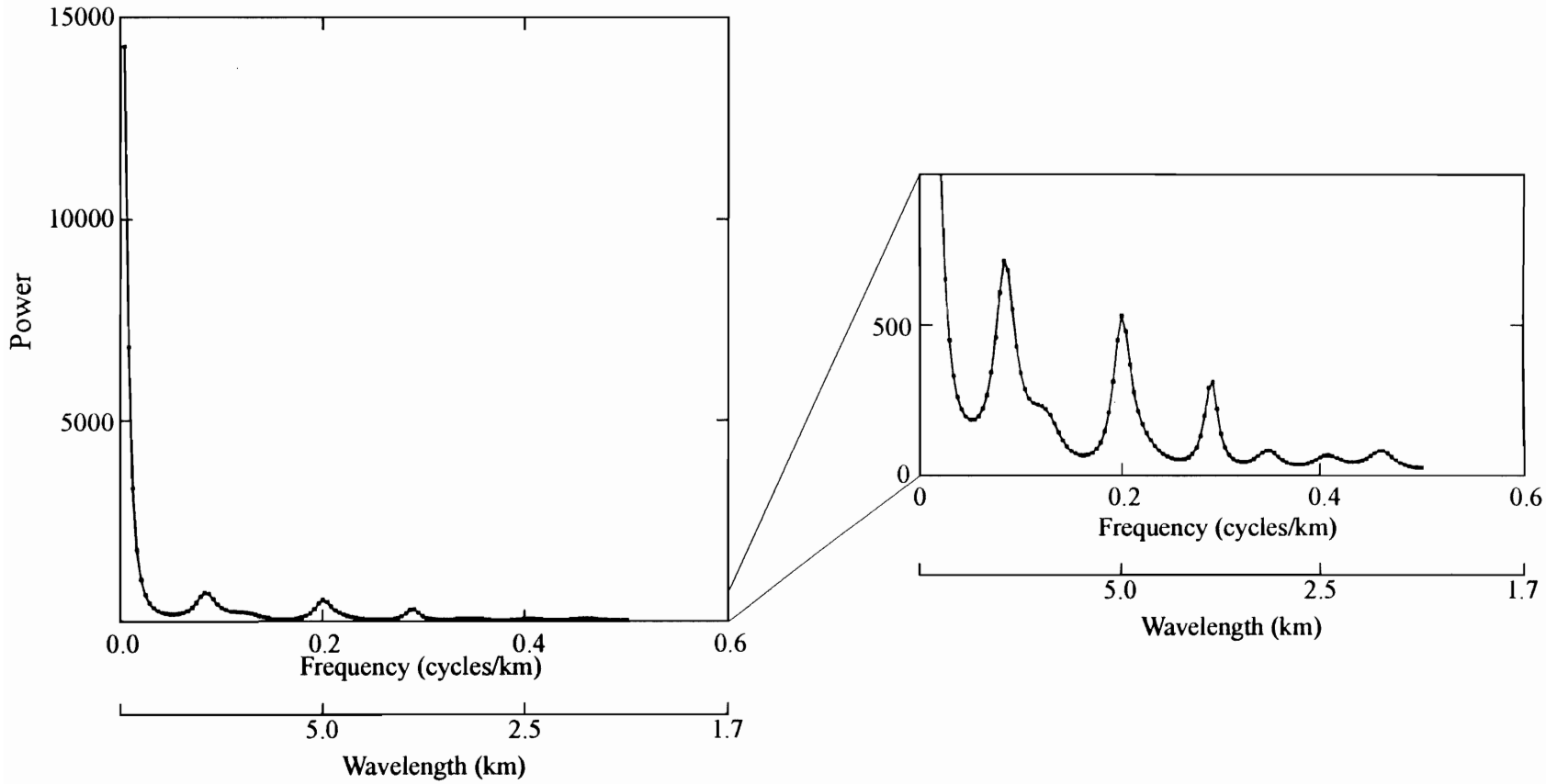

Figure 4.6. Power spectrum of the east-west distribution of mineralization in the Troodos ophiolite.

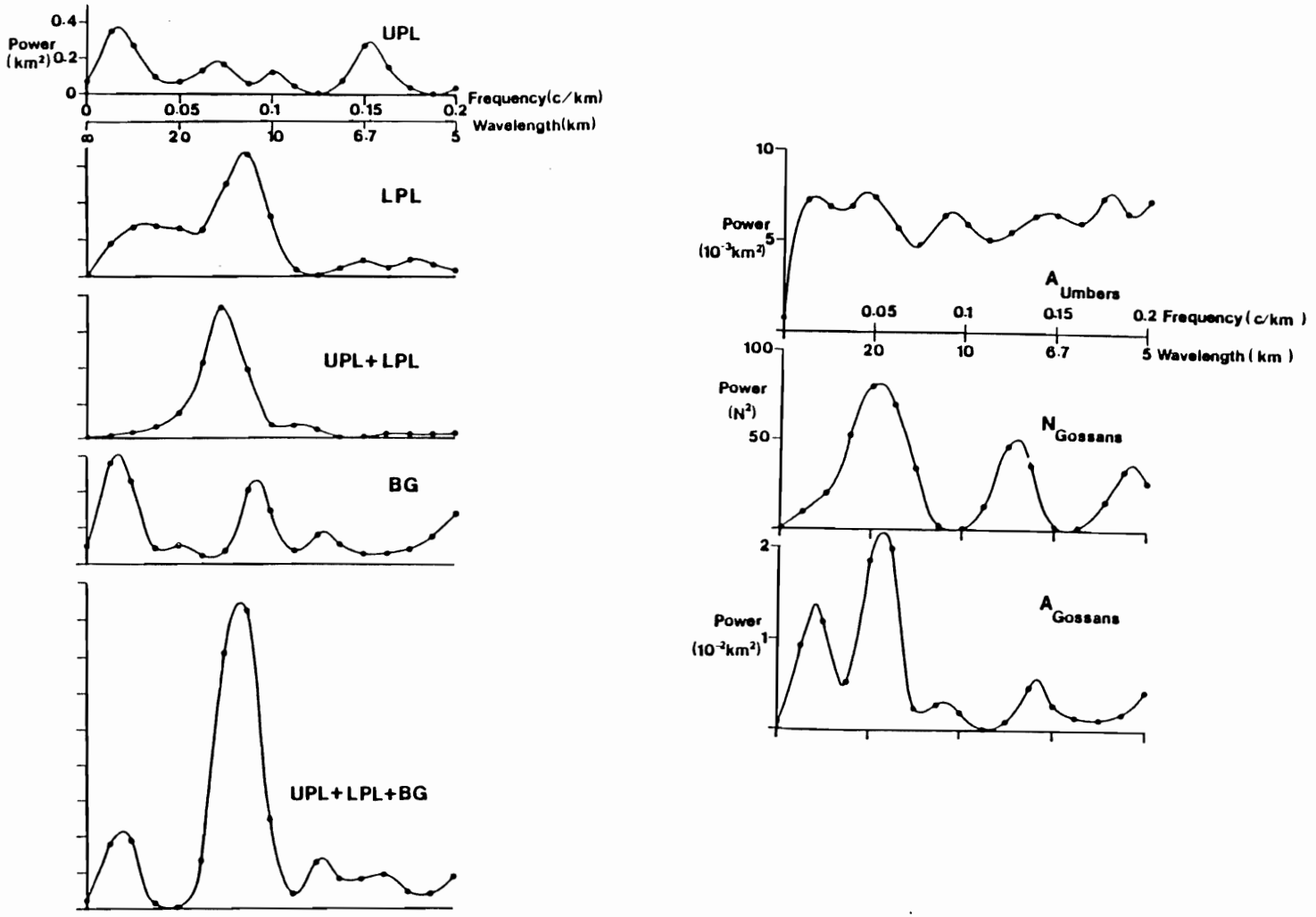

Figure 4.7. Power spectra of features on the northern flank of the Troodos ophiolite. UPL and LPL - pillow lava units which are subdivisions of the Extrusives, BG - Basal Group, A Umbers - area of umbers, N Gossans - number of gossans, A Gossans - area of gossans. From Hall et al. 1989.

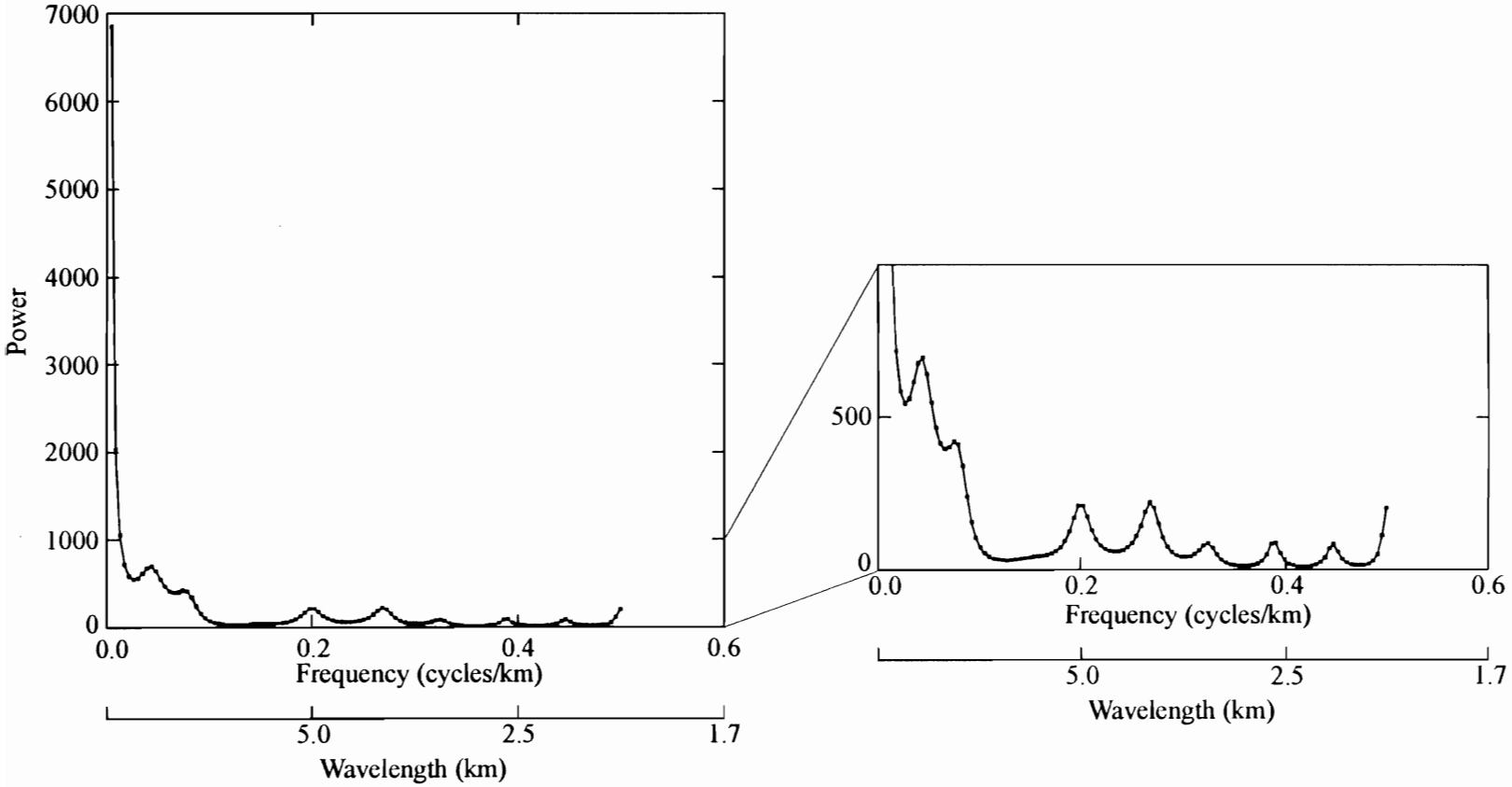

Figure 4.8. Power spectrum of the mineralization data set rotated twenty degrees counterclockwise.

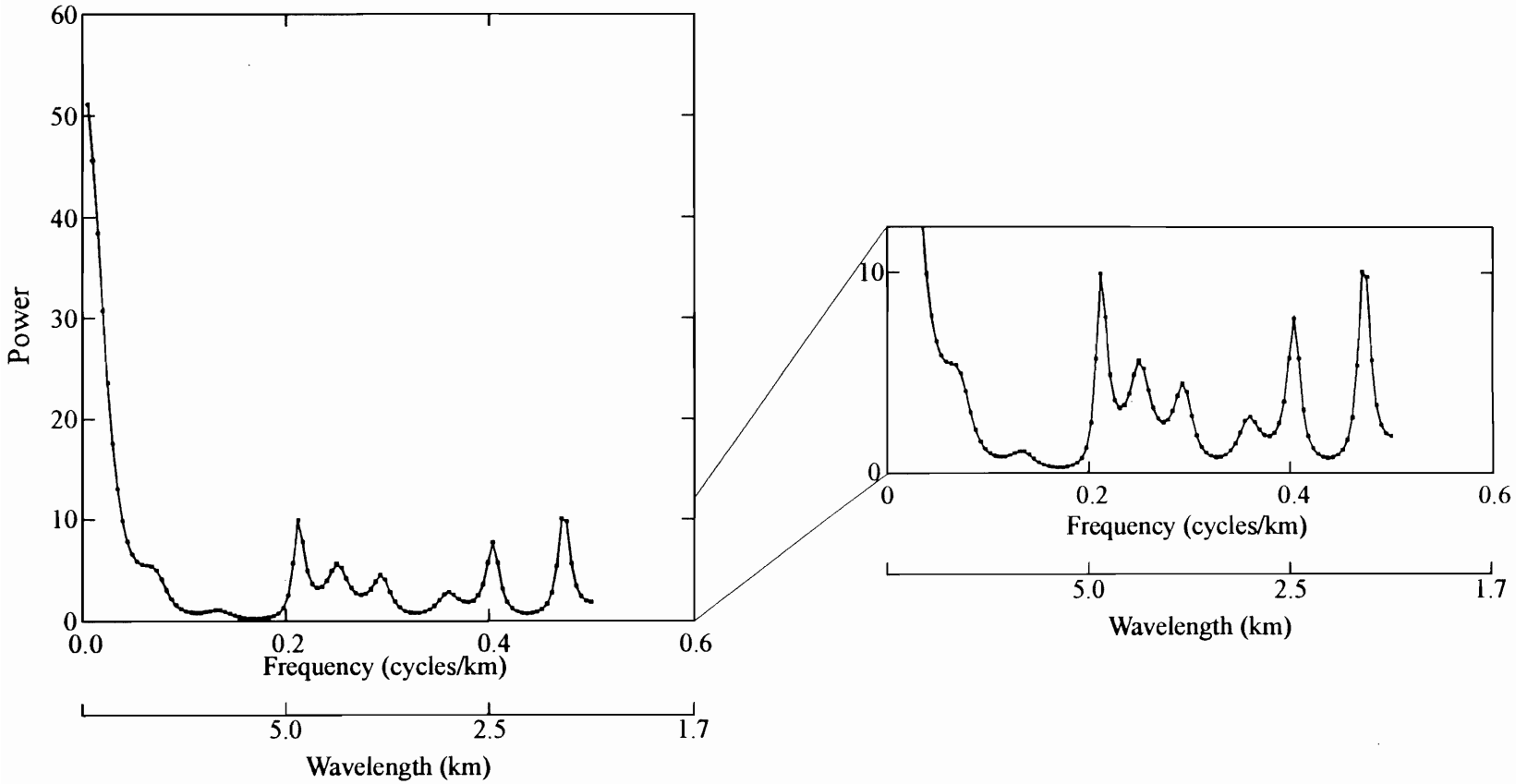

Figure 4.9. Power spectrum of the east-west distribution of mines only in the Troodos ophiolite.

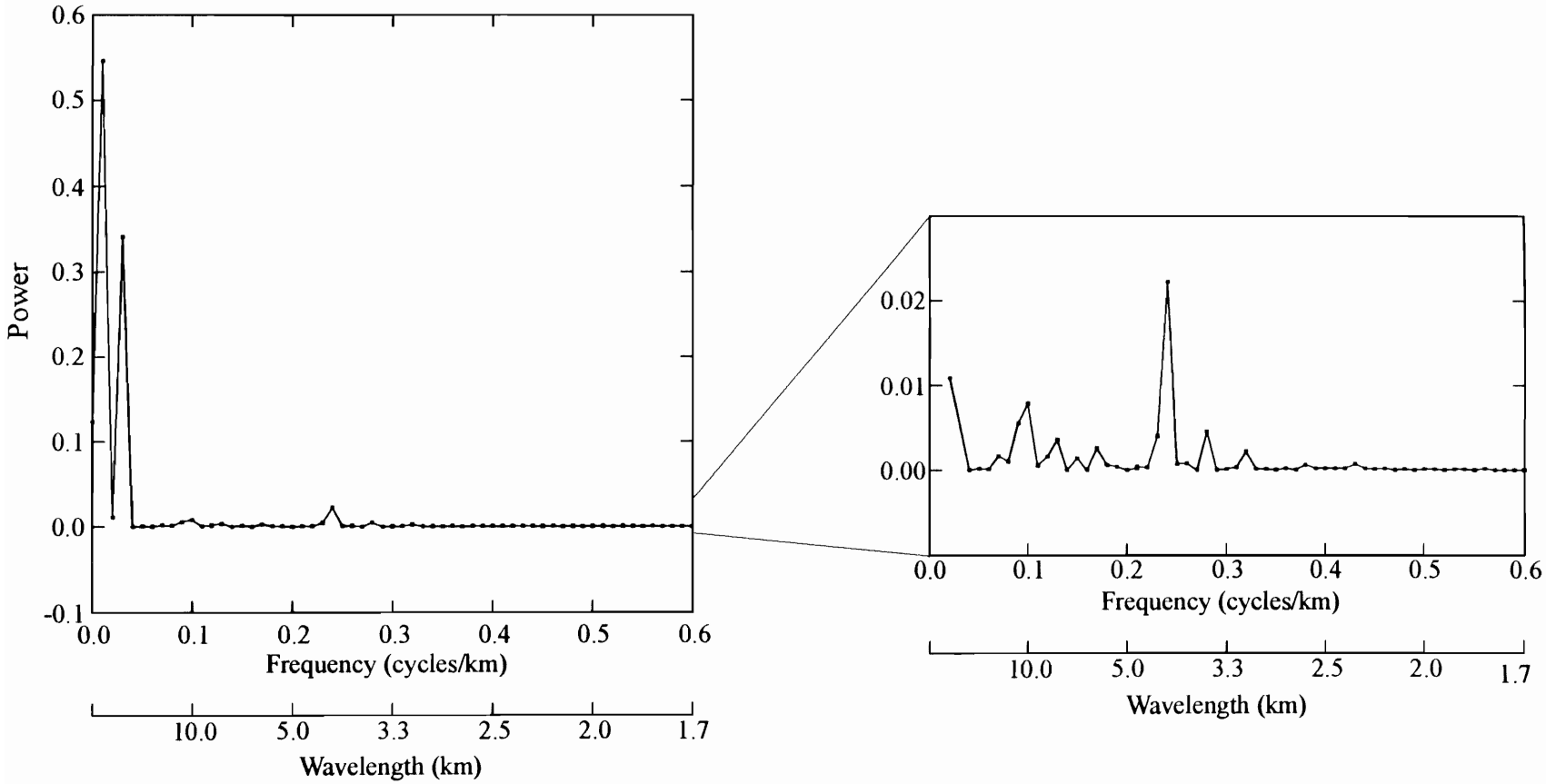

Figure 4.10. Walsh power spectrum of the east-west distribution of mineralization in the Troodos

in the spectrum is due to the average level of the data and could be lowered by subtracting an average value from each point in the data series. The remainder of the lowest frequency peak is due to the "half wave" or single peak shape of the data series. The smaller size of the shorter wavelength peaks indicates a lack of periodicity in the data. By comparison, the spectra in Hall et al. (1989) (figure 4.7) show a much greater proportion of the total power in the higher frequencies and a significant peak at approximately twelve kilometres.

Rotation of the data set (figure 4.8) has the predictable effect of very slightly decreasing the wavelength at which some peaks occur. Unfortunately, no enhancement of the power spectrum was created by the rotation.

A similar analysis of only the mine locations, involving some 41 ore bodies throughout the extrusive units of the ophiolite, is lacking a significant peak in the region near twelve kilometres wavelength (figure 4.9). Most power is again concentrated in the long wavelength part of the spectrum with scattered peaks at less than five kilometres wavelength. Due to the much smaller number of locations than that in the all mineralization data set, the power is much less and more noise may be expected.

The Walsh power spectrum (figure 4.10) has a very small peak at about ten kilometres wavelength, but it is almost lost in the baseline. A slightly larger peak is evident at about 4 kilometres wavelength but, as with the Fourier spectra, it represents a small fraction of the power.

This indicates that very little regular variation is evident in this data set.

While this may be due to a lack of fundamental arrangement, it is possibly also due to the small size and lack of completeness of the data set. Ancient mines have been abandoned and forgotten while other bodies are as yet undiscovered. The designation of mineralization as mine, prospect or gossan is arbitrary, determined by economic and other factors. In addition, uplift and erosion have imposed their own pattern on the data which may excessively bias the original distribution. These factors may combine in statistical errors that overwhelm any signal.

The apparent arrangement seen in mineral maps such as figure 4.1 may be artificial. In addition to the somewhat arbitrary classification of mineralization, the exploitation of mineral bodies may have been concentrated into districts based more on the cost of shipping ore than geographical or geological distribution. The more complete total mineralization data set, which gives equal weight to smaller bodies and gossans and gains better coverage and increased numbers, may destroy the district pattern.

The minor peak at about twelve kilometres wavelength seen in all spectra, including that of Hall et al. (1989) and excepting the mines-only data set, probably indicates weakly developed, regularly occurring features. It is most evident in the limited area of the northern flank and less so in the spatially larger data set.

This cannot be considered as a final definitive spatial analysis of the location of mineralization in the Troodos. Other methods of analysis could be used to analyze the location of mines and mineralization. Cluster analysis,

autocorrelation and other spatial analysis methods might be considered in addition to the Fourier and Walsh analysis.

However, given the limited results in the above study, it is considered to be unlikely that these methods will find regular variation in the east-west dimension. In this case (ie. parallel to the spreading direction) it would seem that the mines and mineralization in the Troodos are not regularly distributed and occur at random intervals.

Chapter 5

Discussion and Conclusions

Discussion of models

In chapter three, three possible scenarios were developed and tested to model the aeromagnetic field in the Kambia study area. The three models are variable magnetization, variable depth of strong magnetization and strongly magnetized bodies at depth. It remains to be discussed which of these are reasonable and likely models of the geology in view of local constraints and general models of hydrothermal circulation in the oceanic crust.

Variable magnetization model

The variable magnetization model accounts for the aeromagnetic anomalies by having a pattern of magnetization in the surface rocks. The model developed to simulate this assigns values of two to ten amperes/metre in the Extrusives and one ampere/metre in the Basal Group.

A cursory glance at the aeromagnetic data indicates that on a coarse scale this model must be important. The anomalies over the Basal Group and Sediments are weaker and broader. The magnetization in samples from the Basal Group is correspondingly smaller.

Several examples of local mineralization coincide with local aeromagnetic

lows. For example, the Kambia mine corresponds spatially to a small aeromagnetic low (figure 5.1a). These anomalies are reasonably expected when a flight line directly crosses non-magnetic ore and gossan material surrounded by strongly magnetic basalt.

While some mines do, as expected, coincide with local aeromagnetic lows, many do not. On such example is the Kaphedes mine (figure 5.1b). The absence of a low may result from missing data between flight lines. Alternately, the stockwork feeding the circulating hydrothermal fluid to the ore body may not directly underlie the body. Bear (1963) observed several cases where the ore forming fluid had travelled laterally in the vicinity of ore bodies. In an area such as Kambia numerous sheet flows would reduce the permeability normal to the flows and channel fluids parallel to the flows.

The magnetization of samples within the Extrusives shows a range of 0.01 to 77.5 amperes/metre. The average magnetization is 8.55 amperes/metre with one standard deviation of 10.24 amperes/metre. The range in sample values is much greater than that within the model.

However, the sample magnetization within the Extrusives does not appear to occur in any pattern. It certainly does not occur in a pattern which matches that of the magnetization within the model. With the available sample coverage, it is unlikely that this pattern would be missed. The average magnetization in the centre low (12.82 amperes/metre) is greater than that in either magnetic high (7.27 and 5.45 amperes/metre).

(a) Kambia

(b) Kaphedes

Figure 5.1. (a) Magnetic low coincident with the Kambia mine. (b) The Kaphedes mine. No local magnetic low is present. Modified from Hunting Geology and Geophysics Ltd, 1969. Scale is approximately 1:39,500. North is up.

The variable magnetization model obviously applies in some situations in the Kambia area, particularly in the Basal Group - Extrusives - Sediment magnetization contrast. It is likely to be a factor in the immediate area of some, but not all, mines and gossans. No systematic variation in rock magnetization, however, corresponds to the larger highs and lows in the magnetic field over the Extrusives.

Variable depth model

The variable depth model accounts for the anomalies within the Extrusives by varying the thickness of a strongly magnetized (ten amperes/metre) layer that outcrops at the surface. This layer is modelled as being underlain by a less magnetic (one ampere/metre) base. The magnetization of the weakly magnetic Basal Group and non-magnetic Sediments is similar to that in the variable magnetization model.

This model is more consistent with the lack of a pattern in the magnetization observed in surface samples. There is no requirement for higher surface magnetization in the area of aeromagnetic highs and lower magnetization in the area of aeromagnetic lows.

Since the erosional surface corresponds to a cross section through the Extrusives, we would expect the two magnetic highs to persist across the exposure. The central low should intensify to the south near the Basal Group where the high magnetization surface layer becomes thinner. This is generally observed to

be the case. For the same reason, we would expect lower sample magnetizations deeper in the Extrusives in the area of the central low. This is not seen. This may be due to the sample distribution which includes only a few samples from this subarea (overlay 3 on figure 3.3).

This lack of a low in the sample magnetization deeper in the section may be due to the way magnetization is distributed in the outcrops in the subarea. Most of the Basal Group and the lowest Extrusives are uniformly weakly magnetized. However, the Basal Group is very much a transition zone between the Sheeted Dikes and the Extrusives. The contact of the Basal Group with the Extrusives above is also gradational. Because of this there can be strongly magnetized dikes and sheet flows within the upper Basal Group and lowest Extrusives. These strongly magnetized units may be over-represented in the small set of samples from this sub-area.

It may be that the exposure-based cross section, in not being vertical, includes a variety of different geological situations instead of being a simple depth profile through a layer cake sequence (figure 5.2). In these circumstances, if features are not elongated perpendicular to the spreading direction, moving south through the ophiolite from the Sediments would sample a variety of different geological and therefore magnetic situations. The geological situation responsible for the magnetic low may not be continuous and thus may not be exposed at the surface.

This situation may also explain the position of the Basal Group boundary

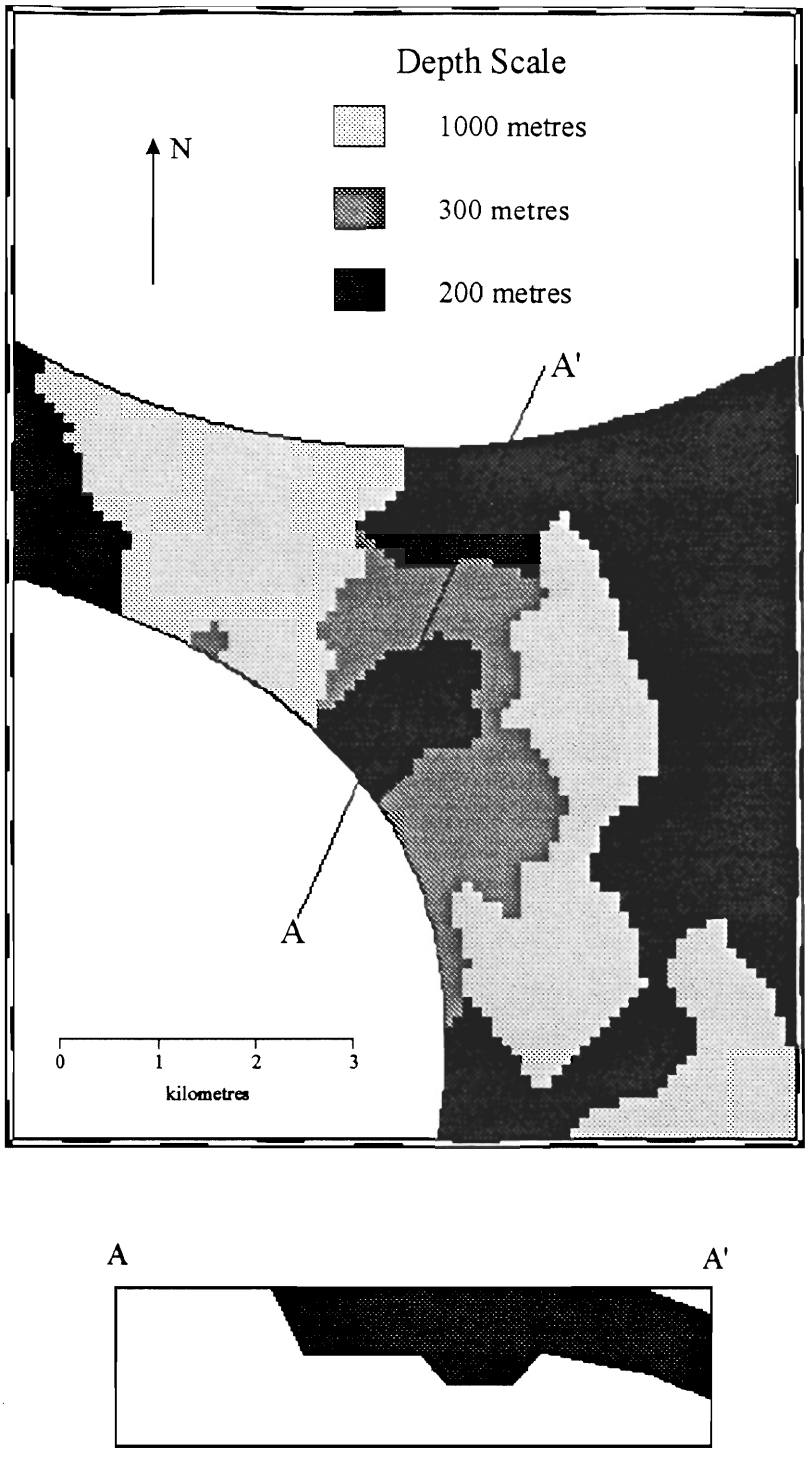

Figure 5.2. Hypothetical cross section across the area of the middle aeromagnetic low showing how the geology of a variable depth model may not be a simple layered structure and may vary across the section.

in the model. On the basis of the southern limit of strong aeromagnetic anomalies, it was necessary to move this boundary further south than originally located in the maps accompanying the Geological Survey Department of Cyprus memoirs. The contact is gradational and is usually mapped approximately. Also, the magnetic boundary may not be exactly co-located with the geologic contact. Such relocation was justified on the basis of sample magnetization, which show higher values further south than the originally mapped Extrusives-Basal Group boundary. Finally, the southward relocation was required to create a significant thickness for the strongly magnetized Extrusives in the southern areas of the aeromagnetic highs.

Strongly magnetized bodies at depth in the Extrusives

This model has a uniform surface magnetization of ten amperes/metre underlain by the Basal Group at one ampere/metre. The large highs are created by relatively small, strongly magnetized (forty amperes/metre) bodies deep in the Extrusives. As the Extrusives thin to the south, these bodies would, if continuous, appear at the surface.

This model has been included as it can account for the aeromagnetic anomalies and does not conflict with any geological evidence. The model is consistent with the sample magnetization as it has no pattern at the surface, with one possible exception. That is, there are a few very high values of magnetization (eg. 77.5 and 68.8 amperes/metre) deep in the Extrusives near the Basal Group contact. These could indicate the local occurrence of very strongly magnetized

material deep in the Extrusives. These very few values could, however, be equally well caused by lightning strikes or other spurious methods of acquisition of magnetization. One of the highly magnetic samples was collected from an exposed hillside where such events are possible. The topographic situations at the locations of the other highly magnetic samples are not known. These samples are the only evidence from the Kambia area suggesting such a model.

Hall et al. (1991b) reported some similar very high magnetization values from samples in drill core from the northern flank of the Troodos. They were interpreted to represent the freshest remnant of original lava that was least affected by alteration processes. The upper limit of sample magnetization values increased with depth, which was interpreted to be due to a decrease in low temperature alteration with depth. The high magnetization values ended abruptly at the depth where high temperature alteration increases.

The highest magnetization values from deep in the Kambia section may be due to the same mechanism. They are above the depth of regional alteration and deep enough to have avoided much of the low temperature alteration. It does not follow that the very high values are concentrated in bodies at the base of the Extrusives.

An alternate explanation for higher magnetization at depth would be higher concentrations of unaltered dikes. Promontories in the 25 and 50 per cent dike contours suggest that more dikes may be present in the regions of the aeromagnetic highs. Where they protrude above the Basal Group, they may

retain strong magnetization and form bodies of higher magnetization. Why they would be more strongly magnetized than the surrounding Extrusives is unclear.

It is also unclear how this model would be compatible with models of hydrothermal circulation. In theoretical studies, the shape and position of circulation cells are primarily determined by the locations of heat sources which provide the energy (Spooner, 1977). If discrete heat sources are present they should create upwelling areas, which are the discharge limbs of the cells. If the dikes either provide the energy, or, as seems more likely, reflect highs in the surface of the underlying gabbros, why do the discharge sites, marked by the mines and mineralization, then preferentially concentrate between the highs?

By these arguments, this is the least likely mechanism to account for the aeromagnetic anomalies. From discussion of the actual evidence, it would seem that hydrothermal circulation generally thinned, by alteration of the lowest part, the strongly magnetized layer in the vicinity of the central low and caused localized lows in some areas of mineralization. Thus, a situation like the variable depth model is most likely the source for most of the aeromagnetic field anomalies in the Kambia area.

Discussion of the general distribution of magnetization on the northern flank of the Troodos ophiolite

The aeromagnetic survey covers most of the northern and eastern

exposures of the Extrusives of which the Kambia detailed study area forms only a small part. As the available dike percentage and pillow to sheet flow ratio data (Hall and Yang, 1994; Yang, 1991) are limited to the northern flank, only this area will be considered here. The question considered here is to what extent do the results from the Kambia area apply to the larger area?

The aeromagnetic survey in this area is shown in figure 5.3 with the geology added from the Geological Survey Department of Cyprus (1982). In the western and central sections of this figure, the geology is a fairly simple layered arrangement. In the eastern section the anticlinal structure becomes less pronounced and the layered arrangement is not apparent at the surface.

Generally, as in the Kambia area, the strongest anomalies occur in the area of the Extrusives. In the Sediments to the north the anomalies are weaker and broader, indicating that their sources are more deeply buried. The few stronger anomalies may indicate shallow or stronger sources. To the south the Basal Group is also quieter magnetically which is consistent with the weaker magnetization seen in the sample measurements discussed earlier.

While the Sediment/Extrusive contact is not always associated with aeromagnetic highs, the strongest, broadest highs are at or just south of this boundary. Strong highs located deeper in the section (ie. further south) tend to be smaller in areal extent. This confirms the variable depth model from the Kambia area where strongly magnetized material is generally present at the surface, but only extends to the base of the Extrusives in more limited areas.

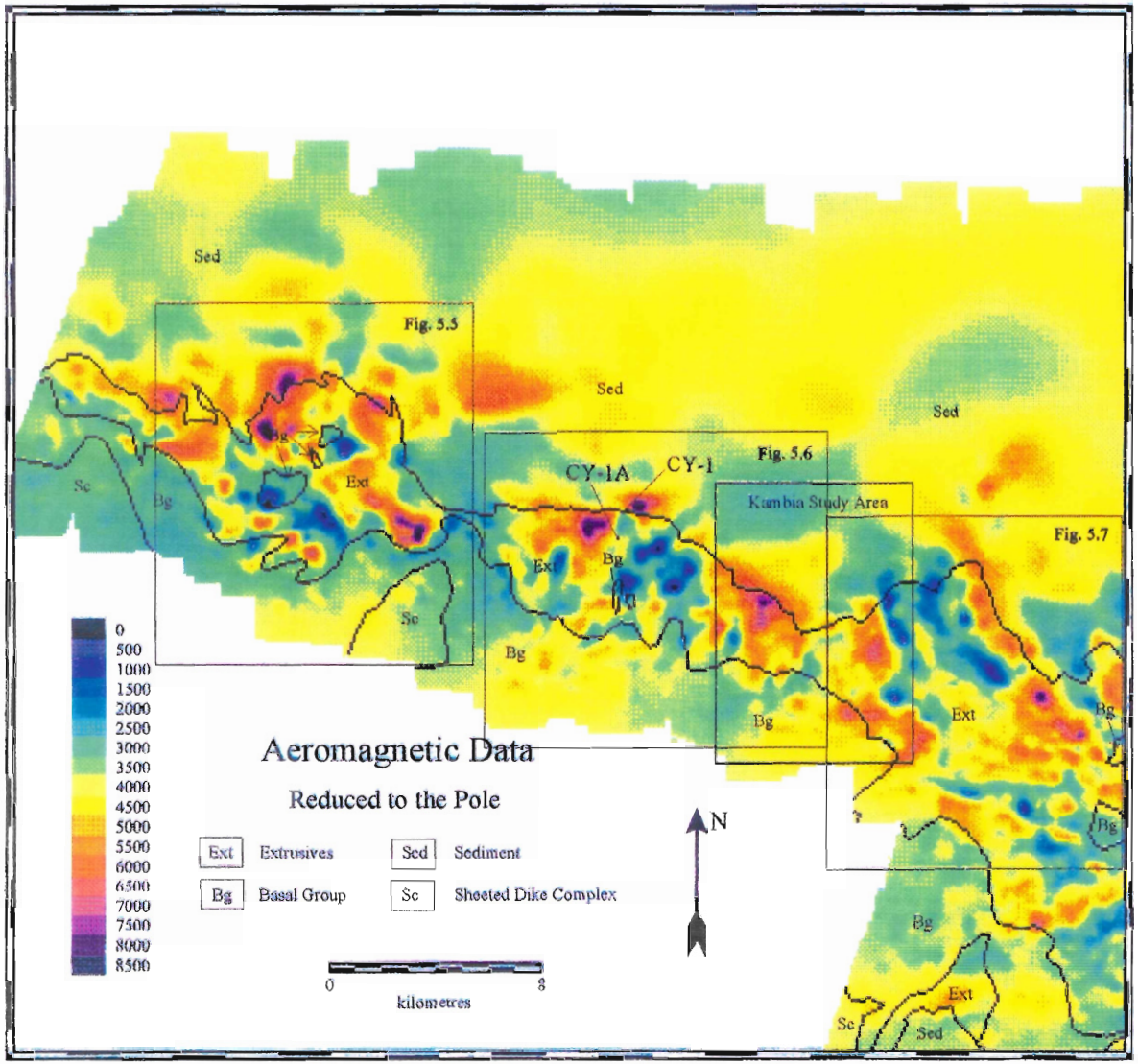

Figure 5.3. The geology and reduced-to-the-pole aeromagnetic field of the northern flank of the Troodos ophiolite.

The pattern of dike percentage (overlay 9 on figure 5.3) from Hall and Yang (1994) tends to match that of the geology. However, on the scale of the northern flank, it is unclear how the pattern of pillow to sheet flow ratio (overlay 10 on figure 5.3) from Yang (1991) might match geological features.

Two drill holes were drilled during the 1980's to investigate the nature of the Extrusives on the northern flank of the Troodos (Robinson, 1991). The locations of holes CY-1 and CY-1A are shown on figure 5.3. Magnetic properties were measured on samples from the holes (Hall et al., 1991b) and we can compare the profiles of magnetization with depth to the aeromagnetic field in the area.

Hole CY-1 was located on the edge of a prominent magnetic high near the Sediment/Extrusives contact. It penetrated approximately 475 metres into the Extrusives. Sample magnetizations (figure 5.4) were generally high but variable, and the variability increased with depth. Very high values were still present at the bottom of the hole (63.8 amperes/metre at 434 metres depth, 5.4 amperes/metre at 435 metres depth, for example). This indicates that the strongly magnetized layer was at least 475 metres thick in this area.

Hole CY-1A was located approximately one kilometre south of the CY-1 hole in an area of moderate magnetic field strength just to the south of a small magnetic low. The hole was 701 metres deep. Samples from the upper part of the hole again show the same high but variable magnetization as the strongly magnetized Extrusives at Kambia (figure 5.4). Below about two hundred metres

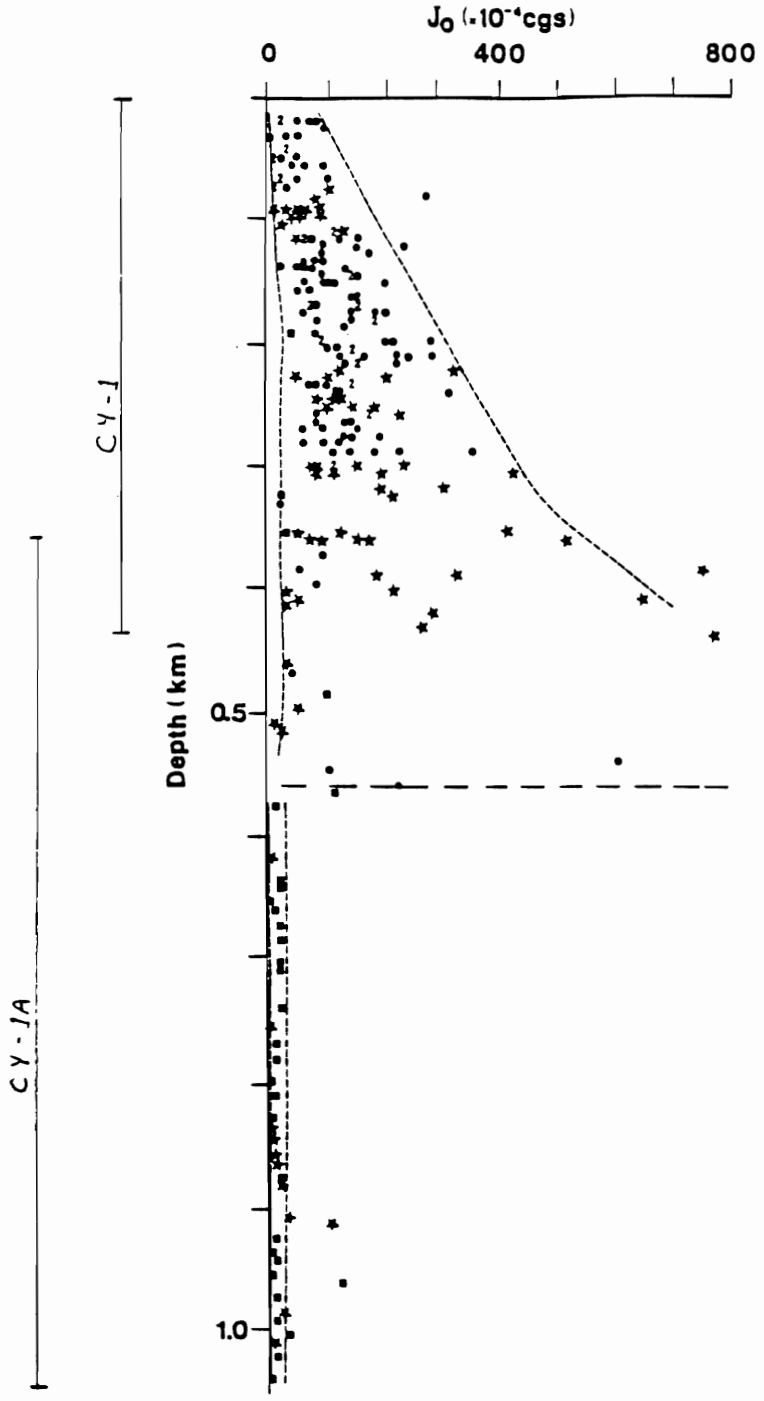

Figure 5.4. A profile of remanent magnetization from the Cyprus Crustal Study Project drillholes CY-1 and CY-1A (from Hall et al., 1991b).

depth the magnetization suddenly drops to values in the order of one ampere/metre. This two hundred metre thickness corresponds to the lower end of the range of thicknesses for intermediate magnetization areas in the Kambia area variable thickness model.

This profile is comparable to the Kambia surface samples. The sample magnetizations are higher and variable in the upper section. Below a single depth they drop suddenly to consistently low values. The highest values and greatest variability are just above this level.

Detailed sub-areas on the northern flank of the Troodos ophiolite

To consider the northern flank aeromagnetic survey in more detail a sub-area was chosen from each of the western, middle and eastern sections. These are shown in figures 5.5, 5.6 and 5.7 respectively.

In the west, strong positive anomalies outline the periphery of a thicker section of Extrusives (figure 5.5a). The centre of this area has been mapped as having three inliers of Basal Group. These again coincide roughly with magnetic lows. Areas of higher dike percentage (figure 5.5b) match these magnetic lows as well. Areas of more abundant sheet flows (from Yang, 1991), marked as 25 per cent or less pillowed flows in figure 5.5c, correspond to a magnetic low and part of a high.

In the middle sub-area, two small outcrops of Basal Group are found just to the south of a large low (figure 5.6a). As they are not exactly coincident with

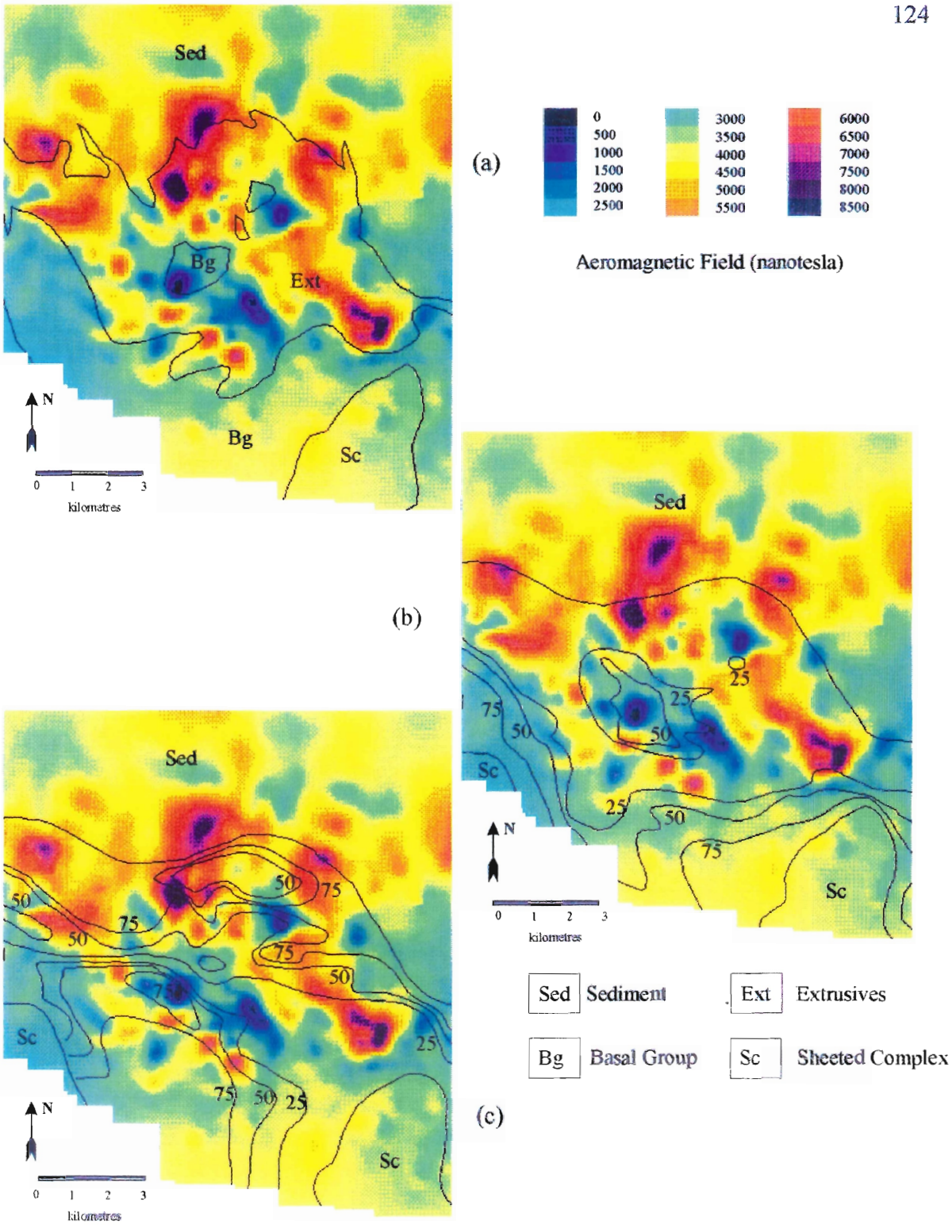

Figure 5.5. A section of the western part of the RTP aeromagnetic survey on the northern flank of the Troodos ophiolite showing (a) the geology, (b) the dike percentage and (c) the pillow/sheet flow ratio.

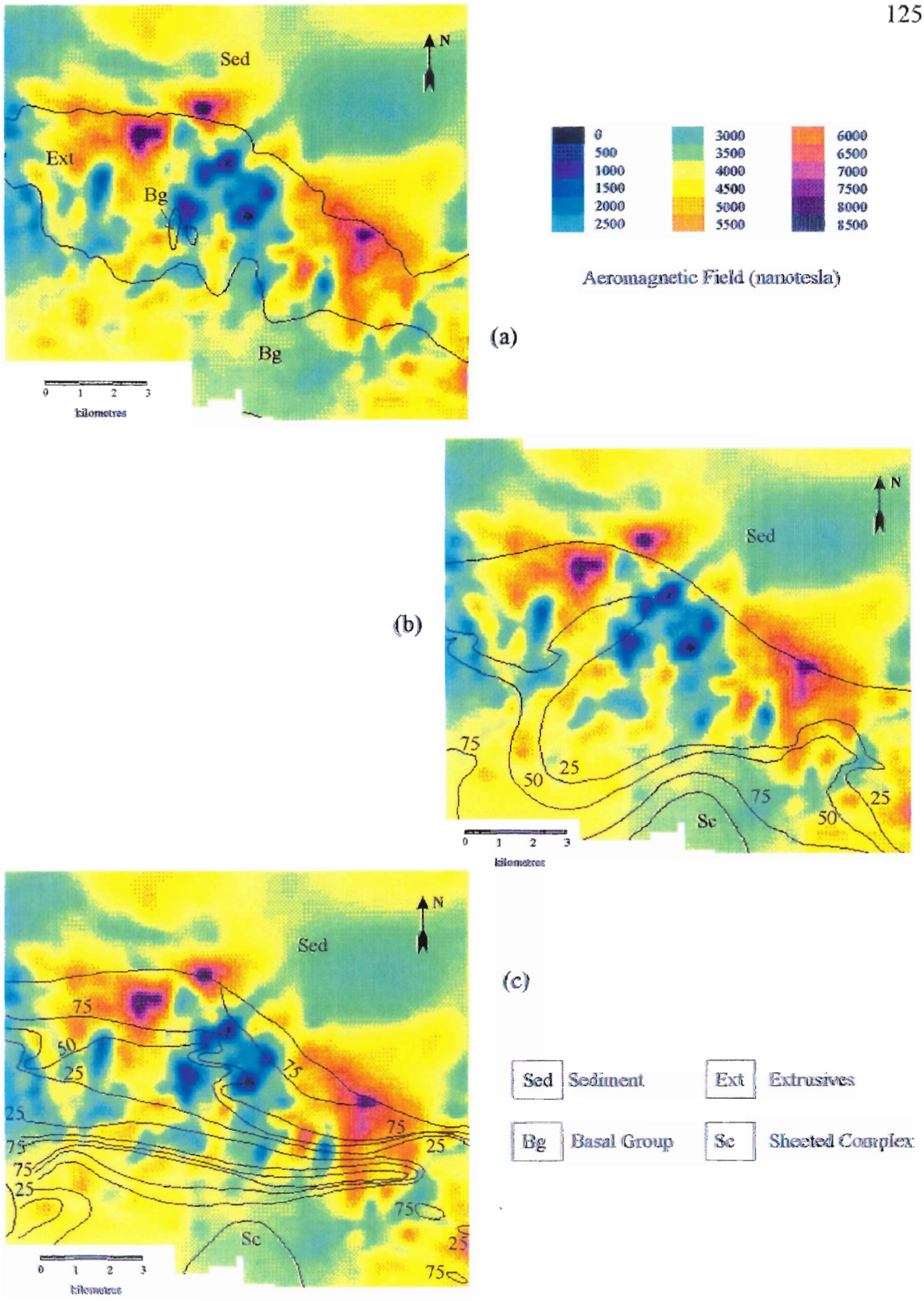

Figure 5.6. A section of the middle part of the RTP aeromagnetic survey on the northern flank of the Troodos ophiolite showing (a) the geology, (b) the dike percentage and (c) the pillow/sheet flow ratio.

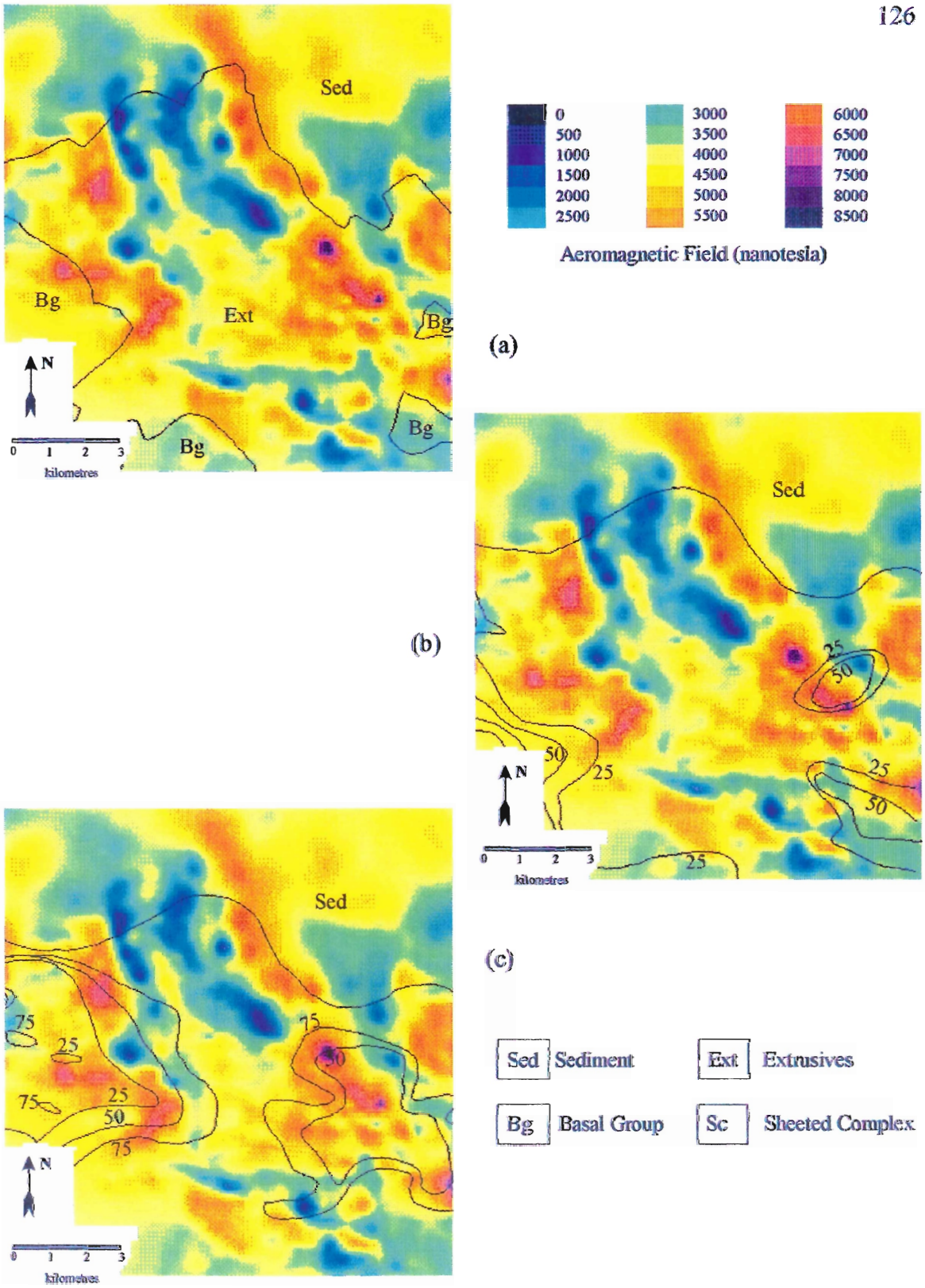

Figure 5.7. A section of the eastern part of the RTP aeromagnetic survey on the northern flank of the Troodos ophiolite showing (a) the geology, (b) the dike percentage and (c) the pillow/sheet flow ratio.

the low it may not be appropriate to correlate them with certainty. A promontory of 25 percent dikes (figure 5.6b) is similarly partially coincident with this magnetic low. The contours of pillow to sheet flow ratio form a sinusoid pattern in the area of this low (figure 5.6c). There is little other correlation between this ratio and the magnetics.

In the east, inliers of Basal Group material visible on the eastern edge of figure 5.7a are again coincident with magnetic lows. The pattern of aeromagnetic anomalies is not obviously related to geological features, which have lost the more regular cross sectional pattern present further west. Outcrops of higher dike percentage (figure 5.7b) are not obviously related to the magnetics. An area dominated by pillow lavas in the centre of figure 5.7c is roughly coincident with a large area of magnetic lows.

Mineralization in the form of mines, prospects and gossans (figure 5.8) does not seem to be associated with a particular area, although it does seem to be more common deep in the Extrusives. This is as was found in Hall and Yang (1994). Mineralization is generally not found in the strong magnetic highs, but it may be found on their periphery as in the Kambia area.

To test the reliability of this relationship, histograms of the number of mineralization occurrences for each level of aeromagnetic field are shown in figure 5.9 for the entire area of the aeromagnetic survey. A histogram showing the number of grid points in the survey for each aeromagnetic field level is shown at the bottom of the figure for comparison. When allowance is made for the

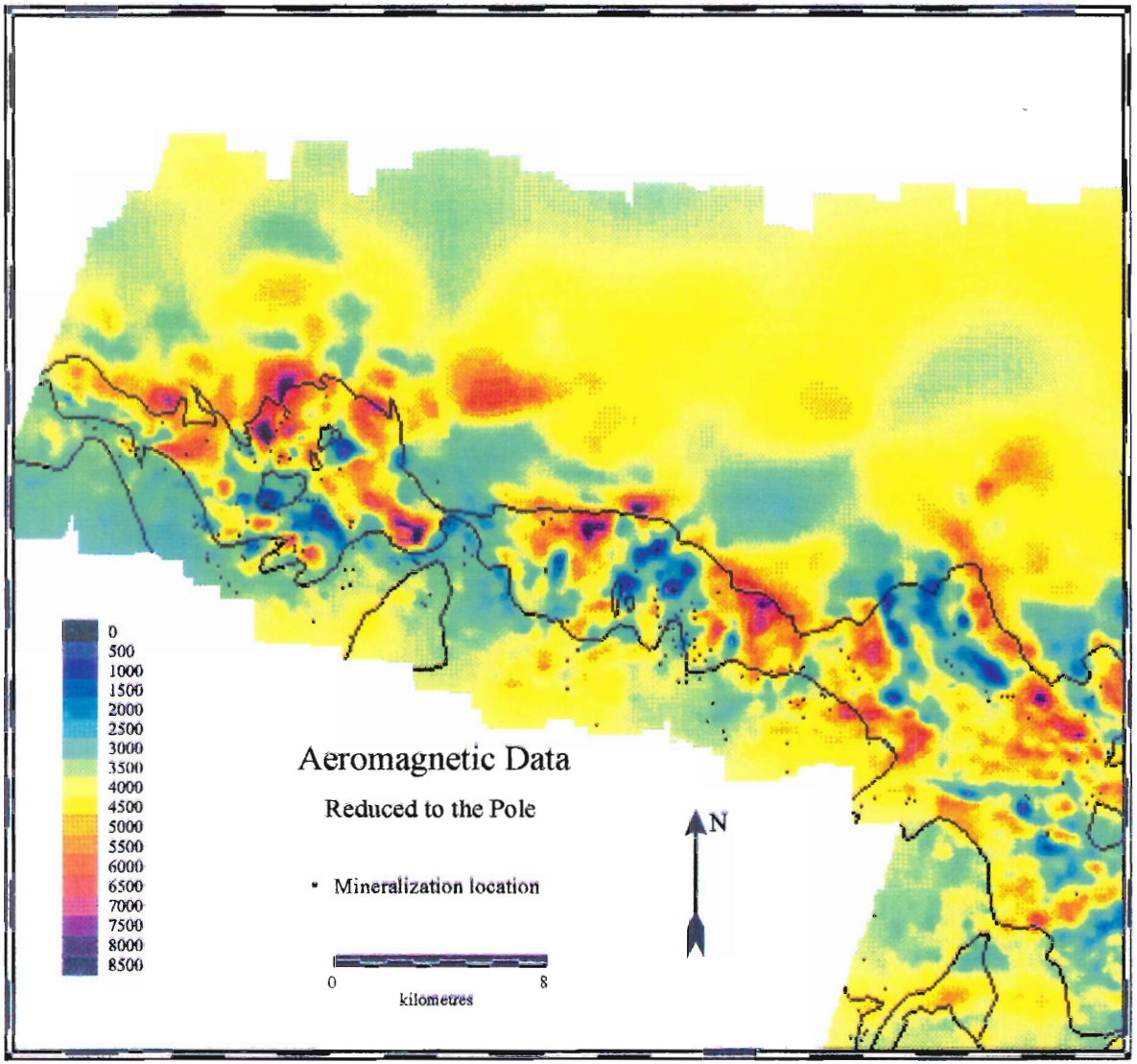

Figure 5.8. Mines, prospects and gossans on the northern flank of the Troodos ophiolite.

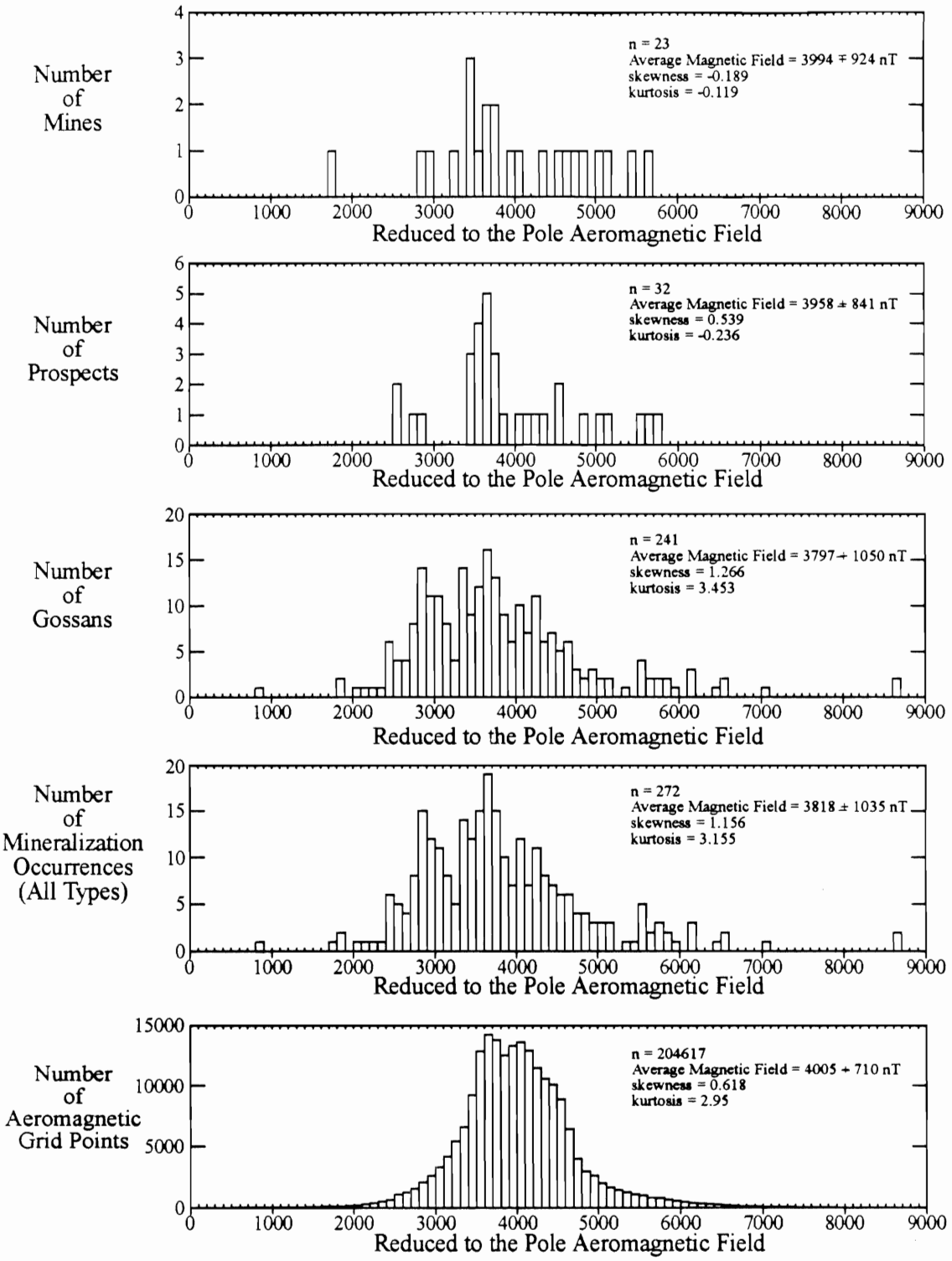

Figure 5.9. Histograms showing the number of mineralization occurrences for different levels of reduced to the pole magnetic field in the area of the aeromagnetic survey in the Troodos ophiolite. The bottom histogram shows the number of aeromagnetic survey grid points at each level for comparison.

difference in numbers of points, all of the histograms show a similar distribution. Thus the absence of mineralization from areas of higher magnetic field values is not necessarily due to their exclusion from these zones, but may be due to their smaller area.

A similar series of histograms is shown in figure 5.10. In these cases only the Extrusives on the northern flank of the ophiolite have been used as this is where most of the strong magnetic highs are concentrated (figure 2.4). The northern Sediments have been excluded as they contain no mineralization. The Basal Group has also been excluded as it contains no strong magnetic anomalies and very few mines.

The distribution of aeromagnetic grid point values (bottom histogram) is symmetrical and unimodal and is centred at about four thousand nanotesla. The histogram of all mineralization and that of gossans only (middle and second from the bottom, respectively) show a bimodal distribution. The higher peak in each histogram is similar to the peak for the entire survey and may thus reflect the distribution of the points in the survey. The lower peak, at about 2800 nanotesla, suggest that at least some mineralization is concentrated at lower aeromagnetic values. The interval between 2400 and 3200 nanotesla contains approximately 28 percent of the mineralization but represents less than 16 percent of the survey grid points. This bimodal distribution is not convincingly present in the mines or prospects histograms (top and second from the top, respectively), perhaps due to the much smaller number of cases.

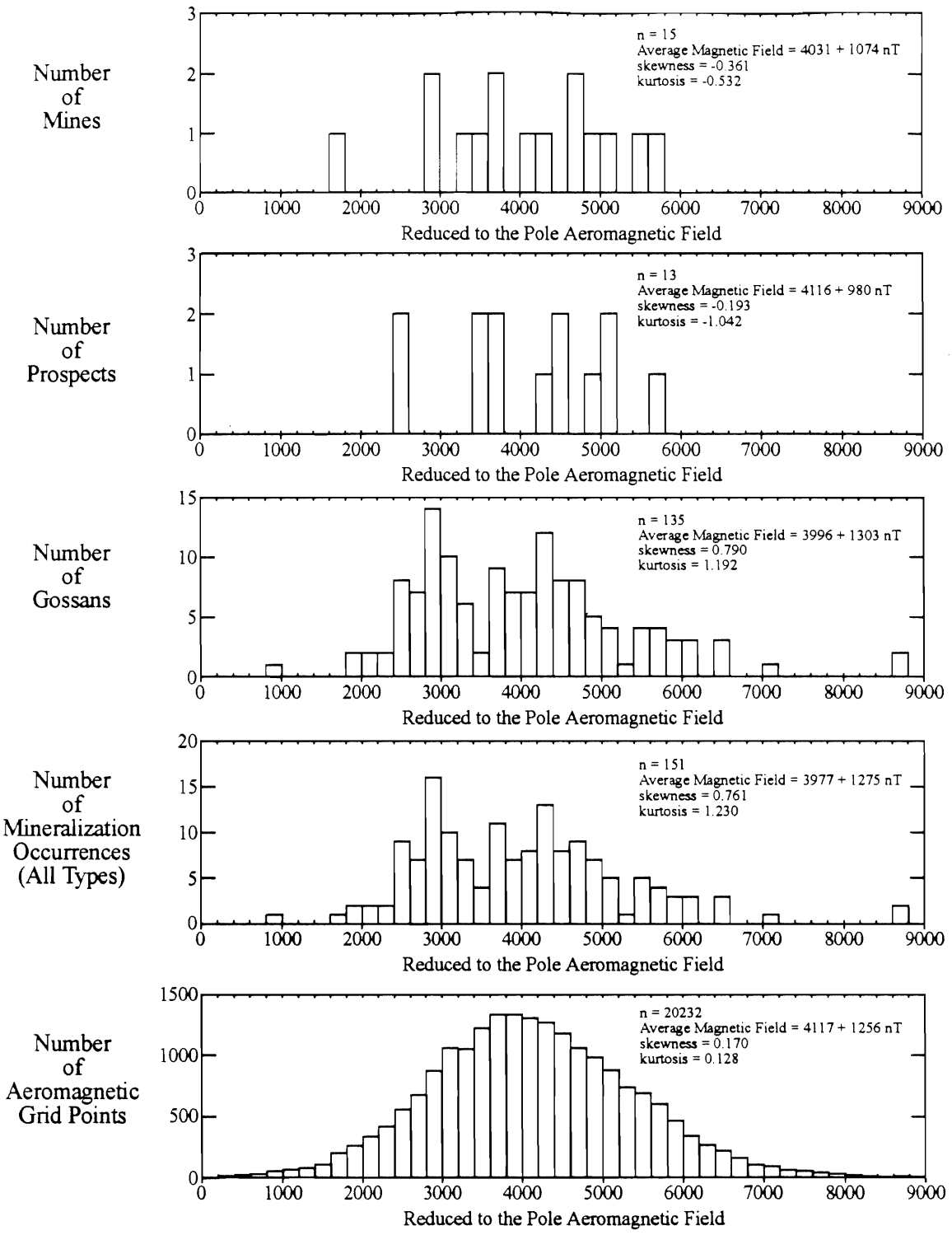

Figure 5.10. Histograms showing the number of mineralization occurrences for different levels of reduced to the pole magnetic field in the area of the Extrusives only on the north flank of the Troodos ophiolite. The bottom histogram shows the number of grid points at each level in the Extrusives for comparison.

The bimodal distribution suggests that a small subset of the mineralization occurs in areas of weaker aeromagnetic field. This subset is small but still significant. It makes a poor prospective criteria since mineralization is found in large numbers across a much wider range of aeromagnetic field strengths. It may indicate that discrete mineralization is, as has been demonstrated for regional hydrothermal alteration, associated with processes that decrease the magnetization of the host rock.

Summary

The magnetic field on the northern flank of the Troodos ophiolite is consistent with a model with strongly magnetized material in the upper layer of the Extrusives. This is underlain by less magnetic lower Extrusives and Basal Group. The less magnetic layer appears to correspond to a level of stronger hydrothermal alteration. The location of this transition varies in depth.

Mineralization does not occur in a regular pattern parallel to the spreading direction, but shows a slight concentration in areas of lower magnetic field.

Consideration of the results in relation to the oceanic crust

What application do these results have to the oceanic crust? In particular, what do they indicate about the magnetic field, hydrothermal circulation and mineralization in the oceanic crust?

A discussion of whether Troodos represents typical oceanic crust has been conducted previously. It will be assumed that it does in this case represent a type of oceanic crust, particularly in respect to magnetization and mineralization.

The results summarized previously indicate that hydrothermal alteration at depth in the oceanic crust causes a decrease in the magnetization. Based on a calculated model which is consistent with detailed geological information, the transition from strongly magnetized to weakly magnetized, altered crust occurs at a variable depth. It is likely to cause anomalies in the magnetic field measured at or above the sea floor.

Several points are worth noting about this. First, the source of these anomalies is in the upper volcanic layer of the oceanic crust. Assuming an average magnetization of ten amperes/metre for this layer, variations in its thickness from two hundred metres to over one kilometre will cause large magnetic anomalies. These may be comparable in magnitude to those due to magnetized topography and magnetic reversals.

These anomalies may take some time to develop. The Troodos ophiolite, at 80+ million years old, is presumably comparable to a type of mature oceanic crust. Some of the alteration and resulting magnetic anomaly variations may continue to develop away from the ridge axis. Alternately, most of the heat driving the hydrothermal system and alteration is found at or near the ridge crest, so activity is more likely to take place there.

In order to be preserved, mineralization must be sealed, usually by burial

under subsequent volcanic material (Hall and Yang, 1994). While they are usually non-magnetic, their relatively small size will make them difficult to detect directly in the magnetic field. Some appear to be weakly related to areas of lesser magnetic field strength but this relationship is not exclusive and could only be a secondary prospective feature. Mineralization anomalies may be larger near the ridge crest where bodies are nearer the surface. Regular spatial arrangements of mineralization have not been detected in this study.

These results may be directly compared to a study by Tivey et al. (1993) which used both near bottom and sea surface magnetic field measurements to investigate subsurface configurations for an active sulphide mound in the TAG hydrothermal field on the Mid-Atlantic Ridge at 26°N. Using a combination of magnetic field inversion, forward modelling and limited geological information, they determined that while the near bottom anomaly could reasonably be caused by a narrow alteration pipe, a larger low-magnetization body must cause the sea surface anomaly. They proposed several possible origins for this larger body including pervasive alteration of the strongly magnetized layer at depth beneath the mound area.

Suggestions for future work

This study has raised additional questions which could be investigated in future studies.

The areas of the deepest aeromagnetic lows were not examined in any

detail. A few well placed, oriented samples from one or more of these areas would determine if they are unmagnetized, rotated or related to some other mechanism. This would have some application to similar areas in the oceanic crust.

It would be of interest to compare gossans from areas where the aeromagnetic field is between 2400 and 3200 nanotesla and gossans from other areas. Any other factors that differentiate these groups could be used to extend the study.

The detailed modelling conducted in the Kambia area could be extended. The western end of the aeromagnetic survey in the Ayia Marina area would be a good candidate. This would suggest more details of the local geological situation, which could be investigated as well.

The analysis of the locations of mineralization failed to find any regular arrangement. Additional methods, using a range of spatial analysis tools and geographic information systems, are becoming available and more need to be developed. Perhaps other methods would discover other, irregular arrangements.

Finally, it would be of interest to search for the Cyprus-type magnetic anomalies in oceanic crust. A detailed deep tow magnetic survey in an area away from the ridge crest and reversal boundaries would be ideal. Good bathymetric data would be necessary to correct for magnetized topography and detailed geological information including oriented samples would be helpful.

Appendix A

Sample Measurements

Site	Northing	Easting	# of samples	J0	J0 Std. Dev.	Susceptibility	Susc. Std. Dev.	Q
301	3874200	524320	1	12.00		11.37		30.49
302	3874100	524270	2	10.10	5.10	10.74	2.21	27.17
303	3874070	524310	2	11.50	1.60	9.79	0.47	33.93
304	3873970	524250	3	11.10	1.50	9.63	0.95	33.29
305	3873930	524270	6	10.30	5.90	9.47	1.26	31.40
306	3873800	524300	2	4.80	2.70	8.53	0.32	16.26
307	3873720	524330	2	2.70	0.00	18.79	1.11	4.15
308	3873600	524350	1	2.80		24.00		3.37
309	3873500	524350	3	3.70	2.00	21.79	6.47	4.90
310	3873450	524400	4	5.50	1.40	15.00	1.74	10.59
311	3873320	524400	2	5.70	1.80	12.00	0.32	13.72
312	3873250	524430	3	12.70	16.00	23.69	9.47	15.49
313	3873150	524460	2	4.00	2.00	12.00	0.16	9.63
314	3873130	524390	2	5.90	4.70	13.90	0.79	12.27
315	3872950	524350	2	2.70	0.00	19.58	8.21	3.98
316	3872870	524440	2	24.20	27.20	12.00	1.58	58.25
317	3872750	524440	2	7.80	3.10	14.37	3.32	15.68
318	3872650	524480	3	2.50	0.80	12.00	4.58	6.02
319	3872560	524400	2	3.80	0.80	11.37	1.42	9.65
320	3872490	524460	2	10.50	8.70	22.42	1.42	13.53
321	3872400	524470	3	20.00	23.90	21.00	3.95	27.51
322	3872300	524450	3	8.30	6.00	20.06	3.32	11.96
323	3872120	524490	2	6.30	2.70	29.21	3.32	6.23
324	3872000	524430	2	7.60	4.00	23.06	1.42	9.52

J0 and J0 Std. Dev. are in amp/m. Susceptibility and Susc. Std. Dev. are in SI units x 10-2. Northing and Easting are in metres. Q is dimensionless.

Appendix A

Sample Measurements

Site	Northing	Easting	# of samples	J0	J0 Std. Dev.	Susceptibility	Susc. Std. Dev.	Q
325	3871920	524500	2	33.00	38.60	34.27	12.32	27.82
326	3871800	524400	2	5.60	0.20	20.84	1.58	7.76
327	3871750	524480	2	5.70	5.00	20.06	6.32	8.21
328	3871650	524500	2	4.60	4.10	23.37	1.11	5.69
329	3871610	524550	3	9.20	8.80	43.90	15.00	6.05
330	3871500	524530	2	15.10	6.50	38.53	5.21	11.32
331	3871350	524520	2	16.50	3.00	27.79	2.05	17.15
332	3871250	524630	3	12.30	9.60	23.21	7.42	15.31
333	3871170	524600	2	68.80	59.60	27.00	3.63	73.60
334	3871000	524700	2	15.30	0.30	22.11	3.47	19.99
335	3870950	524600	2	15.00	16.30	28.58	1.58	15.16
336	3870800	524520	2	15.50	3.80	21.63	2.68	20.70
337	3870800	524480	1	18.80		20.69		26.25
338	3870730	524480	2	9.40	7.30	47.69	15.32	5.69
339	3870640	524450	2	8.00	5.20	27.16	3.32	8.51
340	3870500	524430	2	16.80	11.00	38.69	36.79	12.54
341	3870350	524450	4	6.90	3.30	34.74	12.63	5.74
342	3870270	524270	2	12.30	5.40	60.64	6.63	5.86
343	3870200	524330	2	3.20	0.40	69.01	8.53	1.34
344	3870080	524320	2	1.80	0.30	59.69	9.95	0.87
345	3870300	524550	2	0.10	0.10	1.58	0.16	1.83
346	3870200	524630	2	8.00	9.30	40.43	26.21	5.72
360	3869850	524270	2	2.40	3.30	25.11	22.42	2.76
361	3869750	523950	2	4.50	2.80	46.43	19.58	2.80

J0 and J0 Std. Dev. are in amp/m. Susceptibility and Susc. Std. Dev. are in SI units x 10-2. Northing and Easting are in metres. Q is dimensionless.

Appendix A

Sample Measurements

Site	Northing	Easting	# of samples	J0	J0 Std. Dev.	Susceptibility	Susc. Std. Dev.	Q
362	3869600	523400	2	2.10	1.20	60.48	22.27	1.00
363	3868150	523000	1	2.30		62.22		1.07
364	3868050	522520	3	2.00	0.40	105.96	5.37	0.55
365	3867570	521750	1	4.40		57.01		2.23
366	3867450	521240	2	1.70	0.60	101.06	12.00	0.49
367	3867000	520660	1	1.50		84.48		0.51
368	3868400	523170	1	0.50		59.53		0.24
369	3868650	523220	2	1.60	0.70	90.01	7.11	0.51
370	3868950	523140	2	2.10	1.10	40.90	4.11	1.48
371	3869200	523180	2	1.60	0.50	25.74	4.58	1.80
372	3869350	523230	1	3.50		50.53		2.00
373	3867630	522120	1	4.10		66.96		1.77
374	3867200	520820	5	2.80	2.70	111.65	49.74	0.72
4	3873750	524200	50	13.40	7.20	11.05	2.68	35.02
5	3874050	524350	17	7.30	4.10	11.53	3.79	18.29
6	3873220	524000	5	26.10	17.90	23.69	2.21	31.83
7	3873220	524000	7	11.00	6.50	20.53	6.63	15.48
8	3873150	524000	1	2.10		10.11		6.00
9	3873150	524000	1	1.80		9.63		5.40
10	3873150	524000	1	8.50		10.11		24.30
11	3873200	523950	16	6.60	2.80	11.05	3.16	17.25
12	3873200	523870	21	6.70	3.20	9.63	1.89	20.09
13	3871300	522350	9	2.30	2.05	74.22	17.37	0.90
14	3871300	522350	16	0.84	1.31	12.48	10.11	1.95

J0 and J0 Std. Dev. are in amp/m. Susceptibility and Susc. Std. Dev. are in SI units x 10-2. Northing and Easting are in metres. Q is dimensionless.

Appendix A

Sample Measurements

Site	Northing	Easting	# of samples	J0	J0 Std. Dev.	Susceptibility	Susc. Std. Dev.	Q
15	3871300	522350	4	1.20	0.21	80.54	8.84	0.43
16	3871550	522450	4	3.20	0.17	88.43	4.90	1.05
17	3871550	522450	2	0.80	0.41	7.11	1.26	3.25
18	3871550	522450	2	0.54	0.06	22.11	12.79	0.71
19	3871550	522450	13	6.00	7.60	27.32	18.95	6.34
20	3871750	522550	6	1.40	0.72	34.27	20.53	1.18
21	3871750	522550	4	1.70	0.95	67.90	28.42	0.72
22	3871750	522550	9	2.70	1.30	55.27	17.37	1.41
23	3871750	522550	5	1.20	0.85	45.79	20.53	0.76
24	3871750	522550	6	8.30	11.40	20.53	31.58	11.68
25	3870750	522000	4	5.00	1.00	55.27	15.16	2.61
26	3870750	522000	4	1.80	0.29	83.69	10.74	0.62
27	3870750	522000	4	2.90	0.93	69.48	4.90	1.21
28	3870750	522000	3	1.80	0.14	63.17	12.00	0.82
29	3870750	522000	14	0.06	0.09	3.16	7.58	0.52
30	3870750	522000	5	1.70	0.58	48.95	11.84	1.00
31	3870750	522000	5	2.60	1.30	55.27	8.21	1.36
32	3870750	522000	12	0.38	0.82	9.79	20.53	1.12
33	3870750	522000	5	1.40	0.35	61.59	5.05	0.66
34	3871700	523130	3	15.80	12.00	31.58	5.21	14.45
35	3871700	523130	3	3.60	0.80	47.37	3.00	2.20
36	3871700	523130	3	77.50	51.30	30.00	4.90	74.62
37	3871700	523130	4	12.40	14.40	45.79	3.47	7.82
38	3871700	523130	14	27.00	14.80	26.85	4.26	29.05

J0 and J0 Std. Dev. are in amp/m. Susceptibility and Susc. Std. Dev. are in SI units x 10-2. Northing and Easting are in metres. Q is dimensionless.

Appendix A

Sample Measurements

Site	Northing	Easting	# of samples	J0	J0 Std. Dev.	Susceptibility	Susc. Std. Dev.	Q
39	3871700	523130	4	23.90	30.40	42.64	15.32	16.19
40	3871700	523130	4	24.60	14.60	28.42	3.16	25.00
41	3872300	523550	14	15.10	17.70	18.95	5.21	23.02
L20-A	3872350	521000	3	18.30	18.70	37.90	28.42	13.95
L20-B	3872450	521100	3	7.50	3.50	47.37	12.63	4.57
L20-E	3873050	521250	2	9.70	9.30	26.85	8.84	10.44
L20-F	3873520	521700	3	5.40	2.10	25.27	11.37	6.17
L20-K	3874150	522500	3	10.00	4.60	11.84	3.16	24.39
L20-M	3874230	522550	1	4.00		11.84		9.76
L20-1	3871400	522400	2	0.97	0.70	77.38	7.58	0.36
L20-2	3871300	522300	2	1.20	1.40	64.74	12.63	0.54
L20-3	3868700	521200	3	1.10	0.58	42.64	34.74	0.75
L20-4	3869500	521300	2	3.00	0.80	88.43	28.42	0.98
L20-5	3869900	521700	2	1.20	0.50	101.06	11.37	0.34
L20-6	3870600	522000	3	1.10	0.80	45.79	41.06	0.69
L20-8	3868300	520900	1	3.90		61.59		1.83
L20-9	3868900	521300	2	1.40	1.60	34.74	47.37	1.16
L20-10	3869300	521400	1	5.40		33.16		4.70
L20-11	3869700	521400	2	3.80	2.10	75.80	8.84	1.45
L20-12	3870200	521800	2	0.62	0.77	56.85	60.01	0.32
L20-13	3870800	522100	2	1.40	0.90	83.69	10.11	0.48
116	3870100	526700	2	5.72	5.25	20.53	3.32	8.05
117	3870150	527100	2	11.06	3.46	23.69	5.37	13.49
118	3870250	527200	2	4.92	2.23	23.37	1.74	6.08

J0 and J0 Std. Dev. are in amp/m. Susceptibility and Susc. Std. Dev. are in SI units x 10-2. Northing and Easting are in metres. Q is dimensionless.

Appendix A

Sample Measurements

Site	Northing	Easting	# of samples	J0	J0 Std. Dev.	Susceptibility	Susc. Std. Dev.	Q
119	3870450	527100	2	2.69	0.28	19.11	2.37	4.07
120	3082000	526750	2	10.66	3.73	24.32	5.84	12.66
123	3872200	526450	2	1.47	0.98	16.90	0.63	2.51
124	3872150	526500	2	6.52	0.85	29.37	1.11	6.41
125	3872100	526550	2	5.53	3.18	24.95	1.58	6.40
126	3872100	526600	2	3.35	0.37	25.42	1.58	3.81
127	3872050	526650	2	4.62	0.60	29.21	3.32	4.57
128	3872000	526700	3	19.25	7.28	31.11	10.26	17.88
129	3871800	526580	2	5.82	2.53	25.27	12.48	6.65
130	3871690	526430	2	0.01	0.00	24.32	1.89	0.02
131	3871460	526280	2	6.08	0.30	22.11	1.58	7.94
132	3871400	525900	2	4.41	0.85	23.37	0.63	5.45
133	3871880	526330	2	6.13	1.51	24.16	2.68	7.33
134	3871800	526130	2	3.25	0.20	24.16	1.11	3.89
135	3871830	526210	2	1.98	0.04	24.95	0.47	2.29
137	3872250	525950	2	2.36	0.15	29.69	1.89	2.30
138	3872250	525950	2	1.68	0.06	21.16	0.79	2.29
139	3872150	526000	2	1.78	0.00	22.42	0.00	2.29
140	3872050	526130	2	1.94	0.04	24.32	0.47	2.30
141	3871950	526130	2	4.04	1.55	50.69	19.42	2.30
145	3873050	526930	3	1.08	0.29	13.58	3.63	2.30
147	3872550	525030	2	1.41	0.03	17.69	0.32	2.30
148	3872580	524920	2	0.90	0.04	11.37	0.47	2.29
149	3872550	525150	2	3.06	0.93	11.84	0.47	7.46

J0 and J0 Std. Dev. are in amp/m. Susceptibility and Susc. Std. Dev. are in SI units x 10-2. Northing and Easting are in metres. Q is dimensionless.

Appendix A

Sample Measurements

Site	Northing	Easting	# of samples	J0	J0 Std. Dev.	Susceptibility	Susc. Std. Dev.	Q
150	3872650	525230	2	5.08	2.69	10.11	2.21	14.52
151	3872680	525240	2	6.46	0.58	13.11	1.58	14.24
152	3872790	525240	2	8.96	9.53	14.37	3.32	18.01
153	3872830	525550	2	5.54	0.50	12.00	0.79	13.34
154	3872810	525480	2	3.14	0.23	24.48	2.53	3.71
155	3872830	525740	2	9.34	1.63	13.26	0.16	20.34
156	3872830	525840	2	5.52	0.59	19.27	0.47	8.28
157	3872790	525330	2	2.28	0.12	21.32	1.58	3.09
158	3873300	525350	2	8.25	8.41	13.26	2.68	17.97
159	3873430	525640	2	12.88	10.50	44.22	0.47	8.42
160	3873550	525830	2	2.52	0.75	27.32	2.68	2.66
161	3873830	526250	2	5.02	4.66	21.63	15.32	6.70
162	3873200	522550	2	5.01	5.78	10.58	2.05	13.68
163	3873150	522480	2	6.63	2.79	14.37	0.16	13.33
164	3873070	522560	2	2.40	1.31	15.00	0.95	4.62
165	3872900	522630	2	8.23	1.44	18.00	0.00	13.21
166	3872730	522580	2	6.38	1.39	24.32	1.89	7.58
167	3872610	522630	2	11.75	3.46	34.11	4.74	9.95
168	3873920	522240	2	10.92	2.09	12.48	1.26	25.29
169	3873820	522200	2	1.61	0.40	9.32	0.16	4.99
170	3873580	522100	2	1.22	0.63	9.79	0.79	3.60
171			5	1.07	0.90	37.90	28.27	0.82
172			4	2.54	3.40	38:53	43.58	1.90
173			3	0.49	0.68	25.58	42.48	0.55

J0 and J0 Std. Dev. are in amp/m. Susceptibility and Susc. Std. Dev. are in SI units x 10-2. Northing and Easting are in metres. Q is dimensionless.

Appendix B

Sample Directions

Site	Northing	Easting	# of samples	Declination	Inclination	k	alpha95
4	3873750	524200	42	301.0	73.5	91	2.27
5	3874050	524350	15	318.6	76.4	79	4.07
6	3873220	524000	4	290.3	74.6	179	5.23
7	3873220	524000	7	347.3	74.4	69	6.39
11	3873200	523950	16	296.5	62.0	95	3.58
12	3873200	523870	17	320.4	76.8	107	3.29
13	3871300	522350	5	335.4	42.7	56	8.33
14	3871300	522350	14	342.7	62.1	5	16.05
15	3871300	522350	4	339.9	43.6	63	8.84
16	3871550	522450	3	336.0	59.2	71	9.59
17	3871550	522450	2	321.0	65.1	315	5.58
18	3871550	522450	2	32.7	-10.7	1	138.46
19	3871550	522450	10	6.5	66.9	10	13.98
20	3871750	522550	5	314.1	58.5	87	6.71
21	3871750	522550	4	325.5	57.8	31	12.63
22	3871750	522550	9	310.1	52.4	22	10.03
23	3871750	522550	5	303.1	48.1	10	19.36
24	3871750	522550	6	304.5	62.5	135	4.92
25	3870750	522000	4	314.1	67.5	957	2.26
26	3870750	522000	4	317.8	61.6	601	2.86
27	3870750	522000	4	322.3	58.8	88	7.46
28	3870750	522000	3	310.5	61.7	185	5.95
29	3870750	522000	13	292.5	66.2	178	2.91
30	3870750	522000	5	337.8	63.5	76	7.20
31	3870750	522000	4	324.4	65.1	90	7.37
32	3870750	522000	8	297.8	68.1	103	4.89
33	3870750	522000	4	342.2	51.7	20	15.85
35	3871700	523130	2	305.3	40.6	181	7.36
36	3871700	523130	2	287.3	58.3	78	11.20
37	3871700	523130	2	291.1	58.3	18	23.66
38	3871700	523130	8	26.5	62.7	4	25.94
39	3871700	523130	4	316.4	51.5	28	13.27
40	3871700	523130	2	49.9	62.9	46	14.61
41	3872300	523550	8	285.6	45.6	46	7.30

Declination and Inclination are in degrees.

References

Ade-Hall, J.M. and Johnson, H.P. 1976. Paleomagnetism of basalts, Leg 34. in Yeats, R.S., Hart, S.R., et al. Initial Reports of the Deep Sea Drilling Project, Volume XXXIV. Washington: U.S. Government Printing Office.

Arkani-Hamed, J. 1988. Differential reduction-to-the-pole of regional magnetic anomalies. Geophysics **53**: No. 12, 1592-1600.

Arkani-Hamed, J. 1989. Thermoviscous remanent magnetization of oceanic lithosphere inferred from its thermal evolution. Journal of Geophysical Research **94**: 17421-17436.

Army Map Service. 1942a. Cyprus 1:50000 map, Nicosia. U.S. Army, Washington, D.C.

Army Map Service. 1942b. Cyprus 1:50000 map, Pano Lefkara. U.S. Army, Washington, D.C.

Atwater, T. and Severinghaus, J. 1989. Tectonic maps of the northeast Pacific. in eds. Winterer, E.L., Hussong, D.M. and Decker, R.W. The Eastern Pacific Ocean and Hawaii. Boulder, Colorado: Geological Society of America, The Geology on North America, v. N.

Baranov, V. 1957. A new method for interpretation of aeromagnetic maps: pseudo-gravimetric anomalies. Geophysics **22**: No. 2, 359-383.

Baranov, V. and Naudy, H. 1964. Numerical calculation of the formula of reduction to the pole. Geophysics **29**: No. 1, 67-79.

Bear, L.M. 1960. The geology and mineral resources of the Akaki-Lythrodondha area. Geological Survey Department of Cyprus Memoir No. 3. Cyprus: Government Printing Office.

Bear, L.M. 1963. The mineral resources and mining industry of Cyprus. Bulletin No. 1 of the Geological Survey Department of Cyprus. Cyprus: Ministry of Commerce and Industry, Republic of Cyprus.

Bear, L.M. and Morel, S.W. 1960. The geology and natureal resources of the Agros-Akrotiri area. Geological Survey Department of Cyprus Memoir No. 7. Cyprus: Government Printing Office.

Beauchamp, K.G. 1975. Walsh functions and their applications. London: Academic Press.

Bhattacharyya, B.K. 1965. Two-dimensional harmonic analysis as a tool for magnetic interpretation. Geophysics **30**: No. 5, 829-857.

Bischoff, J.L. and Rosenbauer, R.J. 1989. Salinity variations in submarine hydrothermal systems by layered double-diffusive convection. Journal of Geology **97**: 613-623.

Bleil, U. and Peterson, N. 1983. Variations in magnetic intensity and low-temperature titanomagnetite oxidation of ocean floor basalts. Nature **301**: 384-388.

Briggs, I.C. 1974. Machine contouring using minimum curvature. Geophysics **39**: No. 1, 39-48.

Cande, S.C. and Kent, D.V. 1985. Comment on "Tectonic rotations in extensional regimes and their paleomagnetic consequences for ocean basalts" by Kenneth L. Verosub and Eldridge M. Moores. Journal of Geophysical Research **90**: 4647-4651.

Caress, D.W. and Parker, R.L. 1989. Spectral interpolation and downward continuation of marine magnetic anomaly data. Journal of Geophysical Research **94**: No. B12, 17393-17407.

Carr, J.M. and Bear, L.M. 1960. The geology and mineral resources of the Peristerona-Lagoudhera area. Geological Survey Department of Cyprus Memoir No. 2. Cyprus: Government of Cyprus.

Clube, T.M.M., Creer, K.M. and Robertson, A,H.F. 1985. Palaeorotation of the Troodos microplate, Cyprus. Nature **317**: 522-525.

Constantinou, G. 1980. Metallogenesis associated with Troodos ophiolite. in ed. Panayiotou, A. Ophiolites. Proceedings International Ophiolite Symposium 1979. Republic of Cyprus: Ministry of Agriculture and Natural Resources.

Constantinou, G. and Govett, G.J.S. 1973. Geology, geochemistry, and genesis of Cyprus sulfide deposits. Economic Geology **68**: 843-858.

Cordell, L., Phillips, J.D. and Godson, R.H. 1992. U.S. Geological Survey potential-field geophysical software, version 2.0. United States Geological Survey open file report 92-18.

Corliss, J.B., Dymond, J., Gordon, L.I., Edmond, J.M., von Herzon, R.P., Ballard, R.D., Green, K., Williams, D., Bainbridge, A., Crane, K. and van Andel, T.H. 1979. Submarine Thermal Springs on the Galapagos Rift. Science **203**: 1073-

1083.

Fairey Surveys Ltd. 1973a. 1:50000 map, Pano Lefkara. D Survey, Ministry of Defense, United Kingdom.

Fairey Surveys Ltd. 1973b. 1:50000 map, Palekhori. D Survey, Ministry of Defense, United Kingdom.

Fairey Surveys Ltd. 1973c. 1:50000 map, Nicosia. D Survey, Ministry of Defense, United Kingdom.

Fairey Surveys Ltd. 1973d. 1:50000 map, Paleometokho. D Survey, Ministry of Defense, United Kingdom.

Gass, I.G. 1960. The geology and mineral resources of the Dhali area. Geological Survey Department of Cyprus Memoir No. 4. Cyprus: Government Printing Office.

Gass, I.G. 1980. The Troodos massif: its role in the unravelling of the ophiolite problem and its significance in the understanding of constructive plate margin processes. in ed. Panayiotou, A. Ophiolites. Proceedings International Ophiolite Symposium 1979. Republic of Cyprus: Ministry of Agriculture and Natural Resources.

Geological Survey Department of Cyprus. 1982. Mineral Resources Map of Cyprus. Nicosia, Cyprus: Ministry of Agriculture and Natural Resources.

Gillis, K.M. and Robinson, P.T. 1985. Low-temperature alteration of the extrusive sequence, Troodos ophiolite, Cyprus. Canadian Mineralogist **23**: 431-441.

Gillis, K.M. and Robinson, P.T. 1988. Distribution of alteration zones in the upper oceanic crust. Geology **16**: 262-266.

Grand, T., Lapierre, H., Mascle, G.H., Ohnenstetter, M. and Angelier, J. 1993. Superimposed tectonics of the Cyprus ophiolitic massifs. Tectonics **12**: No. 1, 93-101.

Grauch, V.J.S. and Campbell, D.L. 1984. Does draping aeromagnetic datareduce terrain-induced effects? Geophysics **49**: No. 1, 75-80.

Hall, J.M., Walls, C.C. and Yang, J-S. 1989. Constructional features of the Troodos ophiolite and implications for the distribution of orebodies and the generation of oceanic crust. Canadian Journal of Earth Sciences **26**: 1172-1184.

Hall, J.M., Walls, C.C., Yang, J-S and Hall, S.L. 1991. The magnetization of oceanic crust: contribution to knowledge from the Troodos, Cyprus, ophiolite. Canadian Journal of Earth Sciences **28**: No. 11, 1812-1826.

Hall. J.M., Fisher, B.E., Walls, C.C., Ward, T., Hall, S.L., Johnson, H.P. and Pariso, J. 1991. Magnetic properties, oxide petrography, and alteration: Cyprus Crustal Study Project Drillholes CY-1 and CY-1A; in eds. Gibson, I.L., Malpas, J., Robinson, P.T. and Xenophontos, C. Cyprus Crustal Study Project: Initial Report, Holes CY-1 and 1A. Geological Survey of Canada, Paper 90-20, 235-256.

Hall, J.M. and Yang, J-S. 1994. A preferred environment of preservation for volcanic massive sulfide deposits in the Troodos ophiolite (Cyprus). Economic Geology **89**: 851-857.

Hall, J.M. in preparation. The oceanic crustal constructional setting of a thick sheet and massive flow interval in the extrusive sequence of the Troodos, Cyprus, ophiolite.

Haymon, R.M., Koski, R.A. and Sinclair, C. 1984. Fossils of hydrothermal vent worms from Cretaceous sulfide ores of the Samail ophiolite, Oman. Science **223**: 1407-1409.

Haymon, R.M., Koski, R.A. and Abrams, M.J. 1989. Hydrothermal discharge zones beneath massive sulfide deposits mapped in the Oman ophiolite. Geology **17**: 531-535.

Helsley, C.E. and Steiner, M.B. 1969. Evidence ofr long intervals of normal polarity during the Cretaceous period. Earth and Planetary Science Letters **5**: 325-332.

Huang, Z. 1991. Periodicity in Cretaceous pelagic sequences. Halifax, Nova Scotia: Dalhousie University, unpublished PhD thesis.

Hunting Geology and Geophysics Ltd. 1969. An airborne magnetic and electromagnetic survey in Cyprus. Geological Survey Department of Cuprus, Bulletin No. 3.

Kidd, R.G.W. 1977. The nature and shape of the sources of marine magnetic anomalies. Earth and Planetary Science Letters **33**: 310-320.

Lapierre, H. 1971. Geological map of the Polis-Paphos area. Cyprus: Government Printing Office.

Lowell, R.P. 1990. Thermoelasticity and the formation of black smokers.

Geophysical Research Letters **17**: 709-712.

Lowell, R.P. and Germanovich, L.N. 1994. On the temporal evolution of high-temperature hydrothermal systems at ocean ridge crests. Journal of Geophysical Research **99**: 565-575.

Lowell, R.P. 1995. Seafloor hydrothermal systems. Journal of Geophysical Research **100**: No. B1. 327-352.

Lydon, J.W. 1988. Volcanogenic Massive Sulphide Deposits Part 2: Genetic models. Geoscience Canada **15**: No. 1.

Mason, R.G. and Raff, A.D. 1961. Magnetic survey off the west coast of North America, 32 N. latitude to 42 N. latitude. Geological Society of America Bulletin **72**: 1259-1266.

Miyashiro, A. 1973. The Troodos ophiolite was probably formed in an island arc. Earth and Planetary Science Letters **19**: 218-224.

Moore, T.A. 1960. The geology and natureal resources of the Astromerites-Kormakiti area. Geological Survey Department of Cyprus Memoir No. 6. Cyprus: Government Printing Office.

Muenow, D.W., Garcia, M.O., Aggrey, K.E., Bednarz, U. and Schmincke, H.U. 1990. Volatiles in submarine glasses as a discriminant of tectonic origin: application to the Troodos ophiolite. Nature **343**: 159-161.

Mukasa, S.B. and Ludden J.N. 1987. Uranium-lead isotopic ages of plagiogranites from the Troodos ophiolite, Cyprus, and their tectonic significance. Geology **15**: 825-828.

Natland, J. 1991. Mineralogy and crystallization of oceanic basalts. in ed. Floyd, P.A. Oceanic Basalts. New York: Van Nostrand Reinhold.

Oudin, E., Picot, P. and Pouit, G. 1981. Comparison of sulphide deposits from the East Pacific Rise and Cyprus. Nature **291**: 404-407.

Oudin, E. and Constantinou, G. 1984. Black smoker chimney fragments in Cyprus sulphide deposits. Nature **308**: 349-353.

Pantazis, Th.M. 1967. The geology and natureal resources of the Pharmakas-Kalavassos area. Geological Survey Department of Cyprus Memoir No. 8. Cyprus: Government Printing Office.

Press, W.H., Flannery, B.P., Teukolsky, S.A. and Vetterling, W.T. 1986. Numerical recipes. Cambridge: Cambridge University Press.

Raff, A.D. and Mason, R.G. 1961. Magnetic survey off the west coast of North America, 40 N. latitude to 52 N. latitude. Geological Society of America Bulletin **72**: 1267-1270.

Richardson, C.J., Cann, J.R., Richards, H.G. and Cowan, J.G. 1987. Metal depleted root zones of teh Troodos ore-forming hydrothermal systems, Cyprus. Earth and Planetary Science Letters **84**: 243-253.

Robinson, P.T. 1991. Holes CY-1 and 1A of the Cyprus Crustal Study Project: background and objectives. in eds. Gibson, I.L., Malpas, J., Robinson, P.T. and Xenophontos, C. Cyprus Crustal Study Project: Initial Report, Holes CY-1 and 1A. Geological Survey of Canada, Paper 90-20, p. 1-4.

Rona, P.A. 1978. Magnetic signatures of hydrothermal alteration and volcanogenic mineral deposits in oceanic crust. Journal of Volcanology and Geothermal Research **3**: 219-225.

Rona, P.A. and Scott, S.D. 1993. A special issue on sea-floor hydrothermal mineralization: New perspectives - Preface. Economic Geology **88**: 1935-1975.

Salisbury, M.H., Christensen, N.I., Vine, F.J., Smith, G.C and Eleftheriou, S. 1989. Geophysical structure of the Troodos ophiolite from downhole logging. in eds. Gibson, I.L., Malpas, J., Robinson, P.T. Xenophontos, C. Cyprus Crustal Study Project: Initial Report, Hole CY-4. Geological Survey of Canada Paper 88-9. Ottawa: Ministry of Supply and Services Canada. p. 331-349.

Sharma, P.V. 1986. Geophysical Methods in Geology. New York: Elsevier Science Publishing Co.

Smith, W.H.F. and Wessel, P. 1990. Gridding with continuous curvature splines in tension. Geophysics **55**: No. 3, 293-305.

Spooner, E.T.C. 1977. Hydrodynamic model for the origin of the ophiolitic cupriferous pyrite ore deposits of Cyprus. In Volcanic processes in ore genesis. Geological Society of London, Special publication 7, pp. 58-71.

Spooner, E.T.C. and Bray, C.J. 1977. Hydrothermal fluids of seawater salinity in ophiolitic sulphide ore deposits in Cyprus. Nature **266**: 808-811.

Staudigal, H., Gillis, K. and Duncan, R. 1986. K/Ar and Rb/Sr ages of celadonites from the Troodos ophiolite, Cyprus. Geology **14**: 72-75.

Talwani, M. 1965. Computation with the help of a digital computer of magnetic anomalies caused by bodies of arbitary shape. Geophysics **30**: No. 5, 797-817.

Talwani, M., Windisch, C.C and Langseth, M.G. 1971. Reykjanes Ridge crest: a detailed geophysical study. Journal of Geophysical Research **76**: 473-517.

Thy, P. and Moores, E.M. 1988. Crustal accretion and tectonic setting of the Troodos ophiolite, Cyprus. Tectonophysics **147**: 221-245.

Tivey, M.A., Rona, P.A. and Schouten, H. 1993. Reduced crustal magnetization beneath the active sulfide mound, TAG hydrothermal field, Mid-Atlantic Ridge at 26°N. Earth and Planetary Science Letters **115**: 101-115.

United Nations Development Program. 1970. Survey of groundwater and mineral resources, Cyprus. New York: United Nations.

Varga, R.J. and Moores, E.M. 1985. Spreading structure of the Troodos ophiolite, Cyprus. Geology **13**:846-850.

Verhoef, J. 1986. Magnetic anomalies over two- and three-dimensional structures in relation with some magnetic parameters. Utrecht: Vening Meinesz Laboratoroim, unpublished report.

Verosub, K.L. and Moores, E.M. 1981. Tectonic rotations in extensional regimes and their paleomagnetic consequences for ocean basalts. Journal of Geophysical Research **86**: 6335-6349.

Vine, F.J. and Matthews, D.H. 1963. Magnetic anomalies over oceanic ridges. Nature **199**: 947-949.

Vine, F.J., Poster, C.K. and Gass, I.G. 1973. Aeromagnetic Survey of the Troodos igneous massif, Cyprus. Nature Physical Science **244**: 34-38.

Vogt, P.R. 1979. Amplitudes of oceanic magnetic anomalies and the chemistry of oceanic crust: synthesis and review of "magnetic telechemistry". Canadian Journal of Earth Sciences **16**: 2236-2262.

Watson, D.F. 1992. Contouring. A guide to the analysis and display of spatial data. New York: Pergamon/Elsevier.

Webring, M.W. 1991. Minimum curvature gridding of scattered data. U.S. Geological Survey open-file report 81-1224. in Cordell, L., Phillips, J.D. and Godson, R.H. 1992. U.S. Geological Survey potential-field geophysical software, version 2.0. United States Geological Survey open file report 92-18.

Wilson, R.A.M. and Ingham, F.T. 1959. The geology of the Xeros-Troodos area with an account of the mineral resources. Geological Survey Department of Cyprus Memoir No. 1. Cyprus: Government of Cyprus.

Woolridge, A.L., Haggerty, S.E., Rona, P.A and Harrison, C.G.A. 1990. Magnetic properties and opaque mineralogy of rocks from selected seafloor hydrothermal sites at oceanic ridges. Journal of Geophysical Research **95**: 12351-12374.

Woolridge, A.L, Harrison, C.G.A., Tivey, M.A., Rona, P.A. and Schouten, H. 1992. Magnetic modeling near selected areas of hydrothermal activity on the Mid-Atlantic and Gorda Ridges. Journal of Geophysical Research **97**: 10911-10926.

Yang, J-S. 1991. Constructional and alteration features and their relationships to sulfide deposits in the upper part of the Troodos ophiolite, Cyprus. Halifax, Nova Scotia: Dalhousie University, unpublished PhD thesis.

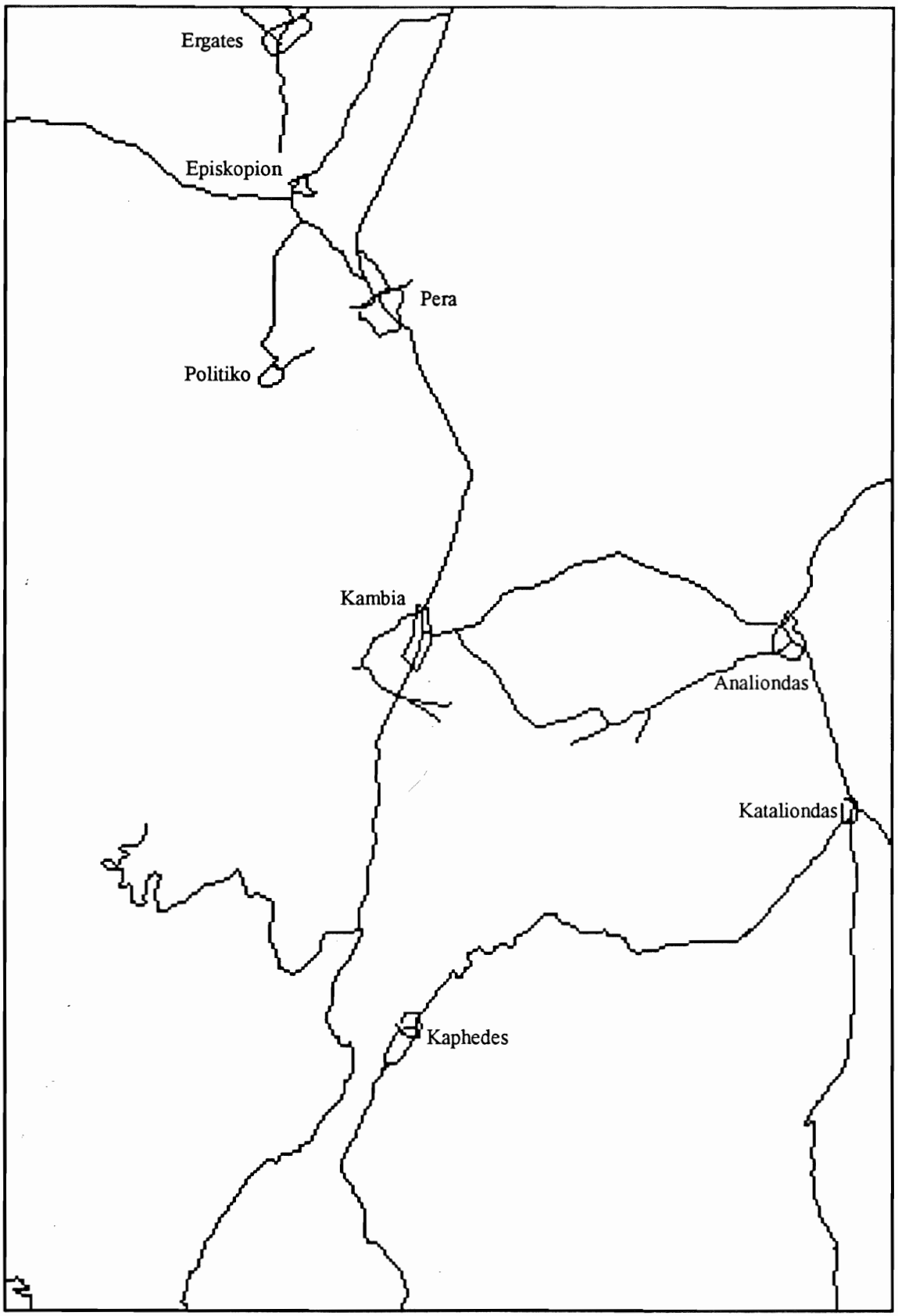

Overlay 1. Roads and villages in the Kambia study area

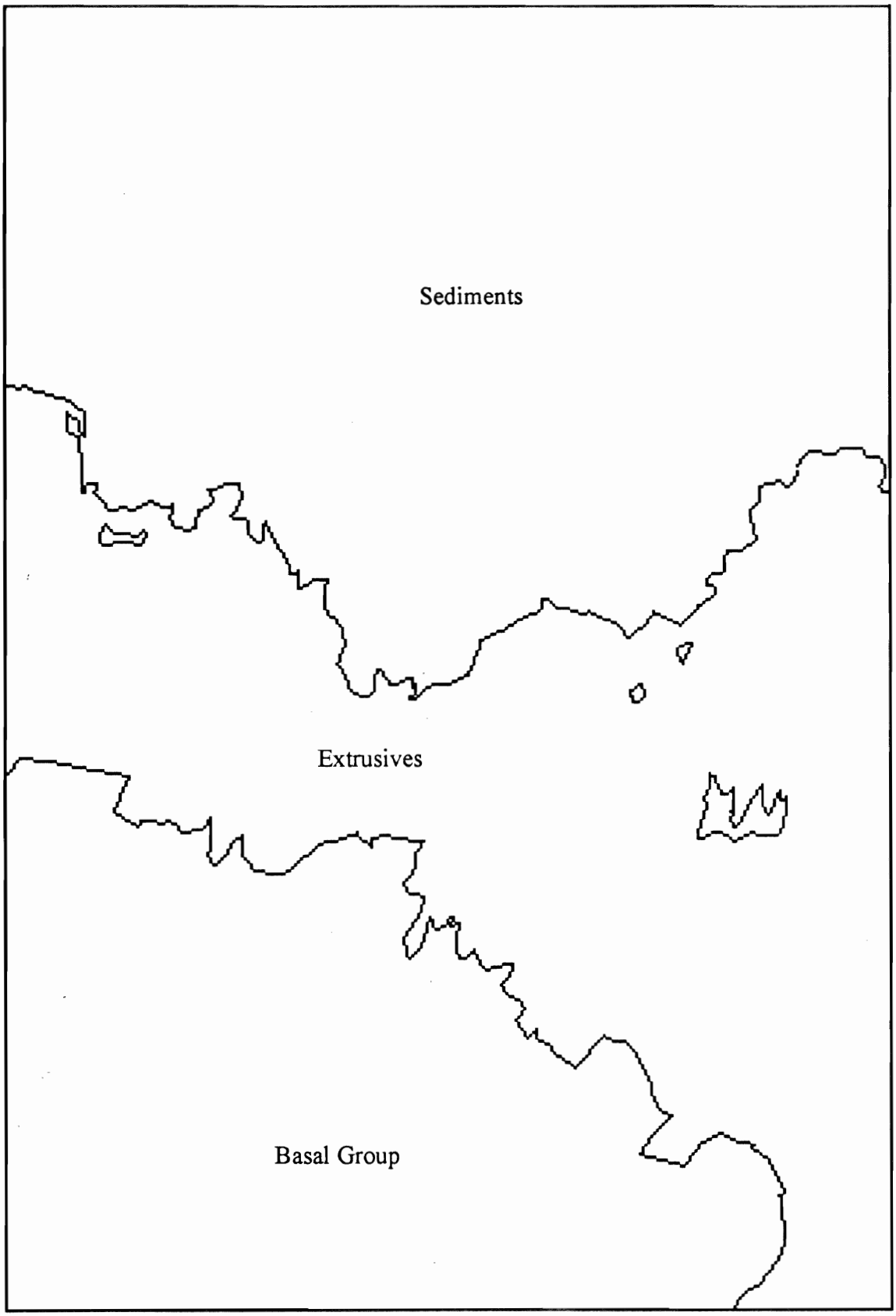

Overlay 2. Major geological units in the Kambia study area

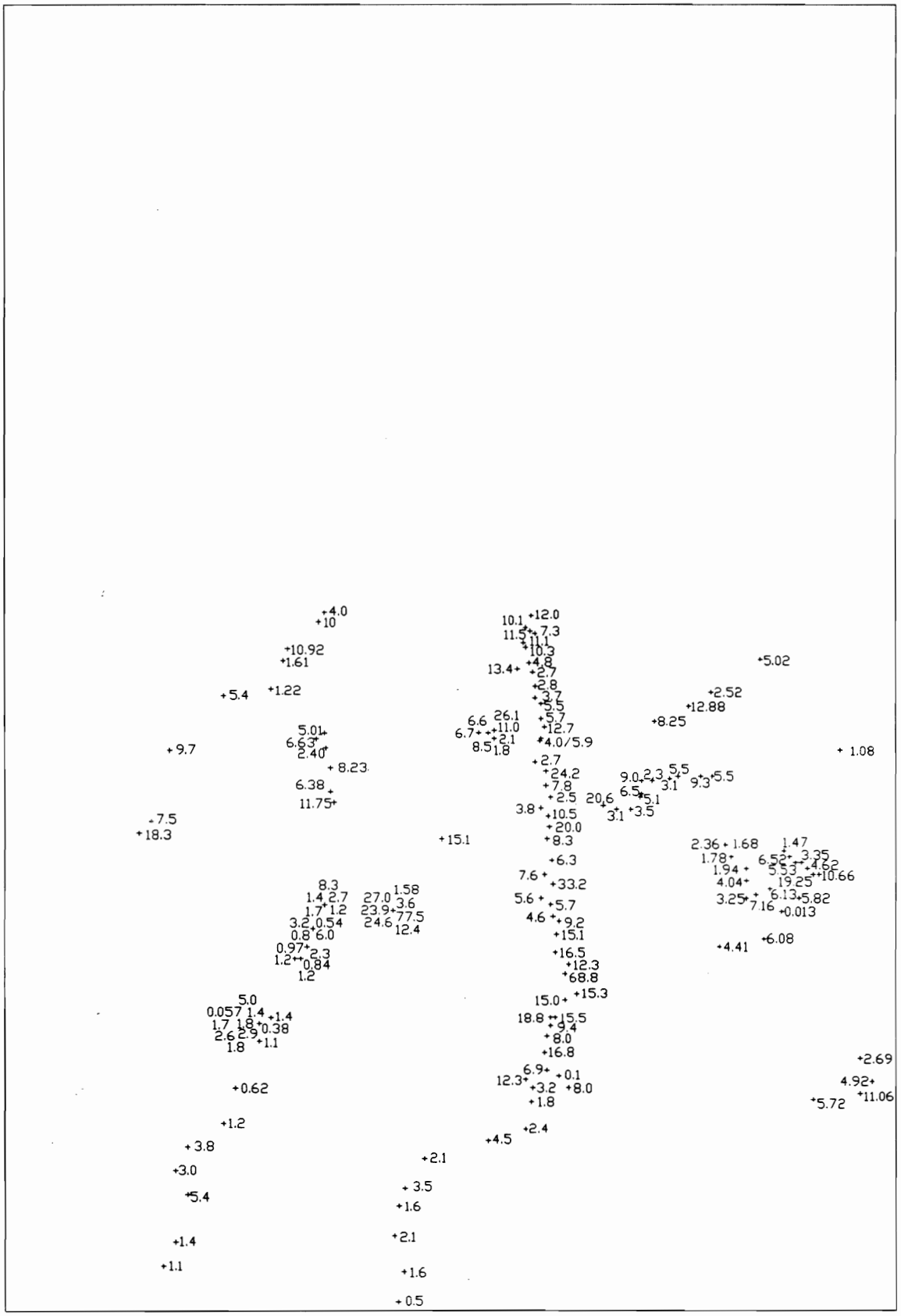

Overlay 3. Locations of magnetic samples and J0

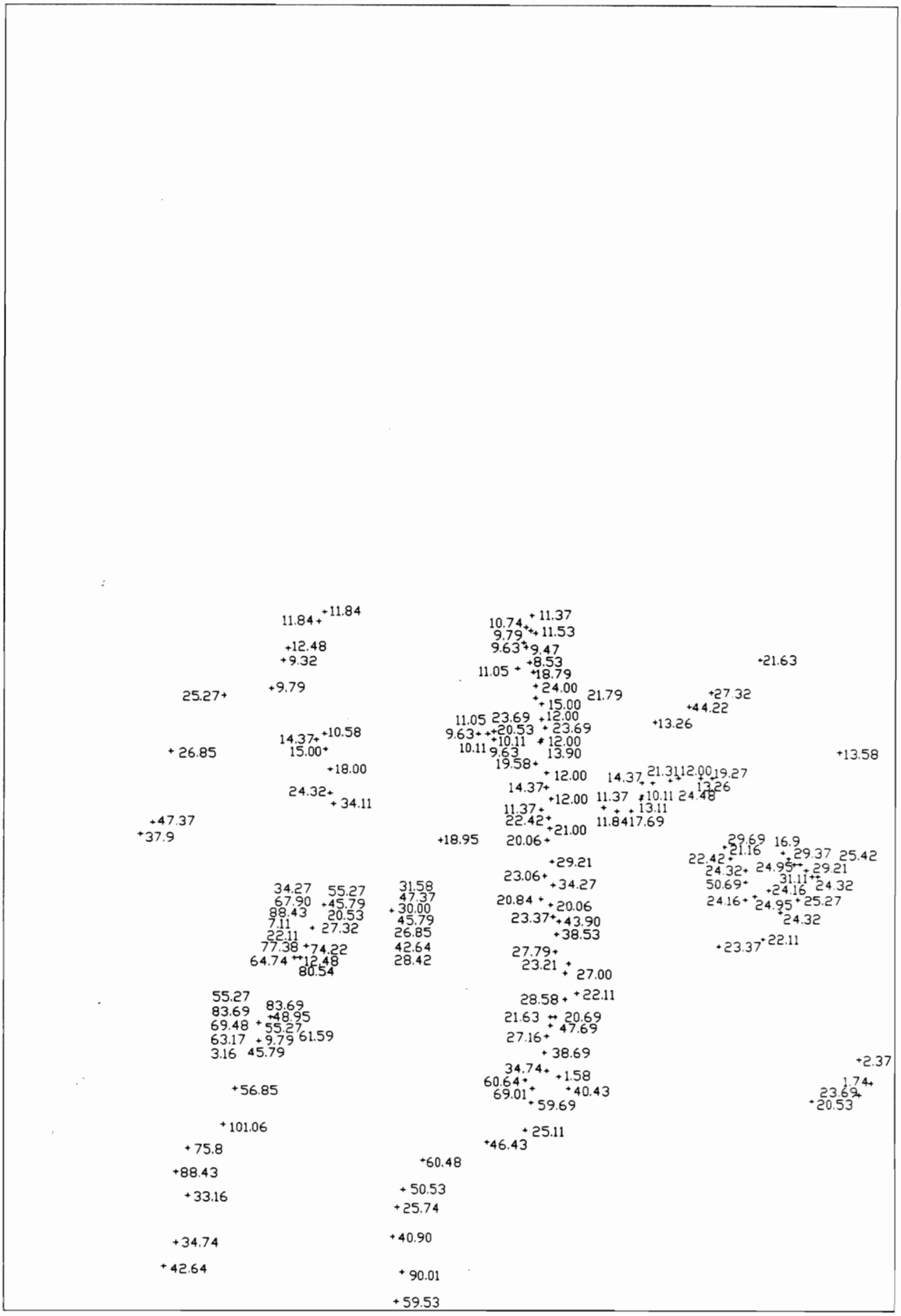

Overlay 4. Locations of magnetic samples and susceptibilities

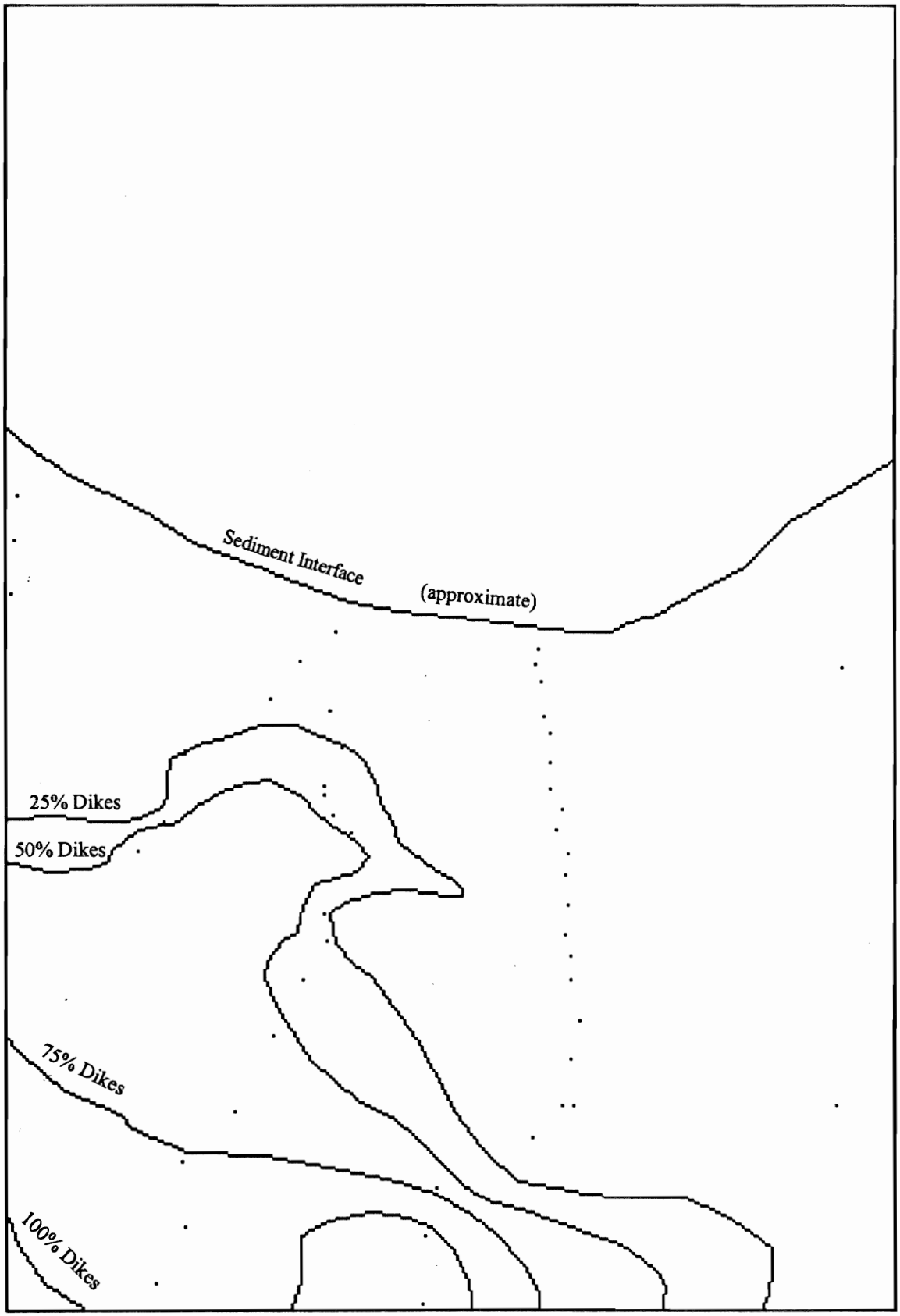

Overlay 5. The percentage of dikes in the Kambia study area.

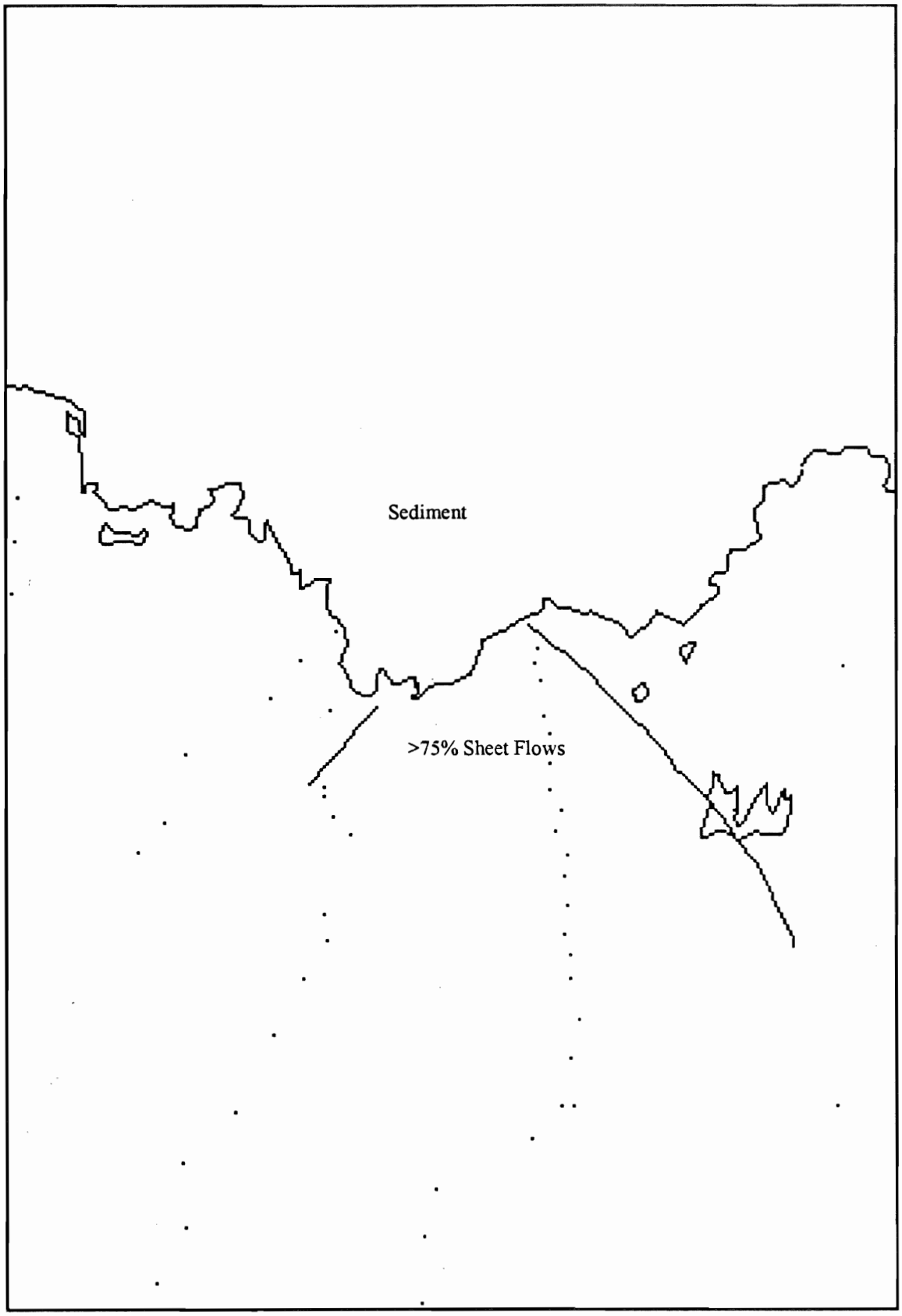

Overlay 6. The region of > 75% sheet flows in the extrusive of the Kambia study area.

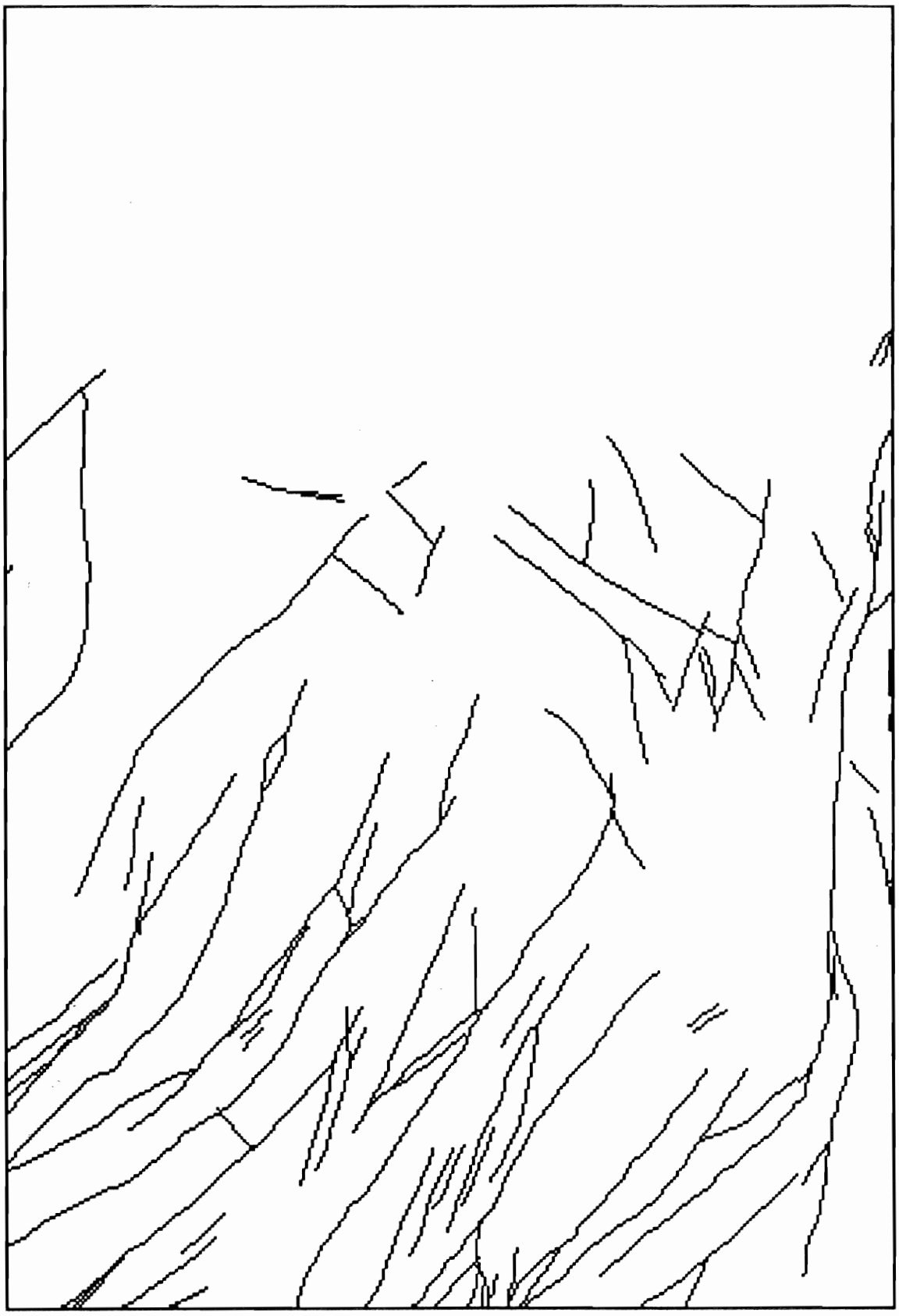

Overlay 7. Faults in the Kambia study area, from Bear,1960 and Gass,1960.

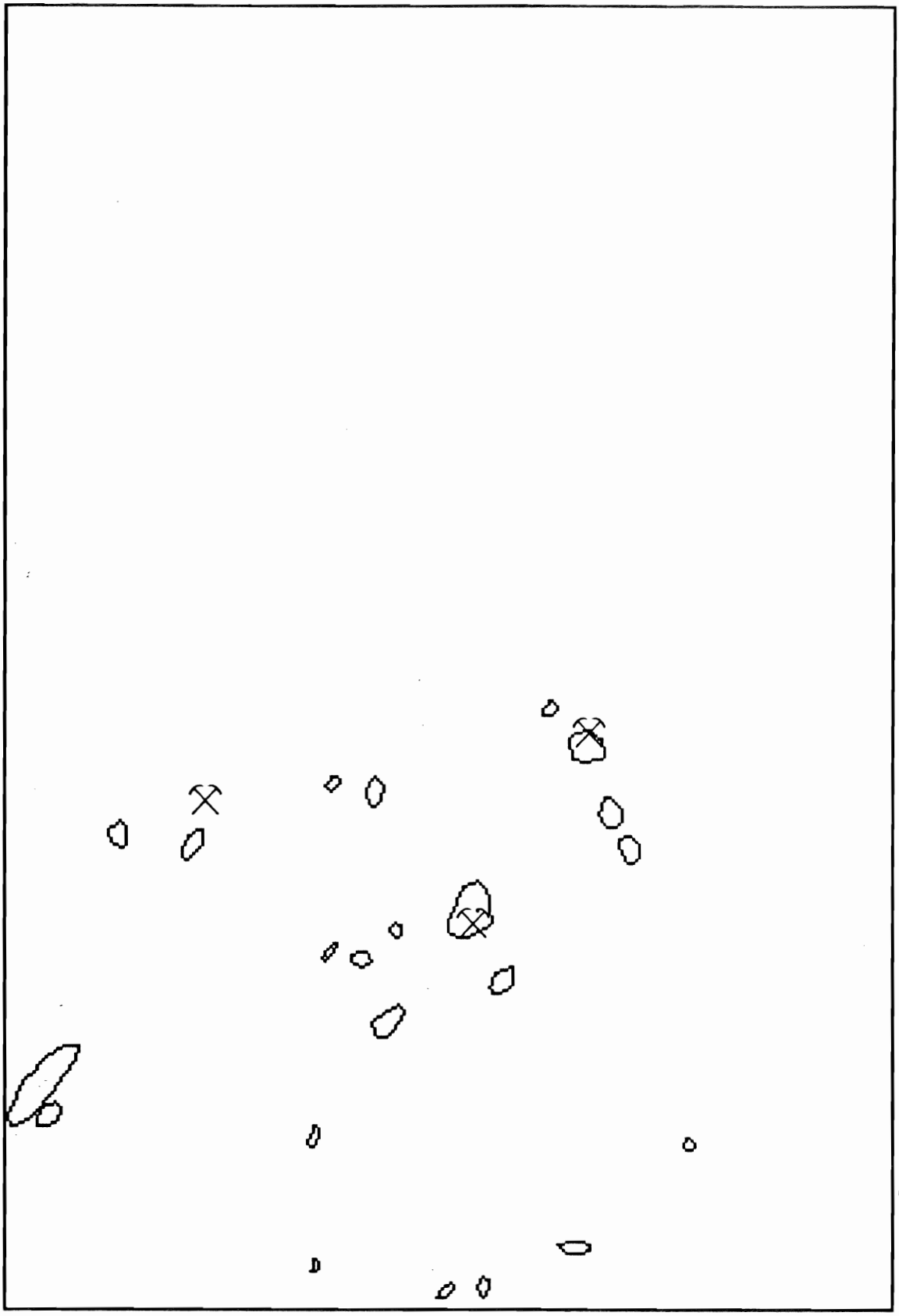

Overlay 8. Mines and gossans in the Kambia Study area, from Bear, 1960 and Gass, 1960.

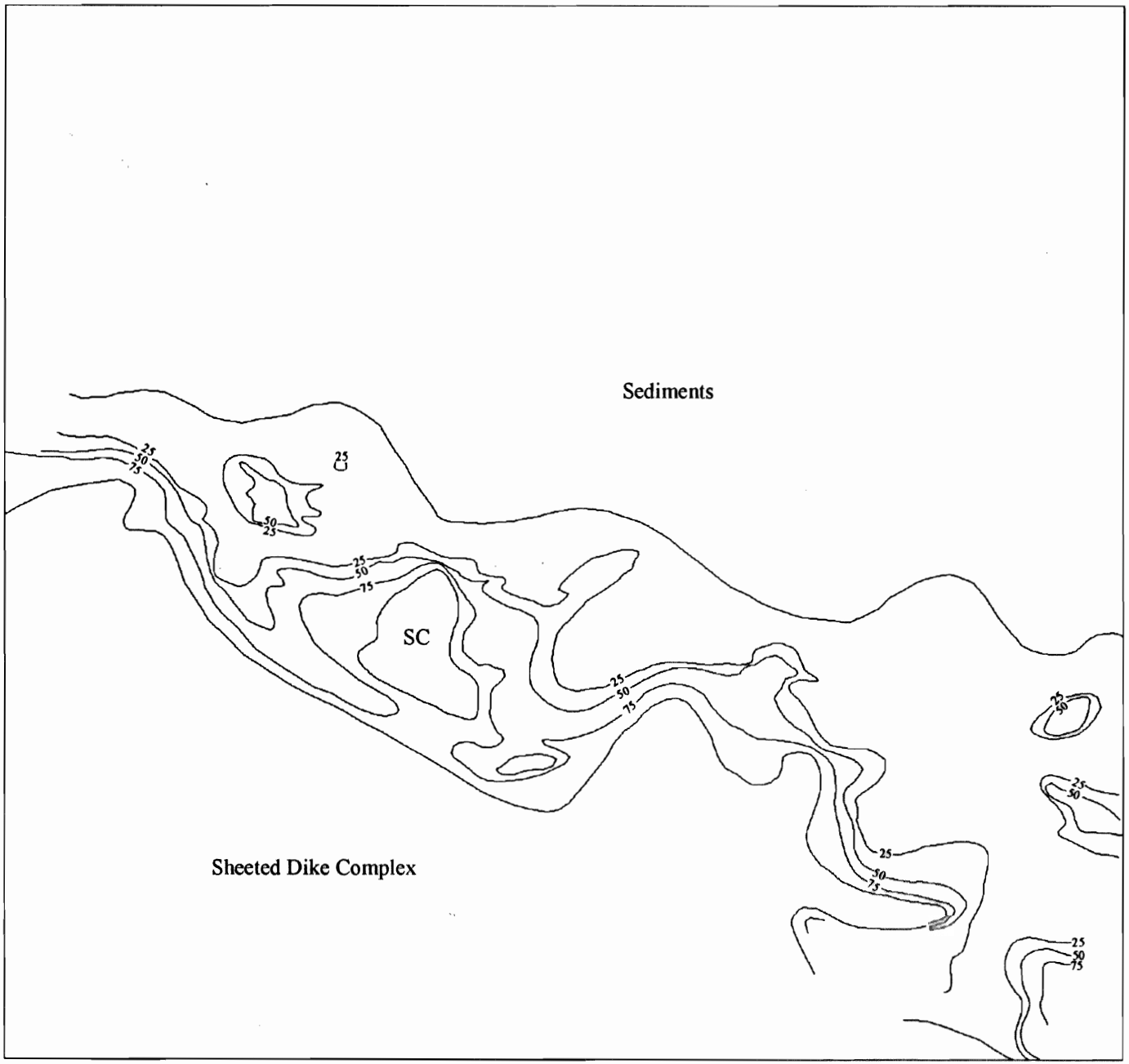

Overlay 9. Dike percentage on the northern flank of the Troodos ophiolite. From Hall et al., 1991.

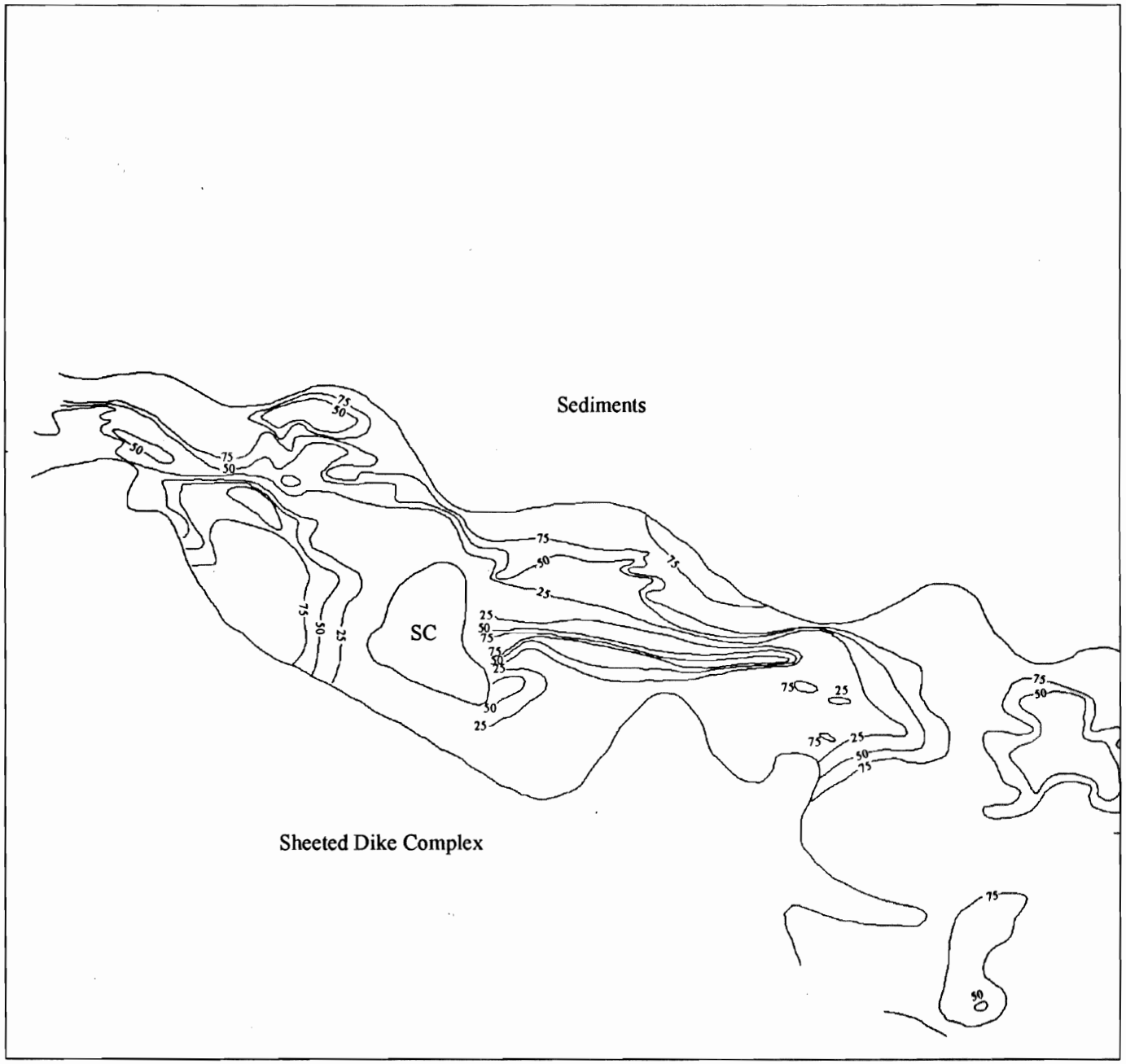

Overlay 10. The ratio of sheet flows to pillowed flows on the northern flank of the Troodos ophiolite, from Yang, 1991.